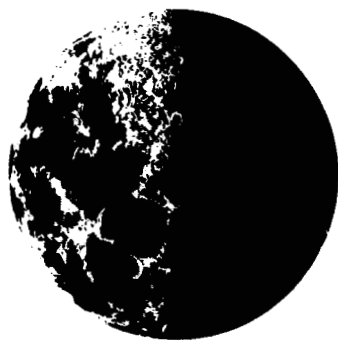


(NASA-CR-117230) DATA REPORT FOR
EXPERIMENTAL HEAT TRANSFER DISTRIBUTIONS
OVER LAUNCH AND ENTRY CONFIGURATIONS ON THE
0.045-SCALE APOLLO MODEL /H-2/ WITH THE
ADDITION OF STRAKES AT A MACH NUMBER OF 10

N79-76582

Unclas
11325

FF 60 ~~NASA CR 117230~~
(NASA CR OR TMX OR AD NUMBER) (CATEGORY)
~~CONTRACTORS ONLY~~



APOLLO

AVAILABLE TO NASA HEADQUARTERS ONLY

Z 65 - 12018

CLASSIFICATION CHANGE

To **UNCLASSIFIED**

By authority of GB-101652

Date 12/13/72

Changed by D. Shirley

Classified Document Master Control Station, NASA
Scientific and Technical Information Facility

Accession No. 57997-64

Copy No. 34

SID 63-1135

DATA REPORT FOR EXPERIMENTAL HEAT TRANSFER
DISTRIBUTIONS OVER LAUNCH AND ENTRY
CONFIGURATIONS ON THE 0.045-SCALE APOLLO
MODEL (H-2) WITH THE ADDITION OF STRAKES
AT A MACH NUMBER OF 10 (U)

NAS9-150

February 1964

Volume 1 (of 6) CONTRACT NAS9-150



Exhibit I, Paragraph 5.5

~~AVAILABLE TO NASA HEADQUARTERS ONLY~~

This document contains information affecting the national defense of the United States within the meaning of the Espionage Laws, Title 18 U.S.C. Section 793 and 794. Its transmission or revelation of its contents in any manner to an unauthorized person is prohibited by law.

NORTH AMERICAN AVIATION, INC.
SPACE and INFORMATION SYSTEMS DIVISION

~~CONFIDENTIAL~~

~~CONFIDENTIAL~~

FOREWORD

The test described herein was conducted from April 2 to April 5, 1963 under NASA Apollo contract NAS9-150. This report was prepared in accordance with Paragraph 5.5, Exhibit I.

The report was prepared by G. A. Udvardy of the Experimental Aerodynamics Unit, Space and Information Systems Division of North American Aviation, Inc.

~~CONFIDENTIAL~~

~~CONFIDENTIAL~~

ABSTRACT

Heat transfer distributions were measured on 0.045-scale models of the Apollo spacecraft at a Mach number of 10 through a Reynolds number range of 190,700 to 1,386,000 (based on maximum command module diameter). The angle-of-attack range for the test was 0 to 15 degrees for the launch configuration and 180 to 130 degrees for the entry configuration. A boundary layer trip was employed on the conical portion of the command module for the launch configuration without LES motor and tower, and on the heat shield for the entry configuration. Oil flow photos were taken of all configurations at several angles of attack.

The results of the test are presented in the form of plotted and tabulated data. Some qualifications and general observations of the data are also made.

~~CONFIDENTIAL~~

~~CONFIDENTIAL~~

CONTENTS

Section		Page
	INTRODUCTION	1
I	MODEL DESCRIPTION	3
	GENERAL	3
	INSTRUMENTATION	3
	INSTALLATION	3
II	TEST DESCRIPTION	5
	TEST FACILITIES	5
	TEST PROCEDURE	5
	DATA REDUCTION	6
	RESULTS	7
	LAUNCH CONFIGURATION	8
	ENTRY CONFIGURATION	9
III	CONCLUSIONS	11
	LAUNCH CONFIGURATION	11
	ENTRY CONFIGURATION	11
	REFERENCES	13
	APPENDIXES	
	A. PLOTTED DATA (VOLUMES 2 AND 3)	A-1
	B. TABULATED DATA (VOLUMES 4, 5, AND 6)	B-1

~~CONFIDENTIAL~~

~~CONFIDENTIAL~~

ILLUSTRATIONS

Figure		Page
1	Typical Launch and Entry Trajectories	27
2	Basic Dimension Sketch of Models	28
3	Configuration Tested with NAA and AEDC Designations	29
4	Photos of Launch Configuration With and Without Service Module Reaction Control Motors (E ₄₃ T ₂₇ C ₂ L ₂₈ R ₅ S ₆ I ₁ B ₈)	30
5	Photos of Command-Service Module Shown With Strakes and With and Without Service Module Reaction Control Motors (C ₂ L ₂₈ S ₂ R ₅)	31
6	Photos of Command-Service Module With Boundary Layer Trip (C ₂ L ₂₈ S ₂ +t _{r16})	32
7	Photos of Entry Configuration With Strakes and Steel Balls Mounted on Entry Face to Simulate Roughness (C ₂ L ₂₈ +t _{r15})	33
8	Photos of Entry Configuration (C ₂) With Sting Attachment	34
9	Thermocouple Installation in Models	35
10	Basic Dimensions of the Strake and Service Module Reaction Control Motors	36
11	Thermocouple Location on Command Module Configuration (C ₂)	37
12	Thermocouple Locations on Launch Configuration HL-1B (E ₄₃ T ₂₇ C ₂ L ₂₈ S ₆ I ₁ B ₈) and Command-Service Module Configuration H-2 (C ₂ S ₂)	38
13	Photos of Instrumentation Entry Configuration (C ₂)	39
14	Sting Arrangement and Angle-of-Attack Range for the Entry Configuration (C ₂)	40
15	Photos of Launch Configuration Installed in Tunnel (E ₄₃ T ₂₇ C ₂ L ₂₈ S ₆ I ₁ B ₈)	41
16	Specific Heat of 310 Stainless Steel Versus Temperature	42
17	H-2 Data Reduction System	43
18	Heating Rate of Thermocouple Number One at Various Angles of Attack on Command Module Configuration.	44

~~CONFIDENTIAL~~



ILLUSTRATIONS (Cont)

Figure		Page
19	Effect of RCS Motors on Launch Configuration Heating Rates With Strakes (E ₄₃ T ₂₇ C ₂ L ₂₈ S ₆ R ₅ I ₁ B ₈) (Re/in. = 27,000)	45
20	Effect of RCS Motors on Launch Configuration Heating Rates With Strakes (E ₄₃ T ₂₇ C ₂ L ₂₈ S ₆ R ₅ I ₁ B ₈) .	46
21	Effect of RCS Motors on Launch Configuration Heating Rates With Strakes (E ₄₃ T ₂₇ C ₂ L ₂₈ S ₆ R ₅ I ₁ B ₈) (Re/in. = 166,000)	47
22	Photos of Oil Flow Photographs of Launch Configuration With Strakes and Service Module Reaction Control Motors at Zero-Degrees Angle of Attack (Re/in. = 27,000)	48
23	Photos of Oil Flow Photographs of Launch Configuration With Strakes and Service Module Reaction Control Motors at 10 Degrees Angle of Attack (Re/in. = 27,000)	49
24	Photos of Oil Flow Photographs of Launch Configuration With Strakes at Zero-Degrees Angle of Attack (Re/in. = 27,000)	50
25	Photos of Oil Flow Photographs of Launch Configuration With Strakes at 10 Degrees Angle of Attack (Re/in. = 27,000)	51
26	Photos of Oil Flow Photographs of Command-Service Modules, With Reaction Control Motors, at Zero Degrees Angle of Attack (Re/in. = 27,000) .	52
27	Photos of Oil Flow Photographs of the Command-Service Module, With Strakes and Reaction Control Motors, at 10 Degrees Angle of Attack (Re/in. = 27,000)	53
28	Photos of Oil Flow Photographs of Command-Service Module With Strakes at Zero-Degrees Angle of Attack (Re/in. = 27,000)	54
29	Photos of Oil Flow Photographs of Command-Service Module With Strakes at 10-Degrees Angle of Attack (Re/in. = 27,000)	55
30	Heating Rates on Windward Side of Strake Versus Angle of Attack (C ₂ Configuration) (Re/in. = 27,000) .	56
31	Heating Rates on Windward Side of Strake Versus Angle of Attack (C ₂ Configuration) (Re/in. = 200,000) .	57

~~CONFIDENTIAL~~

ILLUSTRATIONS (Cont)

Figure		Page
32	Effect of Strakes on Windward Afterbody Heating Rates Near Entry Angle of Attack (C ₂ configuration) (Re/in. = 27,500)	58
33	Effect of Strakes on Windward Afterbody Heating Rate Near Entry Angle of Attack (C ₂ configuration) (Re/in. = 83,300)	59
34	Effect of Strakes on Windward Afterbody Heating Rates Near Entry Angle of Attack (C ₂ configuration) (Re/in. = 200,000)	60
35	The Effect of Strakes on Afterbody Heating at Two Reynolds Numbers (Re/in. = 83,300 and 200,000) ($\alpha = 147^\circ$)	61
36	Mapping of the Command Module Afterbody Heating Rate Ratio (H/H_0) (Re/in. = 200,000) ($\alpha = 147^\circ$)	62
37	Leeward Afterbody Heating Ratio With and Without Strakes (Re/in. = 27,500) ($\alpha = 147^\circ$)	63
38	Leeward Afterbody Heating Ratio With and Without Strakes (Re/in. = 200,000) ($\alpha = 147^\circ$)	64
39	Photos of Oil Flow Photographs of Entry Configuration With Strakes at 147-Degrees Angle of Attack (Re/in. = 27,500)	65
40	Photos of Oil Flow Photographs of Entry Configuration With Strakes at 147-Degrees Angle of Attack and Model Rolled 180 Degrees (Re/in. = 27,500)	66
41	Photos of Oil Flow Photographs of Entry Configuration Without Strakes at 147-Degrees Angle of Attack and Model Rolled 180 Degrees (Re/in. = 27,500)	67
42	Variation of Heat Transfer Rate on Afterbody of Command Module at 147-Degrees Angle of Attack at Various Yaw Angles (Re/in. = 83,300)	68
43	Variation of Heat Transfer Rate on Afterbody of Command Module at 147-Degrees Angle of Attack at Various Yaw Angles (Re/in. = 200,000)	69
44	Variation of Heating Rates on the Command Module Entry Face at Various Angles of Attack (Re/in. = 27,500)	70
45	Variation of Heating Rates on the Command Module Entry Face at Various Angles of Attack (Re/in. = 83,300)	71

~~CONFIDENTIAL~~

~~CONFIDENTIAL~~

ILLUSTRATIONS (Cont)

Figure		Page
46	Variation of Heating Rates on the Command Module Entry Face at Various Angles of Attack (Re/in. = 200,000)	72

TABLES

Table		Page
1	Basic Model Dimensions (Scale 0.045)	14
2	Thermocouple Dimensional Location H ₂ (C ₂).	16
3	Thermocouple Dimensional Location H ₂ (C ₂ S ₂)	18
4	Thermocouple Dimensional Location HL-1B (E ₄₃ T ₂₇ C ₂ L ₂₈ S ₆ I ₁ B ₈).	20
5	H-2 and HL-1B Model Run Summary, AEDC Tunnel C, Mach No. 10	22

~~CONFIDENTIAL~~

~~CONFIDENTIAL~~~~CONFIDENTIAL~~

NOMENCLATURE

Symbols used in the tests are defined as follows:

b	Model skin thickness, ft
c	Specific heat of model material, $\text{BTU}/(\text{lb}_m) (^{\circ}\text{R})$
C_p	Specific heat of air stream, $\text{BTU}/(\text{slug}) (^{\circ}\text{R})$
D	Model characteristic length, ft
H	Enthalpy, BTU/lb
h	Heat transfer coefficient, $\text{BTU}/(\text{ft}^2) (\text{sec}) (^{\circ}\text{R})$
k	Coefficient of conductivity of model skin, $\text{BTU}/(\text{ft}^2) (^{\circ}\text{R})$
M	Mach number
Nu	Nusselt number
P	Pressure, psia
\dot{Q}	Heat transfer rate, $\text{BTU}/(\text{ft}^2) (\text{sec})$
r	Radius of command module at maximum section, in.
Re	Reynolds number
s	Distance of thermocouple from center of (1) entry face of command module (C_2), and (2) apex on both the C_2S_2 and HL-1B configurations, measured along surface, in.
s/r	Nondimensional reference length
s/r*	Nondimensional reference length with s measured from thermocouple number 4 (H-2 model only)
St	Stanton number

~~CONFIDENTIAL~~

~~CONFIDENTIAL~~

T	Temperature, °R
t	Time, sec
V	Velocity, ft/sec
w	Density of model skin, lb_m/ft^3
α	Angle between model centerline and wind vector, degrees $\alpha = 0$ degrees, apex forward
α_s	Angle between reference sting centerline and wind vector, degrees
θ	Angle between command module centerline and reference sting centerline, degrees
μ	Viscosity of air stream, $\text{lb}_F \text{ sec}/\text{ft}^2$
ρ	Density of air stream, slug/ft^3
\emptyset	Angle between meridian lines on which thermocouples are located, degrees
Θ	Roll angle about sting centerline, degrees

Subscripts used in the tests are as follows:

∞	Tunnel free stream conditions
$^{\circ}$	Tunnel stagnation conditions
w	Model wall conditions
STOR	Aerodynamic heating losses not accounted for
AERO	Aerodynamic

~~CONFIDENTIAL~~

~~CONFIDENTIAL~~

INTRODUCTION

The Apollo heat transfer test program has been designed to obtain heat transfer data through the entire range of Reynolds numbers and Mach numbers during both the launch and entry sequence of the Apollo spacecraft flight. However, due to limitations of the existing testing facilities, only parts of the entire flight range can be simulated in any one facility.

A wind tunnel test of 0.045-scale Apollo heat transfer models of the command module (H-2) and of the spacecraft plus the S-IVB adapter (HL-1B) was conducted in Tunnel C of the von Karman Gas Dynamics Facility, Arnold Engineering and Development Center from 2 April through 4 April 1963. This was the fourth in the H-2 series of Apollo heat transfer tests that are planned in various facilities. (See References 1, 2, and 3.)

The primary objectives of the test were to determine the following:

1. The effect on the heat transfer distribution over the launch configuration of the addition of strakes on the command module and reaction control system rockets on the service module
2. The heat transfer distribution over the afterbody of the command module with and without strakes
3. The heat transfer distributions over the entry face and afterbody of the command module with and without a boundary layer trip
4. With the sting located on the windward side of command module afterbody, determine lee side heating rates
5. Induce transition to turbulent flow by means of a boundary layer trip near the apex of the command module plus service module configuration

Oil flow visualization photographs of the various model configurations at several angles of attack were also obtained.

Heat transfer data were obtained at $M = 10$ over a Reynolds number range of 197,000 to 1,388,000 (based on maximum command module diameter) for the entry configuration, and for the launch configuration over a Reynolds number range of 197,000 to 1,155,000. The flight regime simulated in this test is shown in Figure 1. The angle of attack of the launch

~~CONFIDENTIAL~~

~~CONFIDENTIAL~~

configuration was varied from 0 to 15 degrees and the entry configuration from 180 to 130 degrees. The entry configuration was also tested in the yaw plane through a range of 0 to 10 degrees angle of sideslip at 147 degrees angle of attack.

The results of the test are presented in the form of plotted data which show the heat transfer coefficient ratio and the heat transfer rate distribution over every configuration tested. Summary plots are also presented showing the effect of the various model components on the heat transfer rate distribution over the models. Tabulated test results are also presented.

~~CONFIDENTIAL~~

~~CONFIDENTIAL~~

I. MODEL DESCRIPTION

GENERAL

Three 0.045-scale models of the Apollo vehicle were tested. The configurations were the command module with strakes in the entry position (C_2), the command (with strakes) and service modules (C_2S_2), and the launch configuration HL-1B. The HL-1B model includes the escape rocket, tower, command module, strakes, service module, reaction control system rockets, adapter connecting the service module to the instrumentation unit, instrumentation unit, and the Saturn S-IVB booster stage to Station 1039. A sketch showing the basic dimensions of the models is presented in Figure 2. Figure 3 shows all the configurations tested with their NAA and AEDC designations. Table 1 lists the dimensions of the various model components. Photographs of the assembled models are shown in Figures 4 through 7. Figure 8 is two photographs showing the command module model components and the module assembled on the sting.

The models were of thin-skin construction (0.040-inch), with the body shells fabricated from Inconel X. The model body shells were thermally insulated from all body support structure. The insulation material used was Electrobestos. A sketch showing a typical model shell support is presented in Figure 9. Complete model drawings are contained in Reference 4.

Boundary layer trips were used on the entry face of the entry configuration and on the conical surface of the command module plus service module configuration. The trips were 0.069-diameter stainless steel spheres, spot welded to the surface of the models. Figures 6 and 7 show the trips installed on the models.

The strake-on configuration utilized one instrumented and one inert strake. The noninstrumented strake was constructed of 310 stainless steel, thermally insulated from the model by layer of silicon glass laminate. The instrumented strake was a sandwich type of construction using two layers of 310 stainless steel separated by a layer of silicon glass laminate. Thermocouples were mounted on 0.020-inch thick stainless steel. The silicon glass laminate was 0.065-inch thick cut out so that the stainless could be inlaid. Figure 9 shows the installation and construction of the instrumented strake.

Service module reaction control motors were installed on the HL-1B and on the command plus service module models during part of the test. They are located just aft of the command-service module joint on the

~~CONFIDENTIAL~~

7.5-, 97.5-, 187.5-, and 277.5-degree meridian planes. Figure 10 shows a sketch of the motors and their installation.

INSTRUMENTATION

The temperature of the model skin was monitored by ninety-eight 30-gauge constantan thermocouples, fusion welded to the inside surface of the model shell. A typical thermocouple installation is shown in Figure 8. The thermocouples were located on the models within ± 0.01 inch of the dimensions shown in Figures 11 and 12. Figure 13 is a photograph of the instrumentation on the entry configuration. The model shell thickness (b) at each thermocouple location is listed in Tables 2, 3, and 4, along with the s/r and s*/r values for each thermocouple. The b values were obtained by averaging the measured values after the thermocouples were installed.

INSTALLATION

The entry configuration (H-2) was installed in the tunnel using the AEDC 12- and 50-degree split stings and the 22-degree offset sting. With this sting arrangement, the angle-of-attack range obtained was 180 to 126 degrees. The HL-1B and the command-service module configurations were installed in the tunnel using the 22- and 34-degree offset stings, allowing a -27- to 3-degree angle-of-attack range. A sketch showing the sting arrangement and angle range for the entry configuration is presented in Figure 14. Complete installation procedures for the heat transfer models are presented in Reference 5. A photograph of the launch configuration (HL-1B) mounted on the injector is presented in Figure 15.

~~CONFIDENTIAL~~

~~CONFIDENTIAL~~

II. TEST DESCRIPTION

TEST FACILITIES

The test was conducted in Tunnel C of the von Karman Gas Dynamics Facility, Arnold Engineering Development Center. Tunnel C is a 50-inch-diameter, continuous, closed-circuit, variable-density wind tunnel equipped with an axisymmetric, contoured nozzle. The tunnel is designed to operate at a Mach number of 10 through a range of stagnation pressures from 175 to 2400 psi, with stagnation temperatures as high as 1500 F.

The tunnel-model support system is designed so that the model can be retracted from the test section into a cooling tank for model change, modification, or for cooling heat transfer models. When the model is in the retracted position the tank is sealed from the tunnel and tunnel airflow is maintained. When the model is in the test position the tank is evacuated to approximately free-stream static pressure.

In either the retracted or extended positions, the models can be pitched ± 15 degrees with a straight sting and rolled 180 degrees about the sting axis. Using a variety of stings and adapters which are available at the tunnel, coupled with the roll mechanism, various model attitudes in pitch, yaw, and roll may be attained.

Additional information concerning the operation of the tunnel is presented in Reference 6.

TEST PROCEDURE

Transient heat transfer data were obtained by reducing the model wall temperature to approximately 20 F (isothermal conditions) then introducing the model into the hot airstream and recording the change in skin temperature with time. Model exposure time varied from 7 to 10 seconds. Cooling time varied from 2 to 4 minutes after each run. Cooling was accomplished by retracting the model into the cooling tank and blowing compressed air over it.

Oil-flow visualization photos were obtained by: spraying the model with a fine coat of fluorescent impregnated oil in the cooling tank; injecting the model into the stream; and photographing the flow of oil with a motion picture camera.

~~CONFIDENTIAL~~

Nominal tunnel test conditions are presented in the following tabulation:

Condition	Po (psi)	To (° R)	Re/inch x 10 ⁻⁶
1	215	1670	0.27
2	460	1750	0.54
3	750	1805	0.83
4	1285	1865	1.33
5	1645	1885	1.66
6	2000	1900	2.00

A run summary listing the runs by configuration, test group, angle of attack and Reynolds number is presented in Table 4.

DATA REDUCTION

The heating rates and heat transfer coefficient data were obtained using the standard AEDC data reduction equations for heat transfer tests. The heat transfer parameters obtained from the model temperature-time data were heat transfer rate \dot{Q} , heat transfer coefficient h , Stanton number St , and Nusselt number Nu . The general equations used to reduce the data were:

$$Q_{\text{STOR}} = W_{bc} \frac{dT_w}{dt} \frac{\text{BTU}}{\text{Ft}^2 \text{sec}} \quad (1)$$

$$h^*_{\text{STOR}} = \frac{Q_{\text{STOR}}}{H_o - H_w} \frac{\text{LB}}{\text{Ft}^2 \text{sec}} \quad (2)$$

where

$$H_o - H_w = \left(C_{p_o} T_o + \frac{V^2}{2gJ} \right) - C_{p_w} T_w \frac{\text{BTU}}{\text{LB}} \quad (3)$$

$$h_{\text{STOR}} = \frac{Q_{\text{STOR}}}{T_o - T_w} \frac{\text{BTU}}{\text{Ft}^2 \text{sec } ^\circ\text{R}} \quad (4)$$

$$St_{\text{STOR}} = \frac{h_{\text{STOR}}}{\rho_\infty V_\infty C_{p_\infty}} \quad (5)$$

$$Nu = \frac{h_{\text{STOR}} D}{k} \quad (6)$$

~~CONFIDENTIAL~~

~~CONFIDENTIAL~~

Model wall thickness, (b), (Tables 2, 3, and 4) and material density (493 pounds per cubic foot) can be considered constants in equation (1); however, the specific heat of the model skin is a function of temperature. The variation of the specific heat of the model skin as a function of model wall temperature is shown in Figure 16.

Five heat transfer data points are computed for each run. The basis for all the heat transfer data is the temperature-time data. These data are recorded every 0.05 seconds starting at the moment the model starts its movement into the tunnel from the cooling tank, and ceases to be recorded at the instant the model starts its movement back into the cooling tank. When the model reaches tunnel centerline, the next 21 temperature time data points are fitted with a least squares parabolic curve. At the center of this curve (the eleventh time-data point) a $\Delta dT_w/dt$ is evaluated and used to compute the first heat transfer data point. The second heat transfer data point is determined by using the next 21 temperature-time data points. The initial temperature-time data point for the second heat transfer data point is the eleventh point of the preceding heat transfer data point. This sequence is repeated for the next three data points, which are 0.50 seconds apart. The tabulated data for the five times are listed in Appendix B.

A Beckman 210 data acquisition system was used to record the temperature-time data from each run on magnetic tape. The magnetic tape was then programmed into an IBM 7070 digital computer that reduced the temperature-time data to heat transfer parameters. These values, along with the tunnel operating parameters, were printed out on both magnetic tape and tabulated data sheets. The magnetic tapes containing the reduced data were then programmed into an IBM 7090 digital computer for conversion to a machine plotting format. This format was used with an SC-4020 plotter to obtain the machine plotted curves that appear in Appendix A. A block diagram of the data reduction system is shown in Figure 17.

RESULTS

The results of the test are presented in plotted form in Appendix A and tabular form in Appendix B. The plotted heat transfer data are included in pages A-1 through A-997, and tabulated on pages B-1 through B-861. Appendix A is broken up into two volumes; Volumes 2 and 3. Each volume has a plotted data index. Heat transfer plots contain Q and H/H_0 versus s/r and s/r^* . Appendix B is contained in Volumes 4, 5, and 6. Each volume has a tabulated data index.

The H_0 values for the launch configuration are the H values (heat transfer coefficient) obtained during the test at zero-degrees angle of attack for thermocouple number one on the command-service module configuration. This was done for each Reynolds number tested. Stagnation point heat

~~CONFIDENTIAL~~

~~CONFIDENTIAL~~

transfer coefficients that were used as the reference values for all entry configurations curves were obtained by extrapolation. Test values could not be used because of data scatter in the stagnation region of the model at $\alpha = 180$ degrees. Theoretical stagnation point heat transfer coefficients could not be used because of differences in the level of test data from one test to another.

Stagnation point heat transfer rates were determined by plotting curves of Q versus angle of attack for the number one thermocouple located in the geometric center of the entry face, and by extrapolating the value of Q at $\alpha = 156$ degrees to $\alpha = 180$ degrees. Lees distribution for a hemisphere (Reference 10) was used to fit the test data (since the command module in the heat shield forward position is essentially a hemisphere). The value of Q at an angle of attack of 180 degrees (which resulted from making the best fit with the test data) was used at the stagnation point reference value. From this Q stagnation point reference value the H_0 value was calculated using Equation (2). Figure 18 shows the curves used for determining Q stagnation point reference value.

LAUNCH CONFIGURATION

Figures 19, 20, and 21 show the effect of service module reaction control motors on the heating rates on the surface of the launch configuration. The plots are for various Reynolds numbers through an angle-of-attack range of 0 to 15 degrees. The heating rates on a station ($s/r = 2.45$) just forward of the rocket show an increase of approximately four times the heating rates without rockets. The heating rates aft of the rocket nozzles up to the beginning of the S-IVB flare are also increased 100 percent. Aft of the flare the heating is decreased 30 percent, as compared to the heating rate without the rockets nozzles installed.

The addition of strakes also increases the heating rates, by a factor of three, on the service module. This effect is shown by comparing the heating rates at zero angle of attack, with rockets removed on the 0- and 270-degree meridian; the strakes are mounted on the 270 degree meridian, where the increase is noted.

A more graphic presentation of both of these effects is shown in the oil flow photographs of the launch configuration and the command-service module configuration, Figures 22 through 29. These show the flow pattern developed by the addition of strakes and service module reaction control motors; the high heating rate areas are the darkened areas aft of the strakes and just forward of the motors.

~~CONFIDENTIAL~~

~~CONFIDENTIAL~~

Changes in Reynolds number indicated little or no effect on the proportional increase or decrease of the heating rates caused by the addition of strakes or the motors.

ENTRY CONFIGURATION

Figures 30 and 31 show the heating rates on the windward side of strakes at various angles of attack and Reynolds number. The high heating occurred in the entry range at 151-degrees angle of attack. Reynolds number has a large effect on the heating rates on the strake when they are compared to the 180-degree \dot{Q} stagnation heating rate. At an angle of attack of 151 degrees and for a Reynolds number of 27,500 per inch, the \dot{Q}/\dot{Q}_s equals 0.17 and for a Reynolds number of 200,000 per inch the \dot{Q}/\dot{Q}_s equals 0.45.

Figures 32, 33, and 34 show the effect of the strakes on the windward conical region of the command module at entry angles of attack of 147 ± 4 degrees. As shown on Figures 30 and 31 the highest rates occur at 151-degrees angle of attack. There is a definite proportional increase in afterbody heating with an increase in Reynolds number. By comparing the heating rates with and without strakes at Reynolds numbers of 27,500, 83,300, and 200,000 per inch, the rates (\dot{Q} with strake/ \dot{Q} without strake) are 1.4, 2.7, and 3.9, respectively, and show an increase with increasing Reynolds number. As the Reynolds number is increased the high heating area tends to move more towards the apex.

Figure 35 illustrates the effect of the strake on the heating rates on the afterbody of the command module at 147 degrees angle of attack. This graph shows the heating at given s/r's with and without strakes. This figure also shows the effect of Reynolds number on the afterbody heating.

Figure 36 illustrates the area which is affected by the strake. In the vicinity of the strake the high heating rates occur at the apex end on the windward side. The heating rate is about 2 or 3 times higher than the adjacent area out of the effect of strake.

Figures 37 and 38 present the strake leeward heating rates. This data was obtained by rotating the model on the sting 180 degrees. The heating rates with strakes are compared to the rates without strakes. The heating rates along the 285-degree ray located adjacent to the strake on the leeward side shows a decrease up to 70 percent over those with the strake off. The remainder of the rays show a general increase of heating rate up to 2.4 times that without the strake.

~~CONFIDENTIAL~~

~~CONFIDENTIAL~~

Oil flow photographs shown in Figures 39 through 41 show graphically the effect of the strake on the flow pattern on the command module afterbody.

The variation of heat transfer rates on the afterbody of the command module at 147-degrees angle of attack at various yaw angles is shown in Figures 42 and 43. As the yaw angle increases to 10 degrees, the afterbody heating rate increases up to 2 times the heating rate for 0-degree yaw. As the Reynolds number increases from 27,500 to 200,000 per inch, the high heating area moves toward the apex.

Figures 44 through 46 show the variation in heat transfer rate on the heat shield face of the command module at various angles of attack and Reynolds number.

~~CONFIDENTIAL~~

~~CONFIDENTIAL~~

III. CONCLUSIONS

The purpose of this report has been to present the results of heat transfer tests of the spacecraft plus S-IVB adapter incorporating aerodynamic strakes. The tests were conducted in Tunnel C of the von Karman Gas Dynamics Facility, AEDC. Some general conclusions based on a preliminary analysis are summarized below.

LAUNCH CONFIGURATION

1. The service module reaction control motors cause a definite increase in heat transfer rate just forward of the motors.
2. The addition of strakes increases the heating rates on the service module.
3. Changes in Reynolds number appeared to have little or no effect on the heating rates caused by the addition of strakes or motors.

ENTRY CONFIGURATION

1. Highest heating rates on the strakes occur at 151-degrees angle of attack.
2. Reynolds number has a large effect on the proportional increase of the heating on the strake and the command module afterbody.
3. With the model at 147-degrees angle of attack and 10 degrees yaw, the conical surface heating is increased up to twice that of a 0-degree yaw condition.

~~CONFIDENTIAL~~

~~CONFIDENTIAL~~

REFERENCES

1. Biss, W. J. and D. X. Emerson. Experimental Heat Transfer Distributions over Launch and Entry Configurations of an 0.045-Scale Apollo Model (H-2) at Mach Numbers of 8 and 10. NAA S&ID, SID 62-993 (September 1962)
2. Emerson, D. X. Experimental Heat Transfer Distributions over Launch and Entry Configurations of 0.045-Scale Apollo Models (H-2) and (HL-1) at Mach Numbers 2.5 and 3.71. NAA S&ID, SID 63-685 (June 1963)
3. Biss, W. J. Experimental Heat Transfer Distributions over Launch and Entry Configuration of 0.045-Scale Apollo Models H-2, HL-1 and HL-1B at Mach Number of 10. NAA S&ID, SID 63-1184.
4. Model Assembly Modification Apollo H-2 and HL-1 Configuration Heat Transfer Models. S&ID Drawing 7121-01268
5. Model Installation Apollo H-2 in Tunnels B and C at AEDC. S&ID Drawing 7121-01256
6. Arnold Center Test Facilities Handbook. January 1961
7. Fay, J. A. and F. R. Riddell. "Theory of Stagnation Point Heat Transfer in Dissociated Air," Journal of the Aeronautical Sciences. (February 1958) pp. 73-85
8. Structural Analysis of the 0.045-Scale Apollo Heat Transfer Model (H-2). NAA S&ID, SID 63-616 (11 May 1962)
9. Udvardy, G. A. Pretest Information for Heat Transfer Tests of the 0.045-Scale Model with Strake (H-2 and HL-1B) in AEDC-VKF, Tunnel C. NAA SID IOL 223-140-63-023 (March 1963)
10. Lees, L. "Laminar Heat Transfer Over Blunt-Nosed Bodies at Hypersonic Flight Speeds," Jet Propulsions, Vol. 26, No. 4 (April 1956), pp. 259-269, 274

~~CONFIDENTIAL~~



Table 1. Basic Model Dimensions (Scale 0.045)

Item	Full Scale	Model Scale
COMMAND MODULE (C ₂) (DRAWING 7121-01254-8)		
Maximum Diameter, in.	154.000	6.93
Radius of Spherical Blunt End, in.	184.800	8.316
Corner Radius, in.	7.700	0.346
Afterbody Semi-angle, deg	33° 00'	33° 00'
Afterbody Vertex Radius, in.	9.155	0.412
Length of Body, From Apex to Center of Entry Face, in.	142.538	6.4142
Distance From Apex to Center of Launch Face, in.	7.644	0.344
TOWER STRUCTURE (T ₂₇) (DRAWING 7121-01093)		
Length, in. (rocket base to command module attach point)	120.000	5.400
Number of Longitudinal Members	4	4
Diameter of Longitudinal Members, in.	4.000	0.180
Diameter of Cross Braces, in.	2.670	0.120
Distance Between Attach Points at Command Module:		
Pitch Plane	46.840	2.108
Yaw Plane	50.666	2.280
Distance Between Attach Points at Escape Motor:		
Pitch Plane	23.000	1.035
Yaw Plane	36.066	1.623
ESCAPE MOTOR (E ₄₃) (DRAWING 7121-01093-3)		
Total Length, in.	279.500	12.577
Diameter of Motor, in.	26.000	1.170
Maximum Diameter of Skirt, in.	54.820	2.467
Skirt Flare Angle, deg	36° 55'	36° 55'
Nose Included Angle, deg	30° 00'	30° 00'
Nose Radius, in.	2.000	0.090

~~CONFIDENTIAL~~

Table 1. Basic Model Dimensions (Scale 0.045) (Cont)

Item	Full Scale	Model Scale
SERVICE MODULE (S_2) (DRAWING 7121-01268)		
Total Length, in. (measured at tangent point to command module)	154.534	6.954
Diameter, in.	154.000	6.930
SERVICE MODULE PLUS ADAPTER (S_6) (DRAWING 7121-01254-2 (3))		
Service module		
Total Length, in.	140.000	6.300
Diameter, in.	154.000	6.930
Adapter		
Total Length, in.	135.000	6.075
Diameter, in.	154.000	6.930
INSTRUMENT SECTION (I_1) (DRAWING 7121-01261-11)		
Total Length, in.	58.000	2.610
Diameter, in.	154.000	6.930
SATURN S-IVB STAGE (B_8) (DRAWING 7121-01264-2)		
Length, Model, in.	250.000	11.250
Maximum Diameter, in.	260.000	11.700
Flare Angle, deg	25.000	25.000
Flare Length, in.	125.000	5.644
STRAKE (L_{28}) (DRAWING 7121-01268)		
Length, in.	96.400	4.342
Maximum Width, in.	12.000	0.540
Slant Angle, deg	10.250	10.25
SERVICE REACTION CONTROL MOTORS (R_5) (DRAWING 7121-01268)		
Maximum Diameter, Nozzle, in.	5.622	0.253
Length, Nozzle, in.	9.889	0.445
Diameter, Exit, in.	5.622	0.253
Overall Length From Nozzle Exit to Nozzle Exit	31.422	1.414
Overall Width From Nozzle Exit to Nozzle Exit	26.644	1.199
Maximum Height, in.	10.978	0.494

~~CONFIDENTIAL~~

~~CONFIDENTIAL~~Table 2. Thermocouple Dimensional Location - H₂ (C₂)

T/C No.	s/r'	Thickness (ft)	T/C No.	s/r'	Thickness (ft)
1	0	0.00300	41	1.140	0.00320
2	0.401	0.00356	42	1.083	0.00349
3	0.819	0.00320	43	1.140	0.00320
4	0.883	0.00314	44	1.373	0.00332
5	0.927	0.00296	45	1.772	0.00328
6	0.972	0.00296	46	2.115	0.00334
7	1.020	0.00279	47	2.460	0.00325
8	1.083	0.00349	48	1.083	0.00349
9	1.140	0.00326	49	1.140	0.00320
10	1.373	0.00329	50	1.373	0.00332
11	1.772	0.00335	51	1.772	0.00328
12	2.115	0.00337	52	2.115	0.00334
13	2.460	0.00327	53	0.401	0.00360
14	2.880	0.00327	54	0.819	0.00319
15	1.083	0.00349	55	0.927	0.00298
16	1.083	0.00349	56	0.972	0.00296
17	1.083	0.00349	57	1.020	0.00334
18	1.140	0.00320	58	1.083	0.00347
19	1.373	0.00332	59	1.140	0.00325
20	1.772	0.00329	60	1.373	0.00327
21	2.115	0.00334	*61	0.250	0.00350
22	2.460	0.00324	*62	1.701	0.00295
23	1.083	0.00349	*63	0.253	0.00337
24	1.373	0.00328	*64	0.451	0.00342
25	1.772	0.00332	*65	0.653	0.00347
26	2.115	0.00335	*66	0.851	0.00346
27	2.460	0.00329	*67	1.254	0.00320
28	1.083	0.00349	*68	1.371	0.00296
29	1.140	0.00320	*69	1.431	0.00296
30	1.373	0.00332	*70	1.629	0.00348
31	1.772	0.00328	*71	0.251	0.00320
32	2.115	0.00334	*72	1.083	0.00279
33	2.460	0.00325	*73	1.280	0.00348
34	1.083	0.00349	*74	0.254	0.00312
35	1.140	0.00320	*75	0.484	0.00296
36	1.373	0.00332	*76	0.823	0.00349
37	1.772	0.00328	*77	0.145	0.00304
38	2.115	0.00334	*78	0.290	0.00298
39	2.460	0.00325	*79	0.422	0.00297
40	1.083	0.00349	*80	0.504	0.00297

~~CONFIDENTIAL~~

~~CONFIDENTIAL~~Table 2. Thermocouple Dimensional Location - H_2 (C_2) (Cont)

T/C No.	s/r'	Thickness (ft)	T/C No.	s/r'	Thickness (ft)
*81	0.603	0.00349	408	2.367	0.00165
*82	0.416	0.00349	409	2.310	0.00165
			410	2.252	0.00164
401	2.435	0.00168	411	2.194	0.00167
402	2.310	0.00165	412	2.136	0.00167
403	2.194	0.00167	413	2.079	0.00167
404	2.079	0.00167	414	2.021	0.00167
405	1.829	0.00167	415	1.963	0.00168
406	1.713	0.00168	416	2.310	0.00164
407	1.597	0.00171	417	1.828	0.00168

 $r' = 3.465$

*s Value measured from T/C No. 4.

~~CONFIDENTIAL~~

Table 3. Thermocouple Dimensional Location - H_2 (C_2 S_2)

T/C No.	s/r'	Thickness (ft)	T/C No.	s/r'	Thickness (ft)
1	0	0.00328	42	0.870	0.00321
2	0.1157	0.00294	43	1.259	0.00327
3	0.250	0.00319	44	1.650	0.00328
4	0.483	0.00321	45	1.772	0.00331
5	0.870	0.00320	46	2.240	0.00337
6	1.259	0.00326	47	3.025	0.00342
7	1.650	0.00325	48	0.870	0.00317
8	1.772	0.00337	49	1.259	0.00326
9	1.920	0.00342	50	1.650	0.00332
10	2.240	0.00345	51	1.772	0.00332
11	2.636	0.00348	52	1.920	0.00339
12	3.025	0.00347	53	2.240	0.00337
13	3.415	0.00347	54	2.636	0.00337
14	0.1157	0.00295	55	3.025	0.00327
15	0.250	0.00321	56	3.415	0.00340
16	0.483	0.00318	57	0.1157	0.00296
17	0.870	0.00321	58	0.250	0.00319
18	1.259	0.00324	59	0.483	0.00321
19	1.650	0.00327	60	0.870	0.00321
20	1.772	0.00339	61	1.259	0.00323
21	0.483	0.00317	62	1.650	0.00324
22	0.870	0.00324	63	1.772	0.00337
23	1.259	0.00325	64	2.240	0.00343
24	1.650	0.00329	65	3.025	0.00344
25	1.772	0.00333	66	0.1157	0.00296
26	1.920	0.00342	67	0.250	0.00310
27	3.025	0.00342	68	0.483	0.00321
28	3.415	0.00342	69	0.870	0.00321
29	0.870	0.00320	70	1.259	0.00327
30	1.259	0.00324	71	1.650	0.00331
31	1.650	0.00327	72	1.772	0.00338
32	1.772	0.00333	73	1.920	0.00340
33	2.240	0.00336	74	2.240	0.00342
34	3.025	0.00337	75	3.025	0.00342
35	1.259	0.00296	76	3.415	0.00343
37	1.250	0.00312	77	2.636	0.00336
38	1.920	0.00338	78	3.025	0.00340
39	2.240	0.00341	79	3.415	0.00341
40	3.025	0.00346	80	2.240	0.00342
41	3.415	0.00343	81	2.636	0.00336

~~CONFIDENTIAL~~Table 3. Thermocouple Dimensional Location - H_2 ($C_2 S_2$) (Cont)

T/C No.	s/r'	Thickness (ft)	T/C No.	s/r'	Thickness (ft)
82	3.025	0.00337	408	0.513	0.00169
83	3.415	0.00340	409	0.570	0.00171
			410	0.628	0.00171
401	0.445	0.00169	411	0.686	0.00171
			412	0.744	0.00171
403	0.636	0.00169	413	0.801	0.00171
404	0.801	0.00169	414	0.859	0.00169
405	1.051	0.00169	415	0.917	0.00170
406	1.167	0.00169	416	0.570	0.00167
407	1.283	0.00172	417	1.052	0.00171

~~CONFIDENTIAL~~

~~CONFIDENTIAL~~

Table 4. Thermocouple Dimensional Location - HL-1B

T/C No.	s/r'	Thickness (ft)	T/C No.	s/r'	Thickness (ft)
1	0.411	0.00342	49	1.307	0.00337
2	0.711	0.00342	50	1.641	0.00339
3	1.307	0.00342	51	1.772	0.00342
4	1.641	0.00342	52	2.466	0.00342
5	1.772	0.00358	53	3.009	0.00333
6	2.466	0.00337	54	3.393	0.00329
7	3.009	0.00336	55	3.777	0.00323
8	3.393	0.00333	56	0.411	0.00314
9	3.777	0.00333	57	0.711	0.00327
10	5.323	0.00334	58	1.088	0.00335
14	1.088	0.00342	59	1.307	0.00336
15	1.307	0.00342	60	1.641	0.00337
16	1.641	0.00342	61	3.009	0.00332
19	0.411	0.00311	62	3.393	0.00329
20	0.711	0.00326	63	3.777	0.00323
21	1.088	0.00331	64	1.088	0.00342
22	1.307	0.00333	65	1.307	0.00342
23	1.641	0.00328	66	1.641	0.00342
24	3.009	0.00333	69	0.411	0.00342
25	3.393	0.00325	70	0.711	0.00342
26	3.777	0.00327	71	1.307	0.00341
27	0.711	0.00326	72	1.641	0.00342
28	1.088	0.00331	73	3.777	0.00329
29	1.307	0.00336	74	5.323	0.00334
30	1.641	0.00337	77	3.009	0.00339
31	1.772	0.00342	78	3.393	0.00335
32	2.466	0.00337	79	3.777	0.00329
33	3.009	0.00338	80	2.466	0.00343
34	3.393	0.00333	81	3.009	0.00339
35	3.777	0.00319	82	3.393	0.00336
36	1.307	0.00332	83	3.777	0.00333
37	2.466	0.00341	337	7.168	0.00375
38	3.009	0.00333	339	8.113	0.00383
39	3.393	0.00331	340	8.618	0.00375
40	3.777	0.00328	342	7.168	0.00387
41	4.162	0.00321	344	8.113	0.00385
42	4.555	0.00332	347	7.168	0.00375
43	5.323	0.00338	349	8.113	0.00384
47	0.711	0.00329	350	8.618	0.00354
48	1.088	0.00335	352	7.168	0.00366

~~CONFIDENTIAL~~



Table 4. Thermocouple Dimensional Location - HL-1B (Cont)

T/C No.	s/r'	Thickness (ft)	T/C No.	s/r'	Thickness (ft)
354	8.113	0.00383	408	0.513	0.00165
357	7.168	0.00365	409	0.570	0.00168
359	8.113	0.00358	410	0.628	0.00162
			411	0.686	0.00168
401	0.455	0.00169	412	0.744	0.00167
402	0.570	0.00167	413	0.801	0.00169
403	0.686	0.00167	414	0.859	0.00167
404	0.801	0.00168	415	0.917	0.00168
405	1.051	0.00167	416	0.570	0.00156
406	1.167	0.00168	417	1.052	0.00167
407	1.283	0.00171			

$$r' = 3.465$$



Table 5. H-2 and HL-1B Model Run Summary, AEDC Tunnel C, Mach Number 10

Configurations	Group		Angle of Attack (α) (deg)	Angle of Roll (ϕ) (deg)	Angle of Yaw (β) (deg)	Re/in. $\times 10^{-6}$	Plots $q, h/h_0$ vs $s/r, s/r^*$ Page	Remarks
	NAA	AEDC						
E ₄₃ T ₂₇ C ₂ L ₂₈ S ₆ I ₁ B ₈	1	1	0	0	0	0.027	A-6 - A-11	No H/T Data No H/T Data
			0			0.027	A-12 - A-17	
			5			0.027	A-18 - A-23	
			10			0.027	A-24 - A-29	
			15			0.027	A-30 - A-35	
			0			0.027	None	
			10			0.027	None	
			0			0.054	A-36 - A-41	
			0			0.054	A-42 - A-47	
			5			0.054	A-48 - A-53	
			10			0.054	A-54 - A-59	
			15			0.054	A-60 - A-65	
			0			0.083	A-66 - A-71	
			0			0.083	A-72 - A-77	
			0	180		0.083	A-78 - A-83	
			5			0.083	A-84 - A-89	
			10			0.083	A-90 - A-95	
			15			0.083	A-96 - A-101	
			0			0.166	A-102 - A-105	
			0			0.166	A-106 - A-111	
			5			0.166	A-112 - A-117	
			10			0.166	A-118 - A-123	
			15			0.166	A-124 - A-127	
E ₄₃ T ₂₇ C ₂ L ₂₈ S ₆ I ₁ B ₈	1	1	0	0	0	0.027	A-128 - A-131	No H/T Data No H/T Data
			0			0.027	A-132 - A-135	
			0			0.027	A-136 - A-139	
			5			0.027	A-140 - A-143	
			10			0.027	A-144 - A-147	
			15			0.027	A-148 - A-151	
			0			0.027	A-152 - A-155	
			10			0.027	A-156 - A-159	
			15			0.027	A-160 - A-163	
			0			0.027	None	
E ₄₃ T ₂₇ C ₂ L ₂₈ S ₆ I ₁ B ₈	11	11	0			0.027	None	No H/T Data No H/T Data
			10			0.054	A-164 - A-167	
			0			0.054	A-168 - A-171	
			5			0.054	A-172 - A-175	
			10			0.054	A-176 - A-179	
			15			0.054		
			0			0.054		
			5			0.054		
			10			0.054		
			15			0.054		
E ₄₃ T ₂₇ C ₂ L ₂₈ S ₆ I ₁ B ₈	11	11	0	0	0	0.027	A-128 - A-131	No H/T Data No H/T Data
			0			0.027	A-132 - A-135	
			0			0.027	A-136 - A-139	
			5			0.027	A-140 - A-143	
			10			0.027	A-144 - A-147	
			15			0.027	A-148 - A-151	
			0			0.027	A-152 - A-155	
			10			0.027	A-156 - A-159	
			15			0.027	A-160 - A-163	
			0			0.027	None	



Table 5. H-2 and HL-1B Model Run Summary, AEDC Tunnel C, Mach Number 10 (Cont)

Configurations	Group		Angle of Attack (α) (deg)	Angle of Roll (ϕ) (deg)	Angle of Yaw (β) (deg)	Re/in. $\times 10^{-6}$	Plots $q, h/h_0$ vs $s/r, s/r^*$ Page	Remarks
	NAA	AEDC						
$E_{43} T_{27} C_{27} L_{28} S_{28} R_{51} B_8$	11	23	15	0	0	0.054	A-180 - A-183	No H/T Data No H/T Data
			0	0	0	0.083	A-184 - A-187	
$E_{43} T_{27} C_{27} L_{28} S_{28} R_{51} B_8$	11	25	0	0	0	0.083	A-188 - A-191	
		29	0	0	0	0.083	A-192 - A-195	
		26	5	0	0	0.083	A-196 - A-199	
		27	10	0	0	0.083	A-200 - A-203	
		28	15	0	0	0.083	A-204 - A-207	
		41	0	0	0	0.166	A-208 - A-211	
		45	0	0	0	0.166	A-212 - A-215	
		42	5	0	0	0.166	A-216 - A-219	
		43	10	0	0	0.166	A-220 - A-223	
		44	15	0	0	0.166	A-224 - A-229	
$C_{27} L_{28} S_{28}$	2	172	0	0	0	0.027	A-230 - A-235	No H/T Data No H/T Data
		173	5	0	0	0.027	A-236 - A-241	
		174	10	0	0	0.027	A-242 - A-247	
		175	15	0	0	0.027	None	
		176	0	0	0	0.027	None	
		177	10	0	0	0.027	A-248 - A-253	
		160	0	0	0	0.054	A-254 - A-259	
		161	5	0	0	0.054	A-260 - A-265	
		162	10	0	0	0.054	A-266 - A-271	
		163	15	0	0	0.054	A-272 - A-277	
$C_{27} L_{28} S_{28}$	2	156	0	0	0	0.083	A-278 - A-283	No H/T Data No H/T Data
		157	5	0	0	0.083	A-284 - A-289	
		158	10	0	0	0.083	A-290 - A-295	
		159	15	0	0	0.083	A-296 - A-301	
		168	0	0	0	0.027	A-302 - A-307	
		169	5	0	0	0.027	A-308 - A-313	
		170	10	0	0	0.027	A-314 - A-319	
		171	15	0	0	0.027	None	
		178	0	0	0	0.027	None	
		179	10	0	0	0.027	A-320 - A-325	
$C_{27} L_{28} S_{28} R_5$	21	164	0	0	0	0.054	A-326 - A-331	No H/T Data No H/T Data
		165	5	0	0	0.054	A-332 - A-337	
		166	10	0	0	0.054	A-338 - A-343	
		167	15	0	0	0.054	A-344 - A-349	
		152	0	0	0	0.083	A-350 - A-355	
		153	5	0	0	0.083	A-356 - A-361	
		154	10	0	0	0.083	A-362 - A-367	
		155	15	0	0	0.083		
$C_{27} L_{28} S_{28} R_5$	21							



Table 5. H-2 and HL-1B Model Run Summary, AEDC Tunnel C, Mach Number 10 (Cont)

Configurations	AEDC	Group Number	Angle of Attack (α) (deg)	Angle of Roll (ϕ) (deg)	Angle of Yaw (β) (deg)	Re/in. $\times 10^{-6}$	Plots $q, h/h_0$ vs $s/r, s/r^*$ Page	Remarks
$C_2 L_{28} S_2^{+t} r$	22	127	0	0	0	0.027	A-368 - A-373	No H/T Data
		128	5	0	0	0.027	A-374 - A-379	
		129	10	0	0	0.027	A-380 - A-385	
		130	15	0	0	0.027	A-386 - A-391	
		139	0	0	0	0.054	A-392 - A-397	
		140	5	0	0	0.054	A-398 - A-403	
		141	10	0	0	0.054	A-404 - A-409	
		142	15	0	0	0.054	A-410 - A-415	
		143	0	0	0	0.083	A-416 - A-421	
		144	5	0	0	0.083	A-422 - A-427	
		145	10	0	0	0.083	A-428 - A-433	
		146	15	0	0	0.083	A-434 - A-439	
		131	0	0	0	0.027	A-440 - A-443	
		132	5	0	0	0.027	A-444 - A-447	
		133	10	0	0	0.027	A-448 - A-451	
		134	15	0	0	0.027	A-452 - A-455	
$C_2 L_{28} S_2 R_5^{+t} r$	23	135	0	0	0	0.054	A-456 - A-459	No H/T Data
		136	5	0	0	0.054	A-460 - A-463	
		137	10	0	0	0.054	A-464 - A-467	
		138	15	0	0	0.054	A-468 - A-471	
		147	0	0	0	0.083	A-472 - A-475	
		148	5	0	0	0.083	A-476 - A-479	
		149	10	0	0	0.083	A-480 - A-483	
		150	15	0	0	0.083	A-484 - A-487	
		151	15	0	0	0.083	None	
		99	180	0	0	0.027	A-494 - A-499	
		100	168	0	0	0.027	A-500 - A-505	
		85	151	0	0	0.027	A-506 - A-511	
		109	151	180	0	0.027	A-512 - A-519	
		86	149	0	0	0.027	A-520 - A-525	
		110	149	180	0	0.027	A-526 - A-533	
		87	147	0	0	0.027	A-534 - A-539	
$C_2 L_{28}$	30	111	147	180	0	0.027	A-540 - A-547	No H/T Data
		91	147	0	5	0.027	A-548 - A-553	
		113	147	0	10	0.027	A-554 - A-559	
		93	147	180	0	0.027	None	
		88	145	0	0	0.027	None	
		30	145	0	0	0.027	A-560 - A-565	



CONFIDENTIAL

Table 5. H-2 and HL-1B Model Run Summary, AEDC Tunnel C, Mach Number 10 (Cont)

Configuration	AEDC	Group Number	Angle of Attack (α) (deg)	Angle of Roll (θ) (deg)	Angle of Yaw (μ) (deg)	Re/in. $\times 10^{-6}$	Plots $q, h/h_0$ vs $s/r, s/r^*$ Page	Remarks
$C_2 L_{28}$	30	112	145	180	0	0.027	A-566 - A-573	
		89	143	0		0.027	A-574 - A-579	
		90	130	0		0.027	A-580 - A-585	
		97	180	0		0.083	A-586 - A-591	
		98	168	0		0.083	A-592 - A-597	
		77	151	0		0.083	A-598 - A-603	
		105	151	180		0.083	A-604 - A-609	
		78	149	0		0.083	A-610 - A-615	
		106	149	180		0.083	A-616 - A-621	
		79	147	0		0.083	A-622 - A-627	
		107	147	180	0	0.083	A-628 - A-633	
		83	147	0	5	0.083	A-634 - A-639	
		84	147	0	10	0.083	A-640 - A-645	
		80	145	0	0	0.083	A-646 - A-651	
		108	145	180		0.083	A-652 - A-659	
		81	143	0		0.083	A-660 - A-665	
		82	130	0		0.083	A-666 - A-671	
		94	180	0		0.200	A-672 - A-679	
		95	180	0		0.200	A-680 - A-685	
		96	168	0		0.200	A-686 - A-693	
		69	151	0		0.200	A-694 - A-701	
		101	151	180		0.200	A-702 - A-709	
		70	149	0		0.200	A-710 - A-717	
		102	149	180		0.200	A-718 - A-725	
		71	147	0		0.200	A-726 - A-733	
		103	147	180	0	0.200	A-734 - A-741	
		75	147	0	5	0.200	A-742 - A-747	
		76	147	0	10	0.200	A-748 - A-753	
		72	145	0	0	0.200	A-754 - A-761	
		104	145	180	0	0.200	A-762 - A-769	
		73	143	0	0	0.200	None	No H/T Data
		74	130	0	0	0.200	A-770 - A-775	No H/T Data
$C_2 L_{28}^{+t} r_{15}$	31	53	160	0	0	0.083	A-776 - A-783	
		53a	160	0		0.083	None	No H/T Data
		52	157	0		0.083	A-784 - A-791	
		51	153	0		0.083	A-792 - A-799	
		65	151	180		0.083	A-800 - A-805	
		50	149	180		0.083	A-806 - A-813	
$C_2 L_{28}^{+t} r_{15}$	31	54	149	180		0.083	A-814 - A-821	
		66	147	180	0	0.083	A-822 - A-829	

CONFIDENTIAL



Table 5. H-2 and HL-1B Model Run Summary, AEDC Tunnel C, Mach Number 10 (Cont)

Configuration	AEDC	Group Number	Angle of Attack (α) (deg)	Angle of Roll (θ) (deg)	Angle of Yaw (β) (deg)	Re/in. $\times 10^{-6}$	Plots q, h/h ₀ vs s/r, s/r*	Remarks
C ₂ L ₂₈ ⁺⁺ r ₁₅	31	67	143	180	0	0.083	A-830 - A-837	No H/T Data
		68	140	180	0	0.083	A-838 - A-845	
		57	157	180	0	0.166	A-846 - A-853	
		56	153	180	0	0.166	A-854 - A-861	
		61	151	180	0	0.166	A-862 - A-869	
		55	149	180	0	0.166	A-870 - A-877	
		60	147	180	0	0.166	A-878 - A-885	
		64	147	180	0	0.166	A-886 - A-893	
		63	145	180	0	0.166	A-894 - A-901	
		59	143	180	0	0.166	A-902 - A-909	
		62	143	180	0	0.166	A-910 - A-917	
		58	140	180	0	0.166	A-918 - A-925	
		114	151	180	0	0.027	A-926 - A-931	
		115	149	180	0	0.027	A-932 - A-937	
		116	147	180	0	0.027	A-938 - A-943	
C ₂ L ₂₈ ⁺⁺ r ₁₅	32	118	147	180	0	0.027	None	No H/T Data
		117	145	180	0	0.027	A-944 - A-949	
		119	151	180	0	0.086	A-950 - A-955	
		120	149	180	0	0.086	A-956 - A-961	
		121	147	180	0	0.086	A-962 - A-967	
		122	145	180	0	0.086	A-968 - A-973	
		123	151	180	0	0.200	A-974 - A-979	
		124	149	180	0	0.200	A-980 - A-985	
		125	147	180	0	0.200	A-986 - A-991	
		126	147	180	0	0.200	A-992 - A-997	

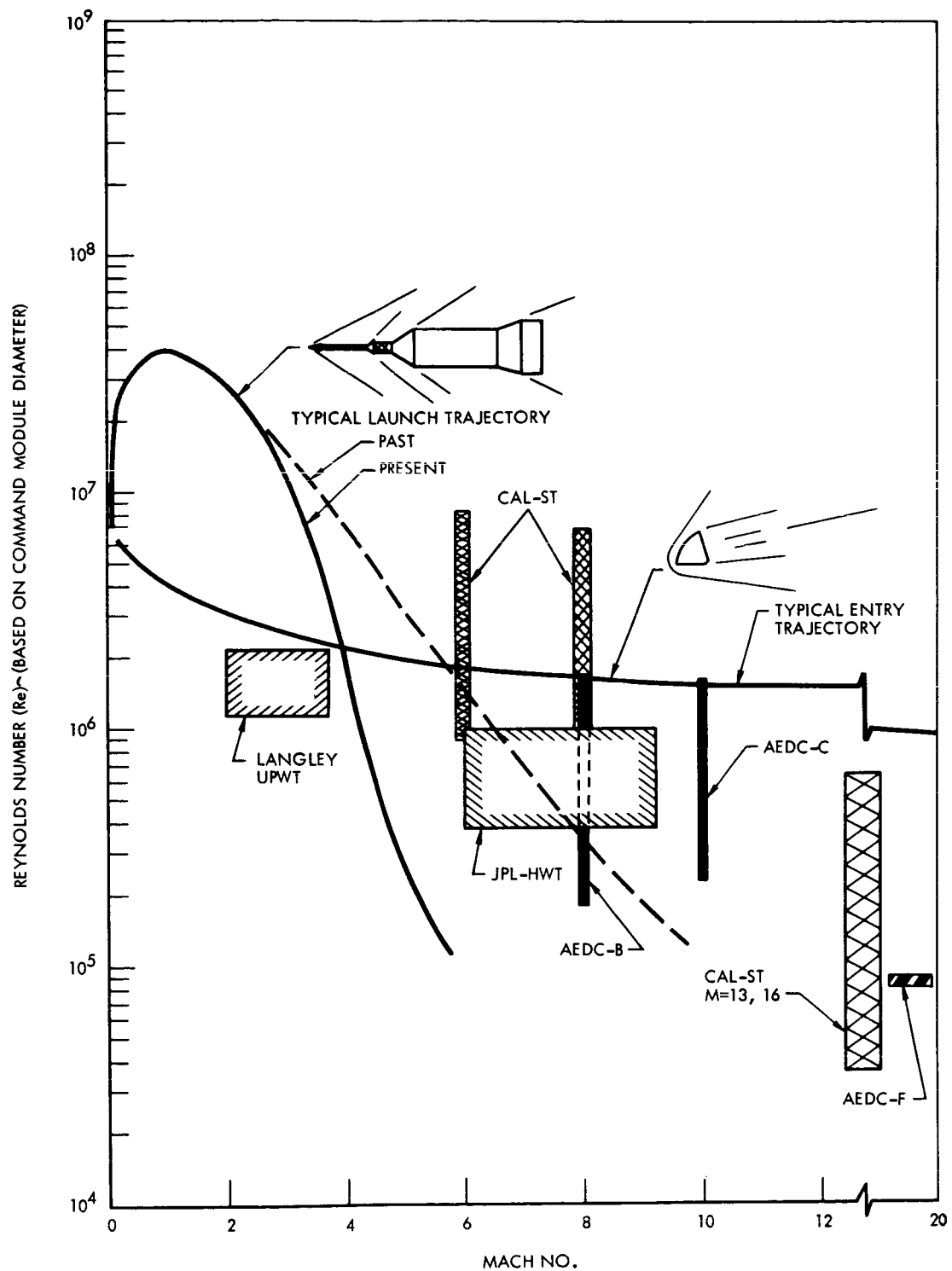
~~CONFIDENTIAL~~

Figure 1. Typical Launch and Entry Trajectories

~~CONFIDENTIAL~~

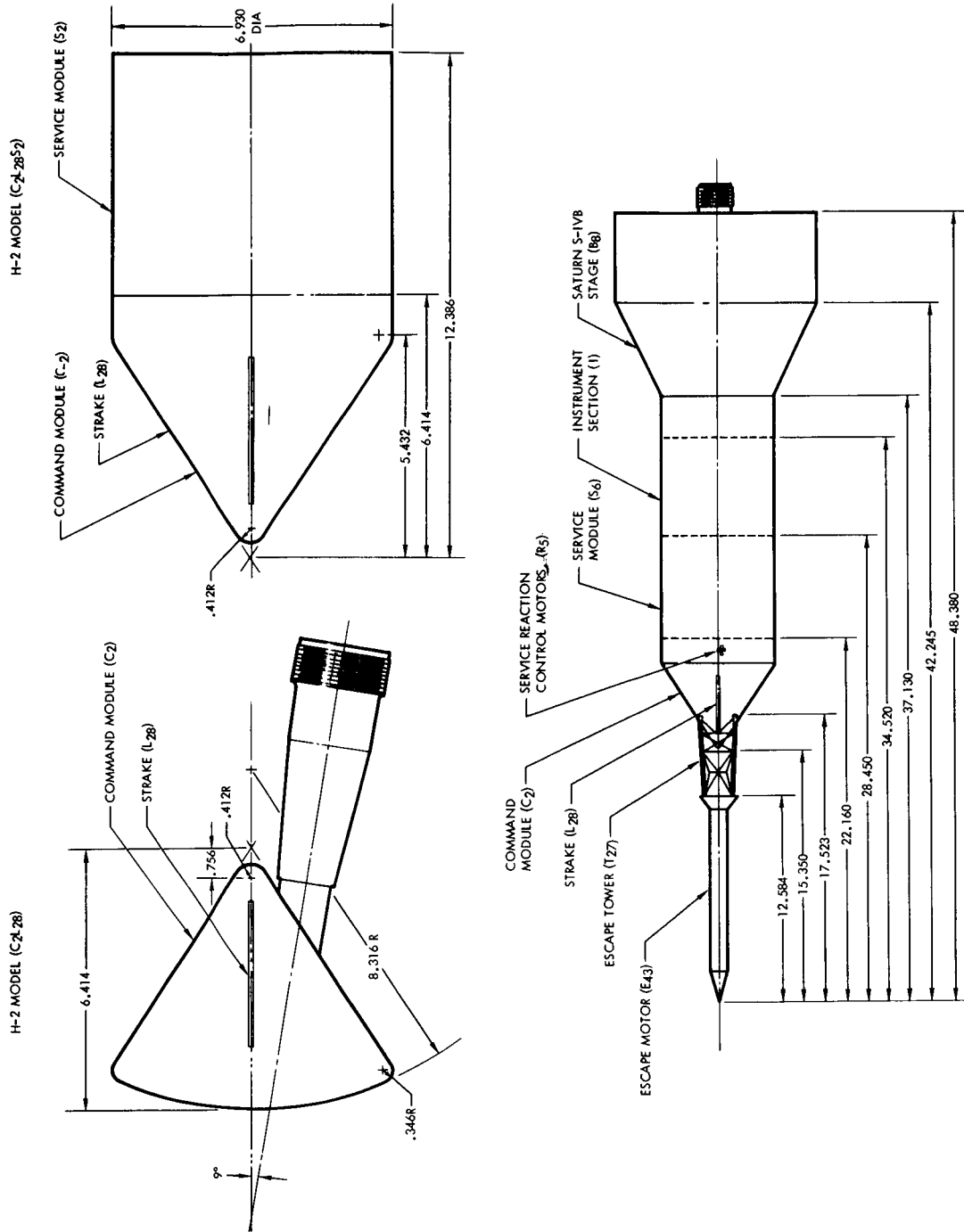
~~CONFIDENTIAL~~

Figure 2. Basic Dimension Sketch of Models

~~CONFIDENTIAL~~

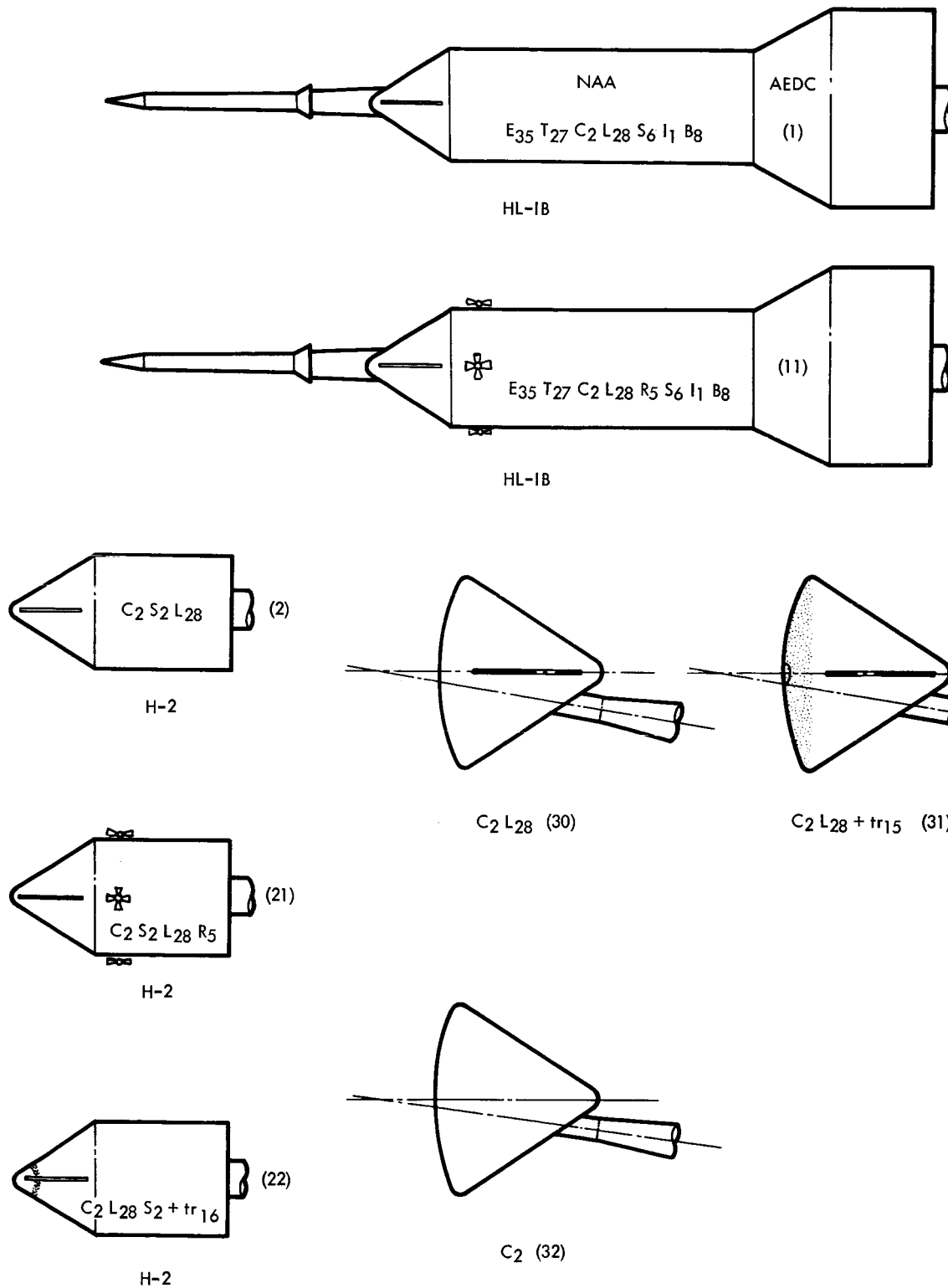
~~CONFIDENTIAL~~

Figure 3. Configuration Tested with NAA and AEDC Designations

~~CONFIDENTIAL~~

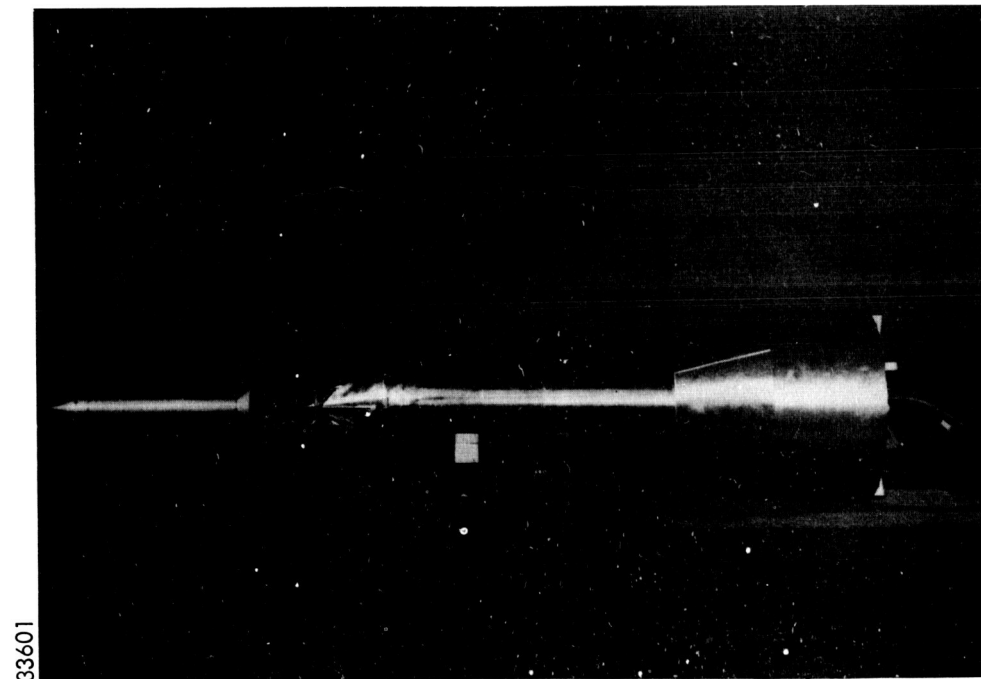
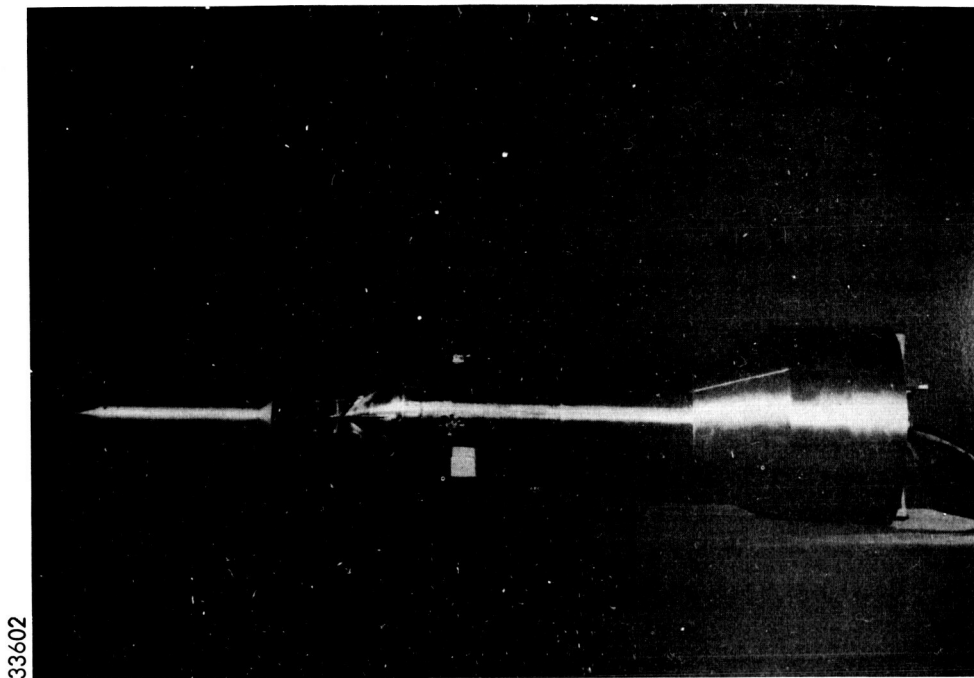
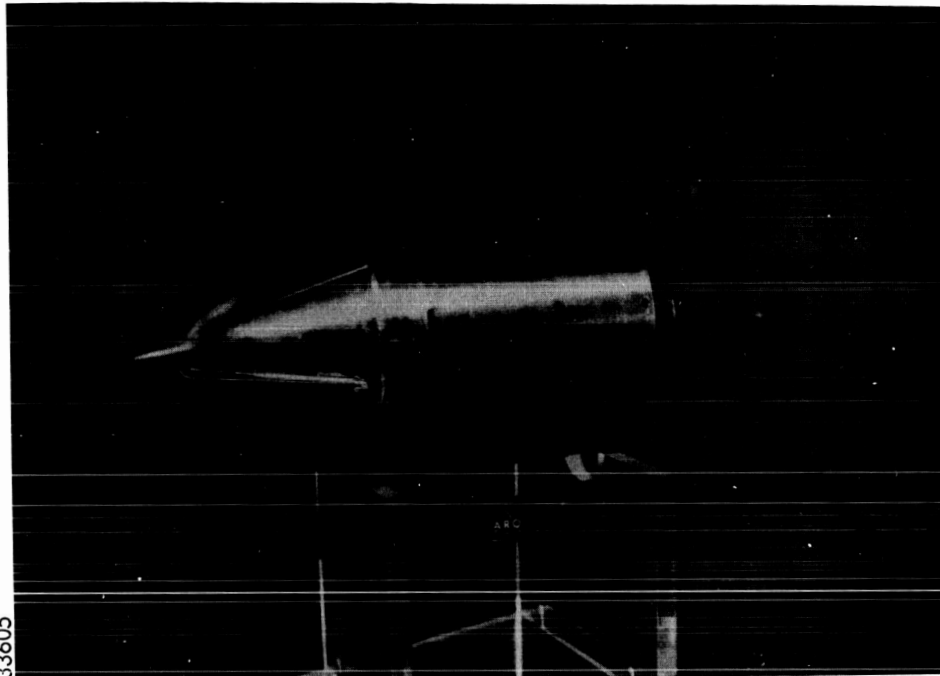
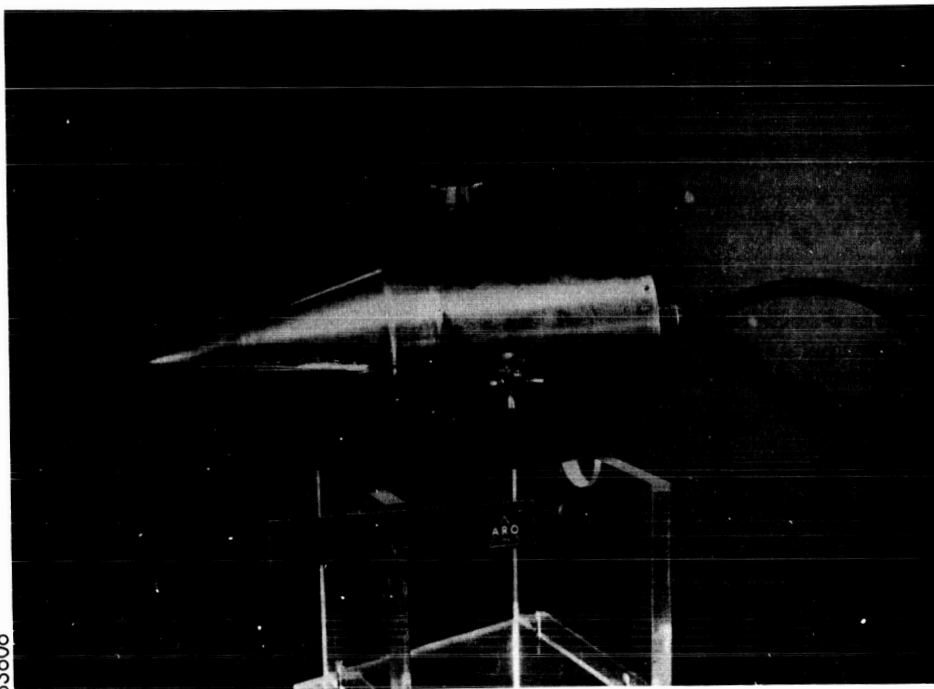
~~CONFIDENTIAL~~

Figure 4. Photos of Launch Configuration With and Without Service Module Reaction Control Motors (E43T27C2L28R5S6I1B8)

~~CONFIDENTIAL~~

~~CONFIDENTIAL~~

33605



33606

Figure 5. Photos of Command-Service Module Shown With Strakes and With and Without Service Module Reaction Control Motors (C₂L₂₈S₂R₅)

~~CONFIDENTIAL~~

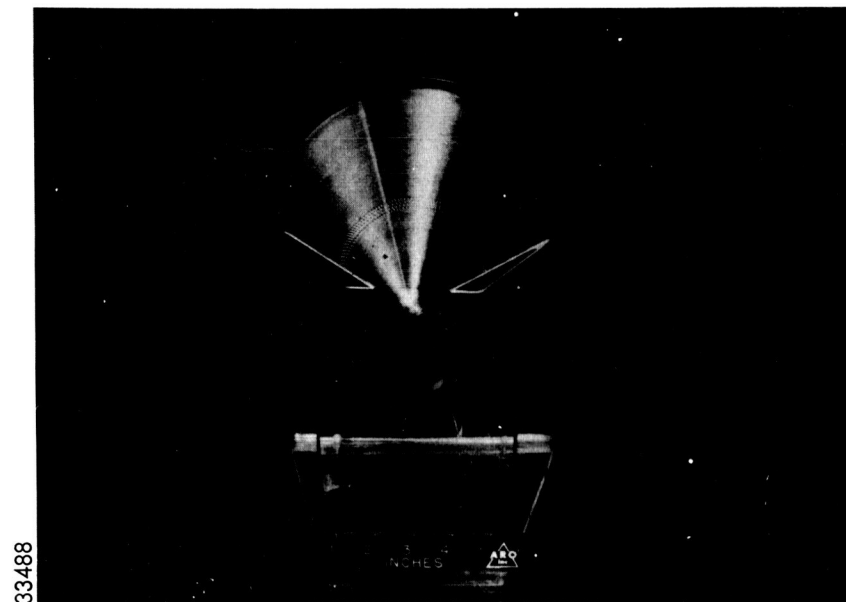
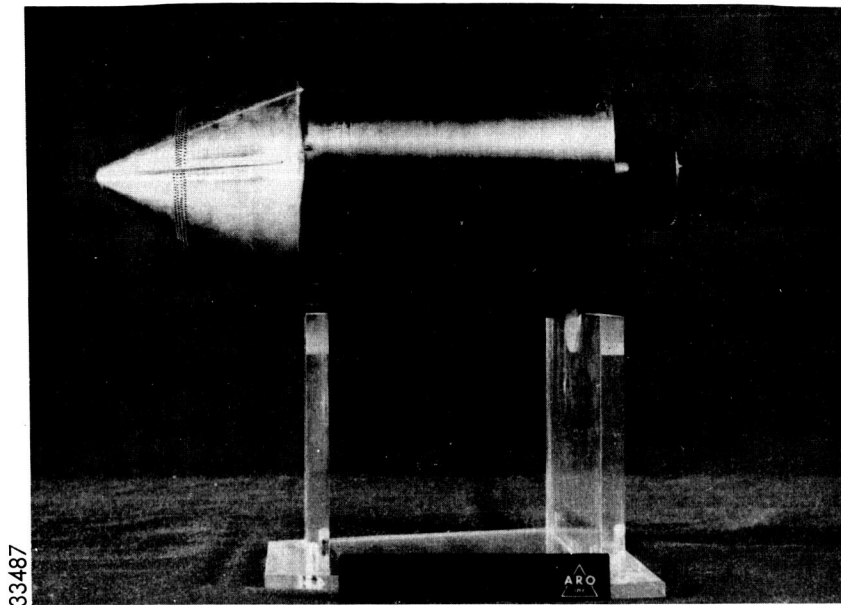
~~CONFIDENTIAL~~

Figure 6. Photos of Command-Service Module With Boundary Layer Trip (C2L28S2+t_R16)

~~CONFIDENTIAL~~

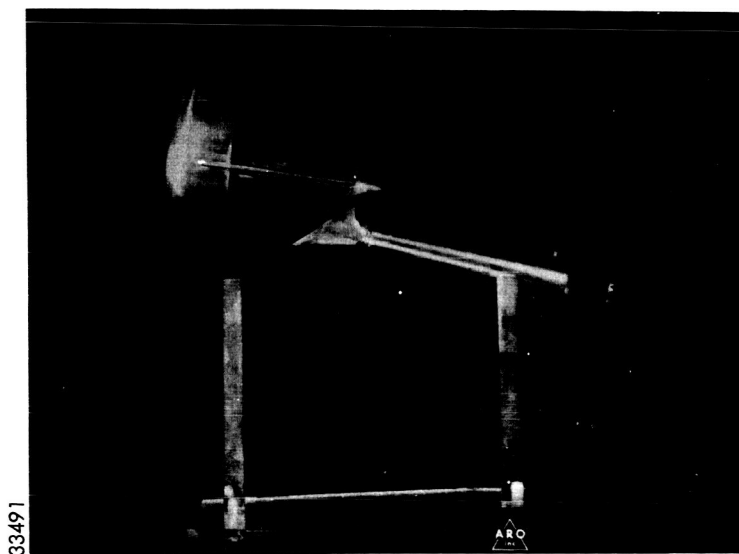
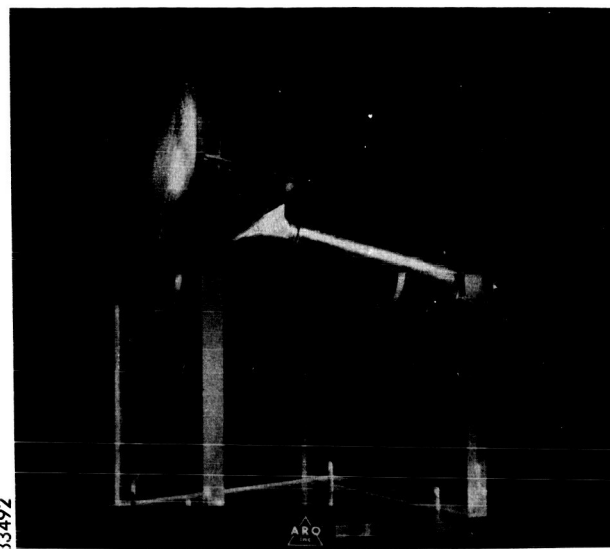
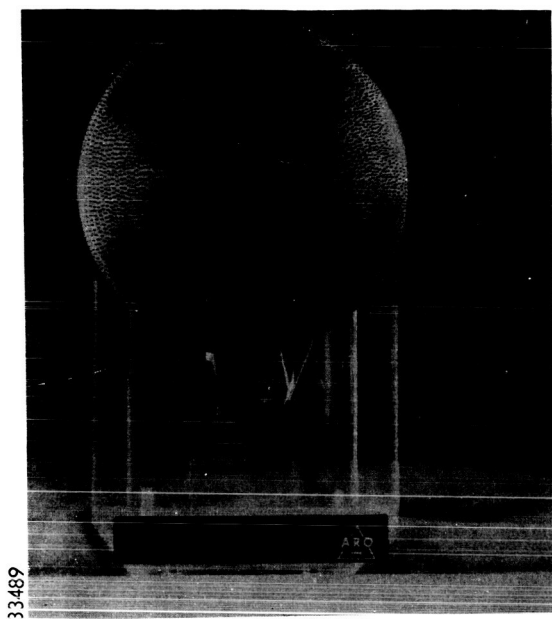
~~CONFIDENTIAL~~

Figure 7. Photos of Entry Configuration With Strakes and Steel Balls Mounted on Entry Face to Simulate Roughness (C2L28+t_{r15})

~~CONFIDENTIAL~~

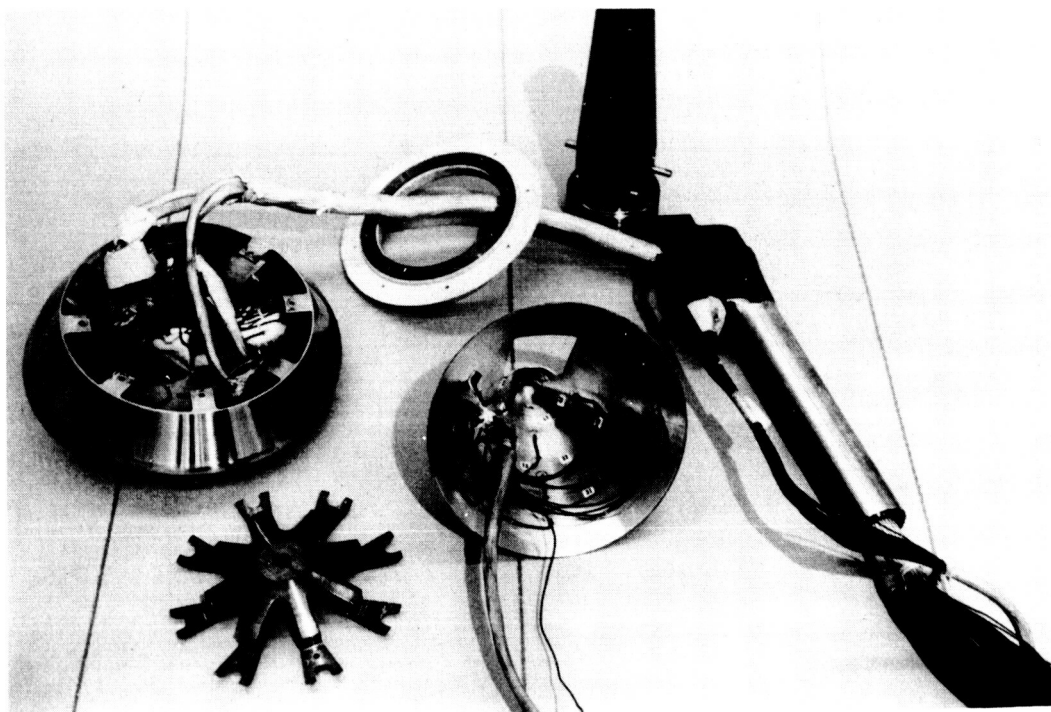
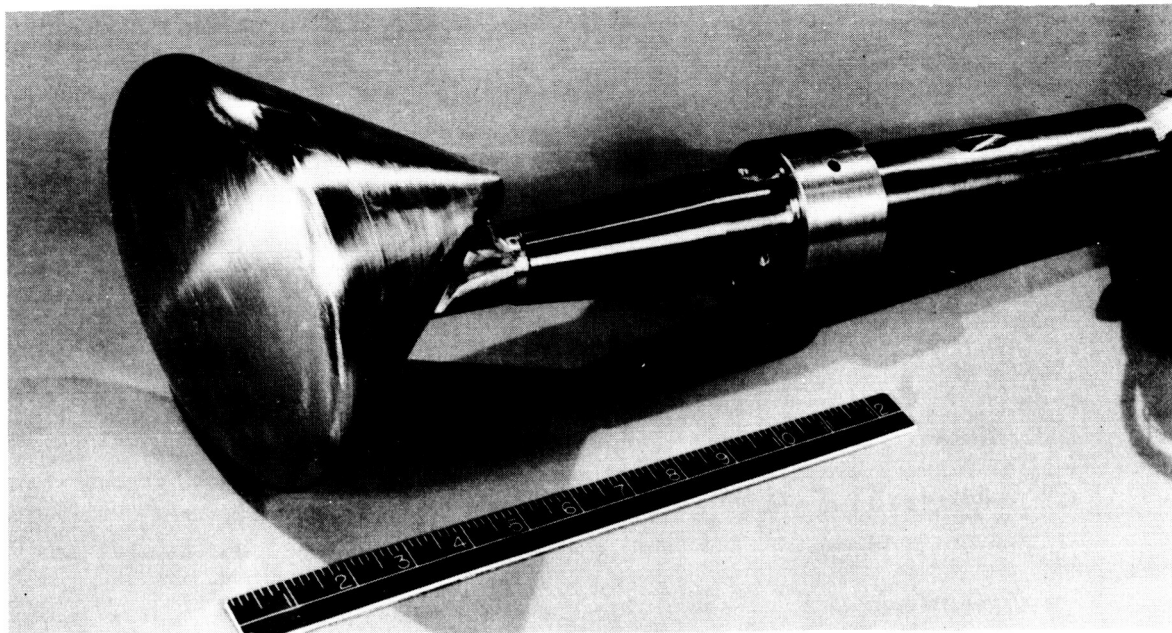
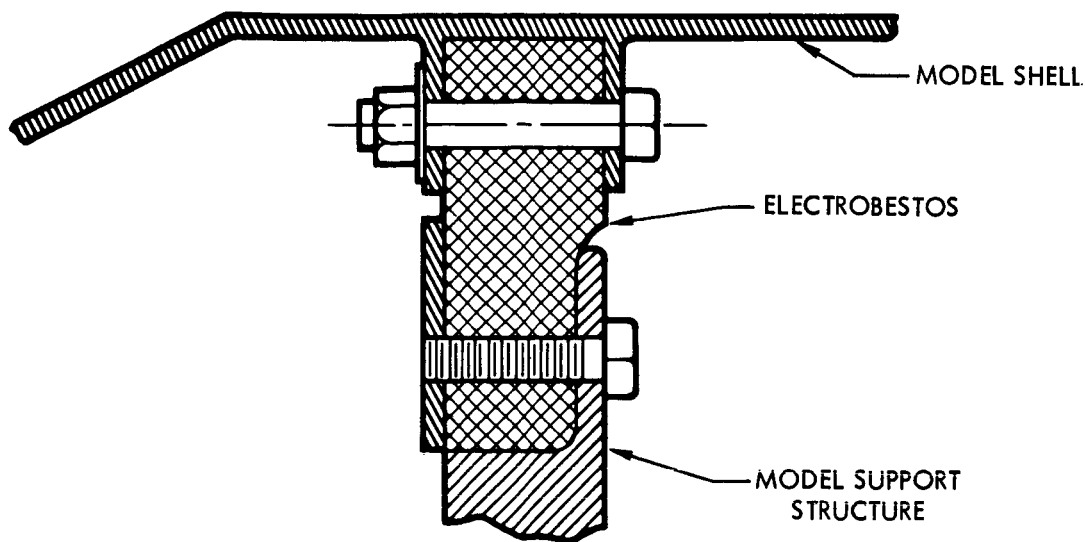
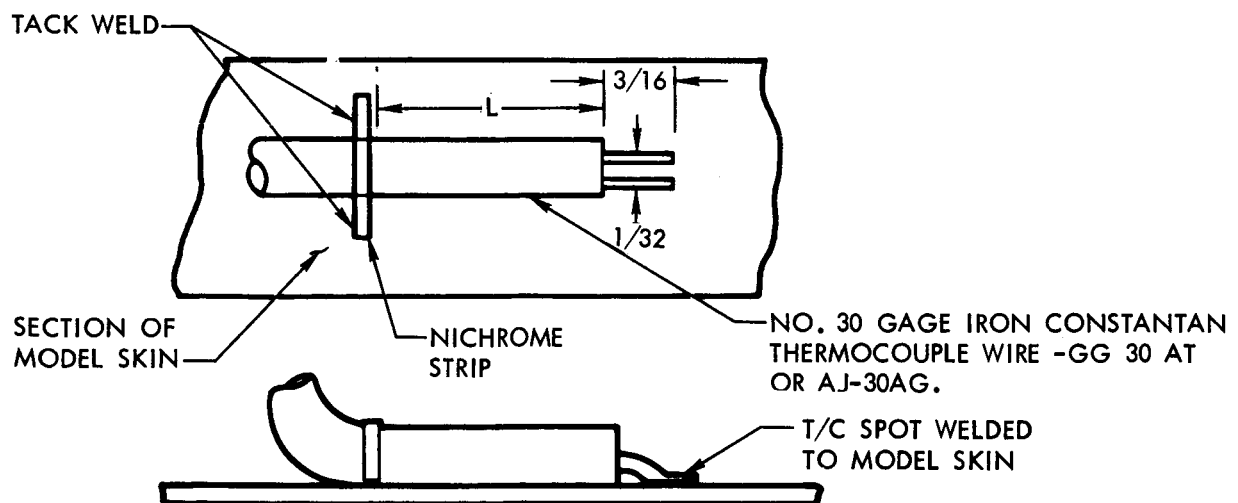
~~CONFIDENTIAL~~

Figure 8. Photos of Entry Configuration (C₂) With Sting Attachment

~~CONFIDENTIAL~~

~~CONFIDENTIAL~~

TYPICAL MODEL SHELL SUPPORT



L-THE THERMOCOUPLE LEAD IS BROUGHT AWAY FROM THE JUNCTION PARALLEL TO THE SKIN FOR A DISTANCE OF AT LEAST 0.50 IN.

Figure 9. Thermocouple Installation in Models

~~CONFIDENTIAL~~

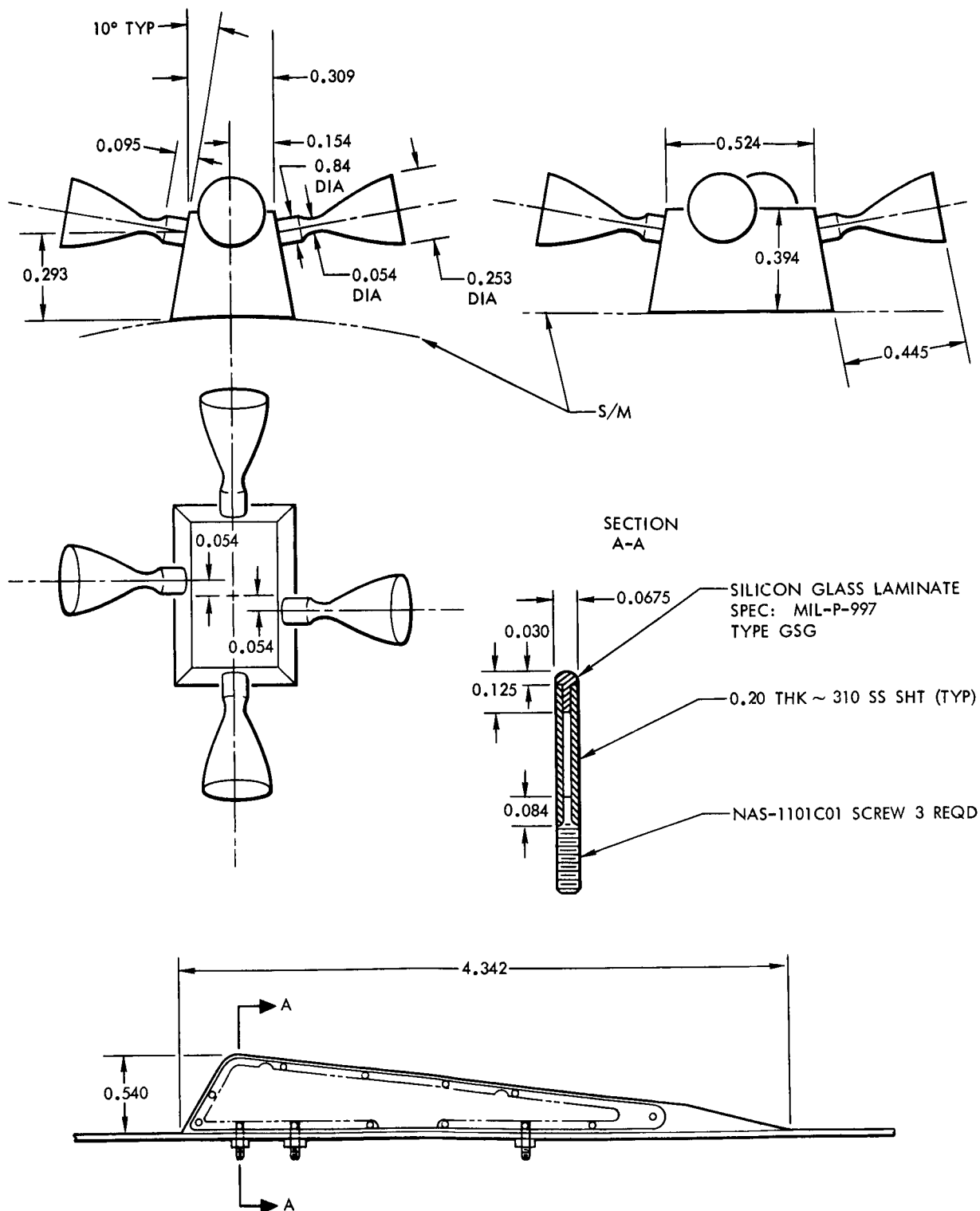


Figure 10. Basic Dimensions of the Strake and Service Module Reaction Control Motors



~~CONFIDENTIAL~~

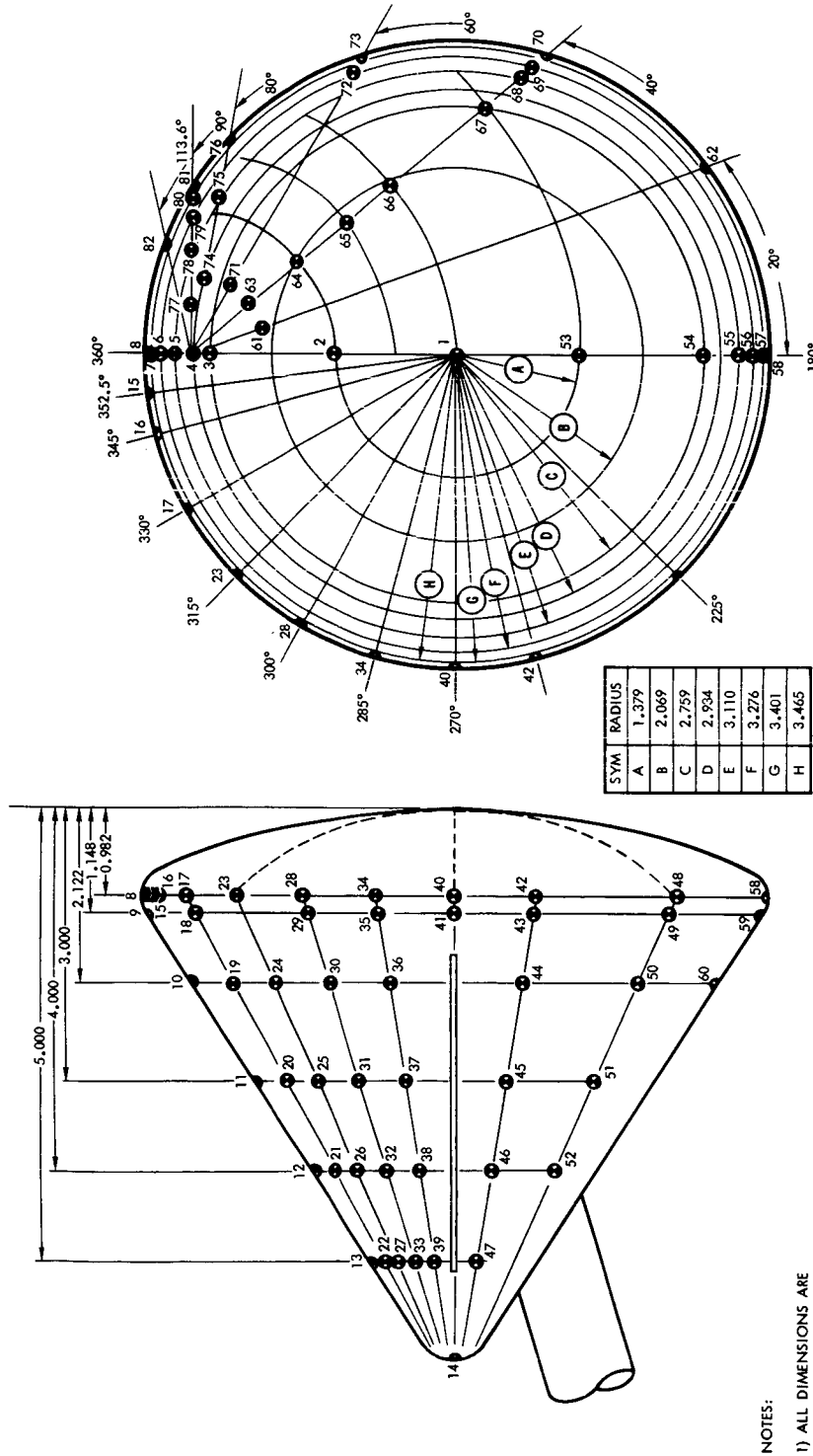


Figure 11. Thermocouple Location on Command Module Configuration (C2)

~~CONFIDENTIAL~~

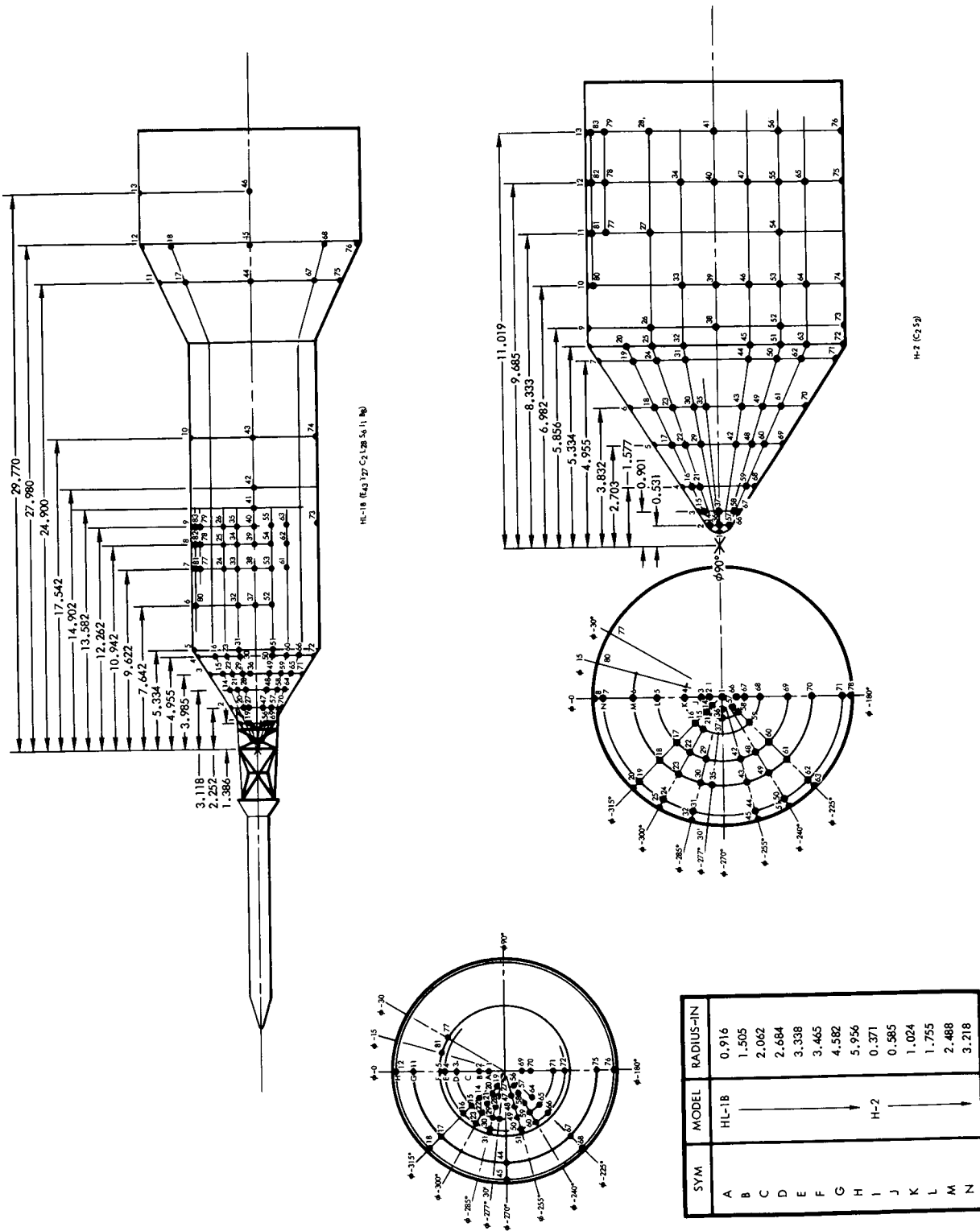
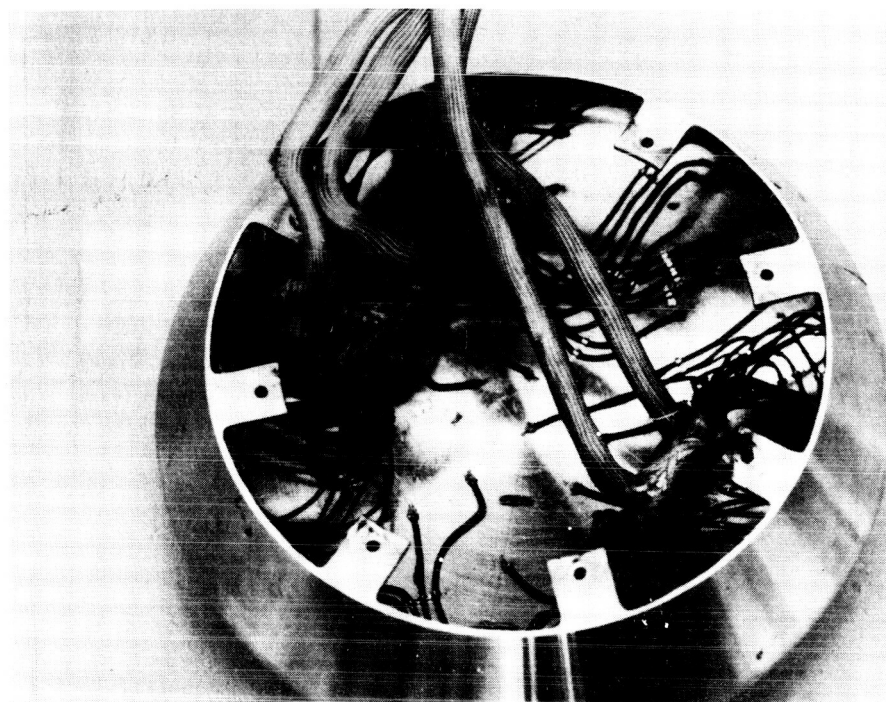
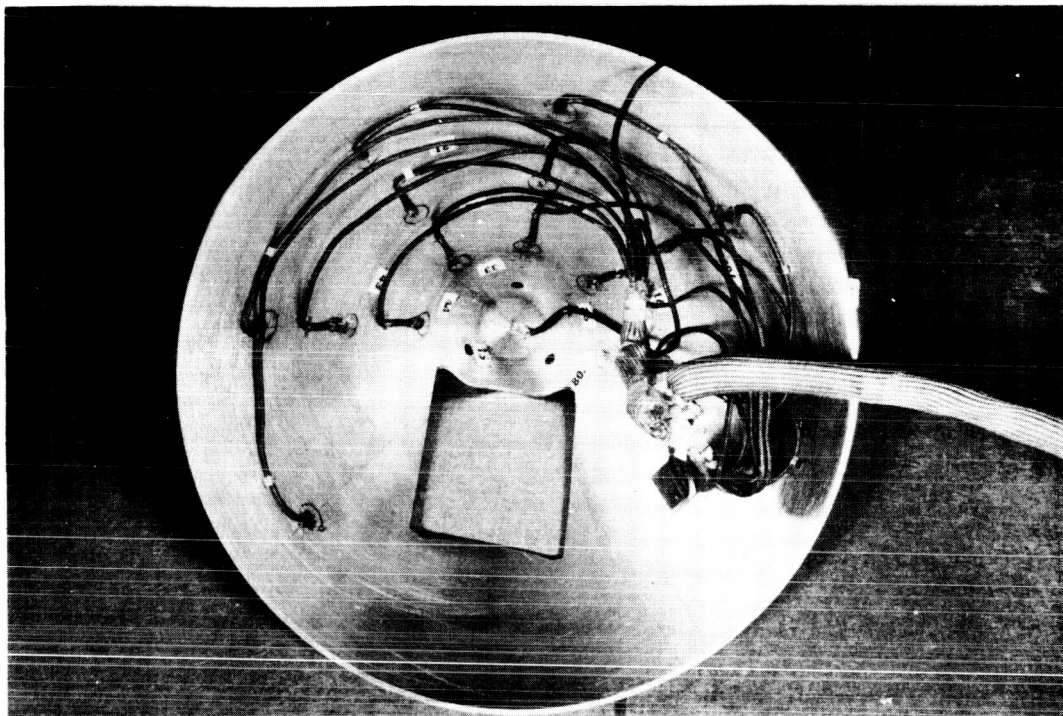


Figure 12. Thermocouple Locations on Launch Configuration HL-1B (E43 T27 C2 L28 S6 I1 B8) and Command-Service Module Configuration H-2 (C2 S2)

~~CONFIDENTIAL~~

700-98-104

Figure 13. Photos of Instrumentation Entry Configuration (C₂)

~~CONFIDENTIAL~~

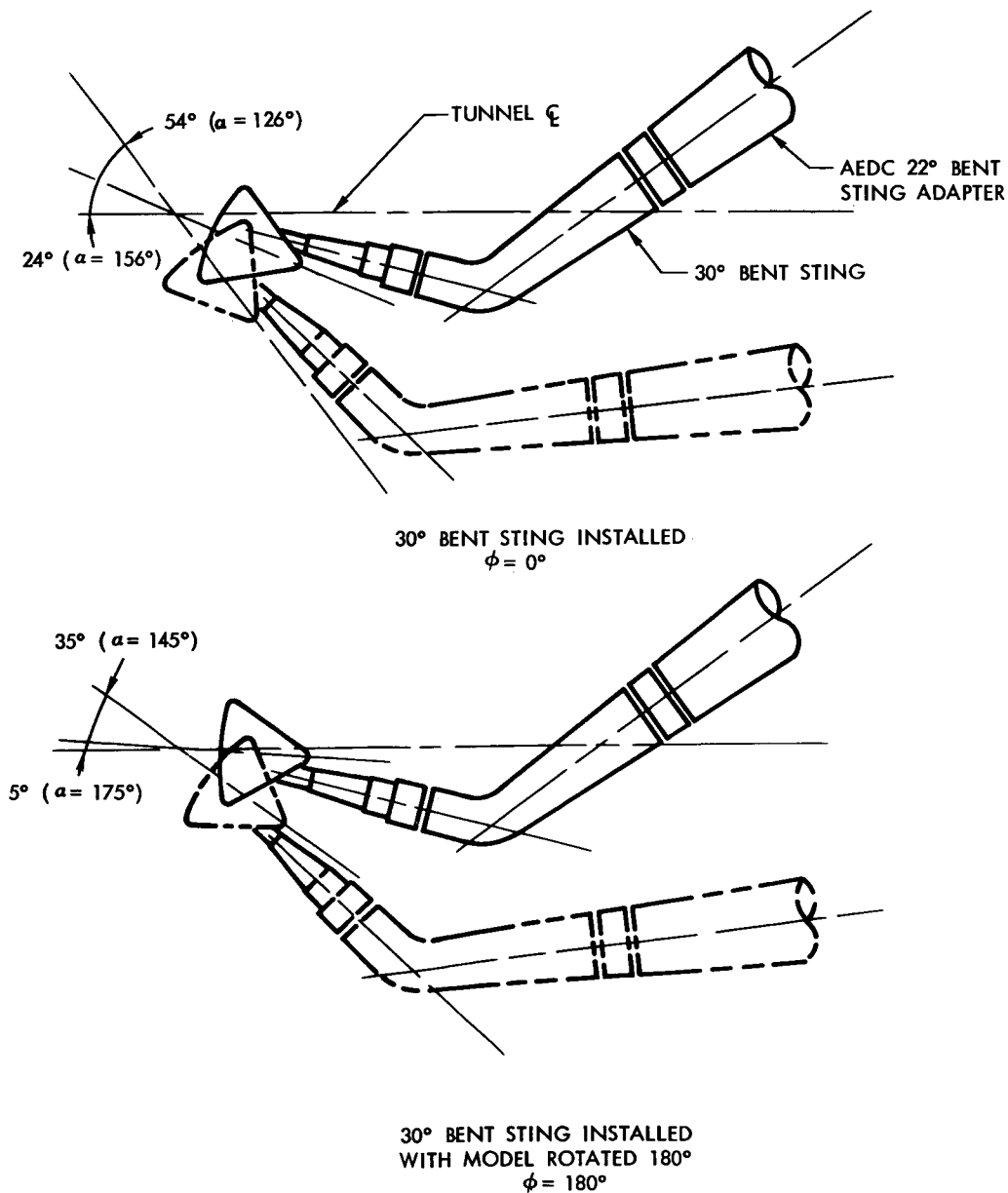
~~CONFIDENTIAL~~

Figure 14. Sting Arrangement and Angle-of-Attack Range for the Entry Configuration (C₂)

~~CONFIDENTIAL~~

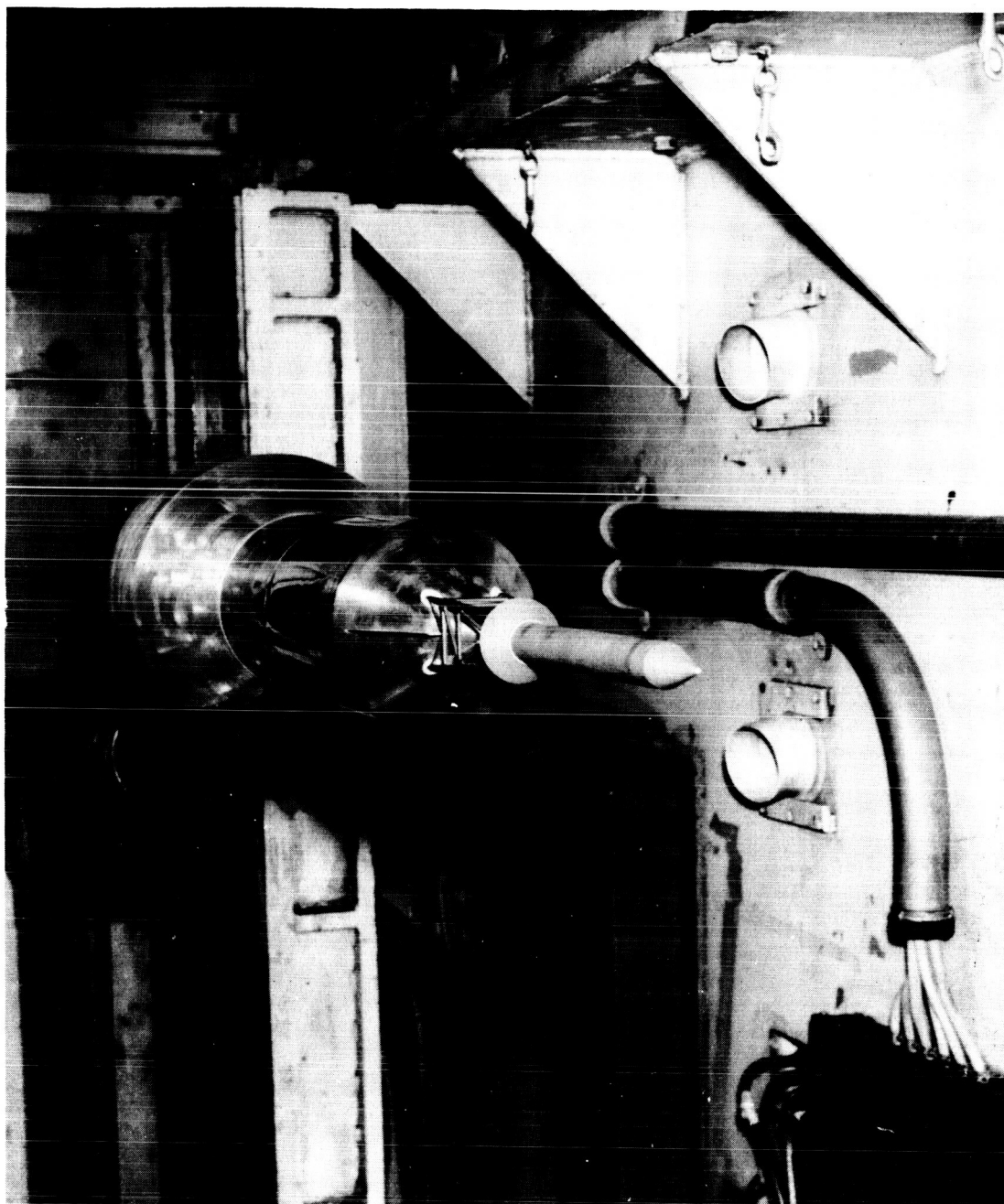
~~CONFIDENTIAL~~

Figure 15. Photos of Launch Configuration Installed
in Tunnel (E₄₃T₂₇C₂L₂₈S₆I₁B₈)

~~CONFIDENTIAL~~



~~CONFIDENTIAL~~

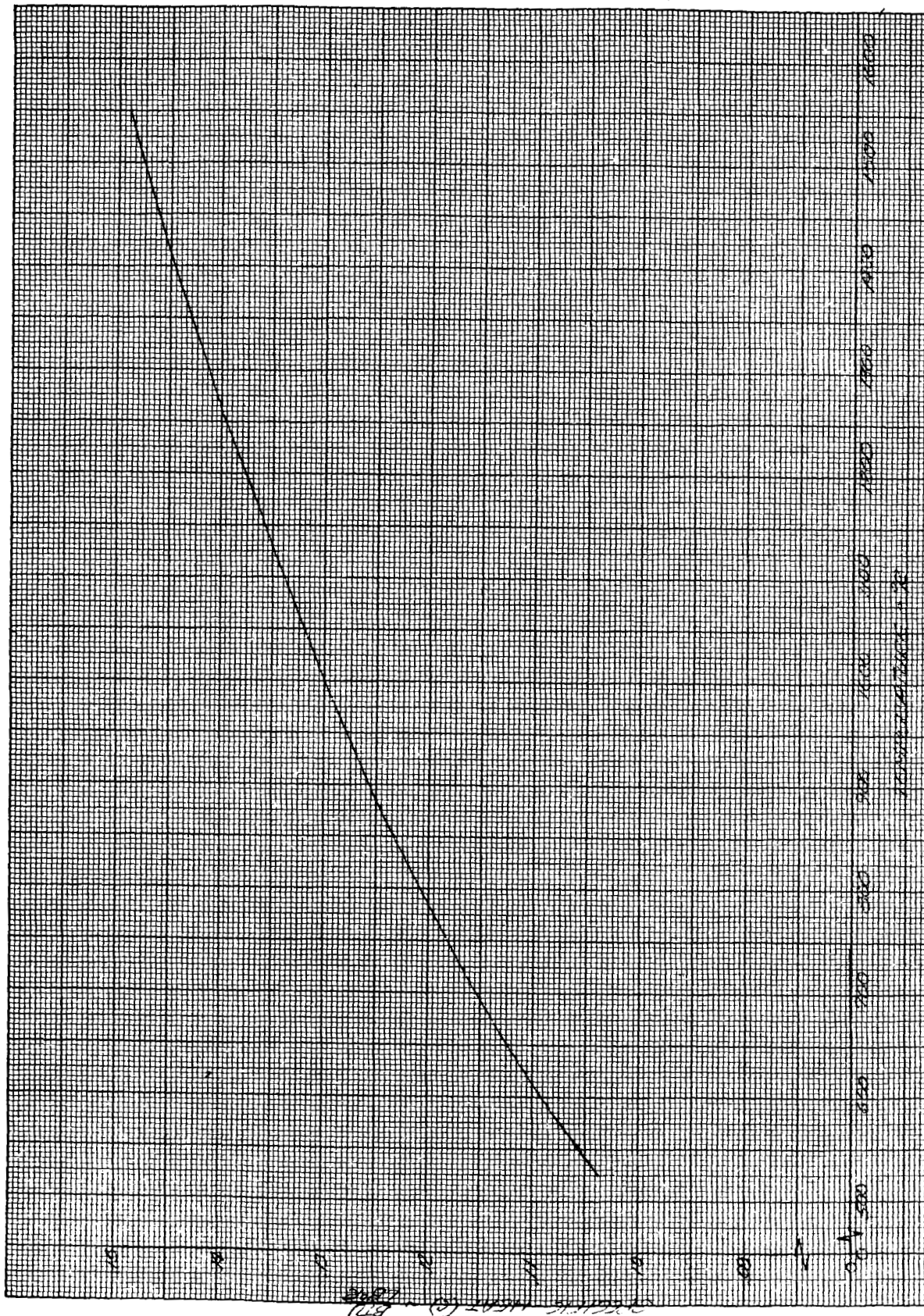


Figure 16. Specific Heat of 310 Stainless Steel Versus Temperature

~~CONFIDENTIAL~~

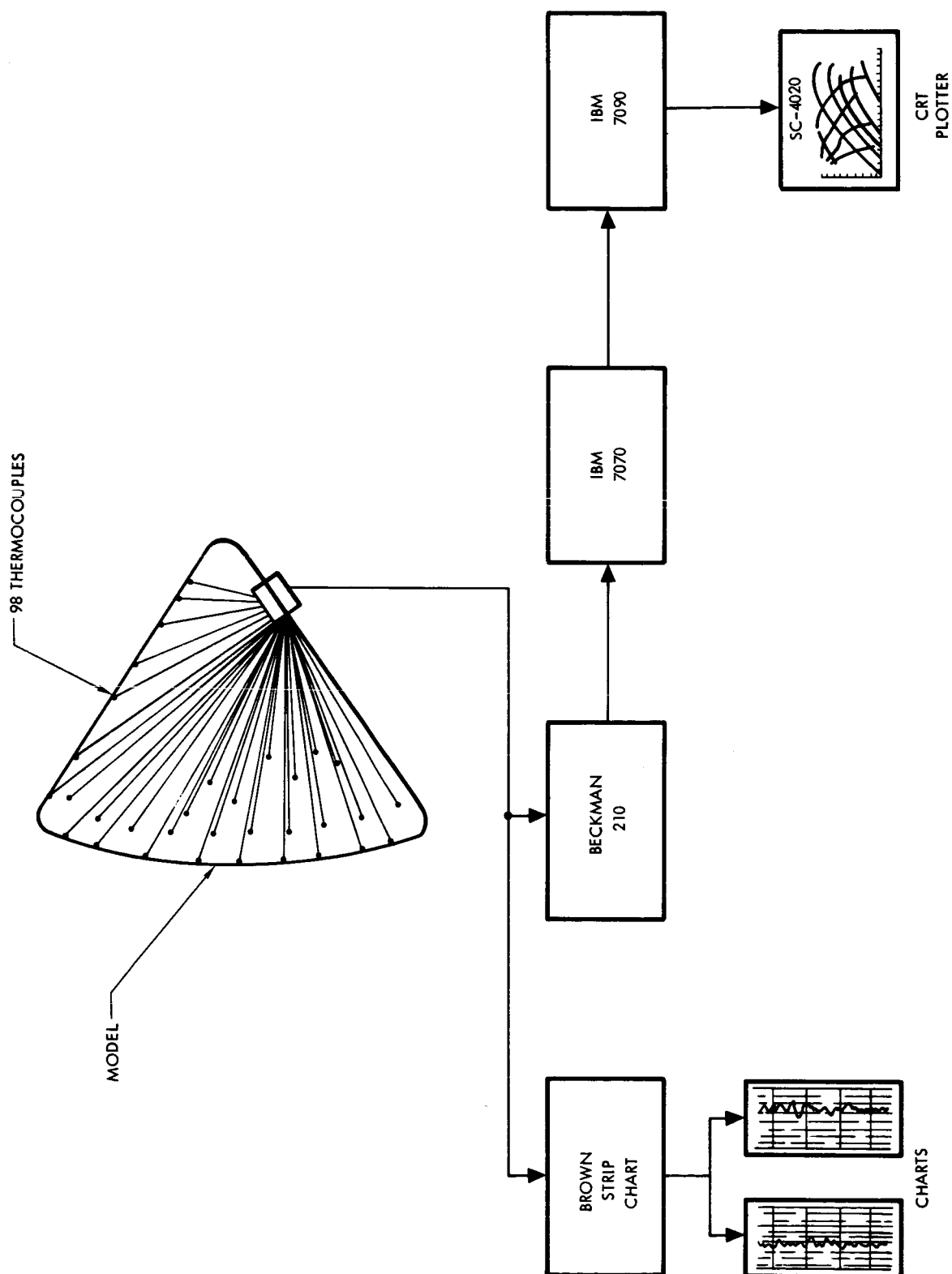
~~CONFIDENTIAL~~

Figure 17. H-2 Data Reduction System

~~CONFIDENTIAL~~



~~CONFIDENTIAL~~

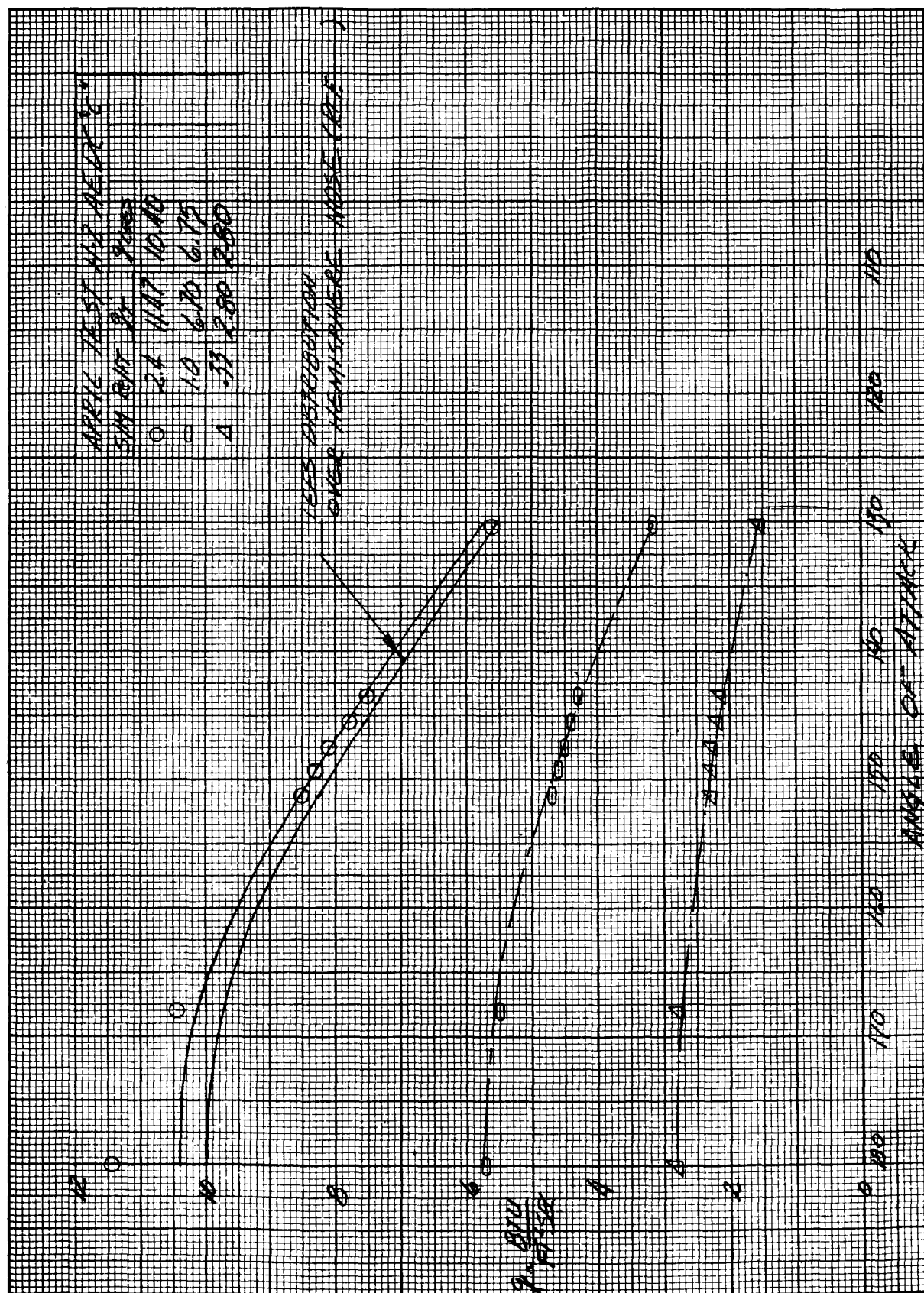


Figure 18. Heating Rate of Thermocouple Number One at Various Angles of Attack on Command Module Configuration

~~CONFIDENTIAL~~



CONFIDENTIAL

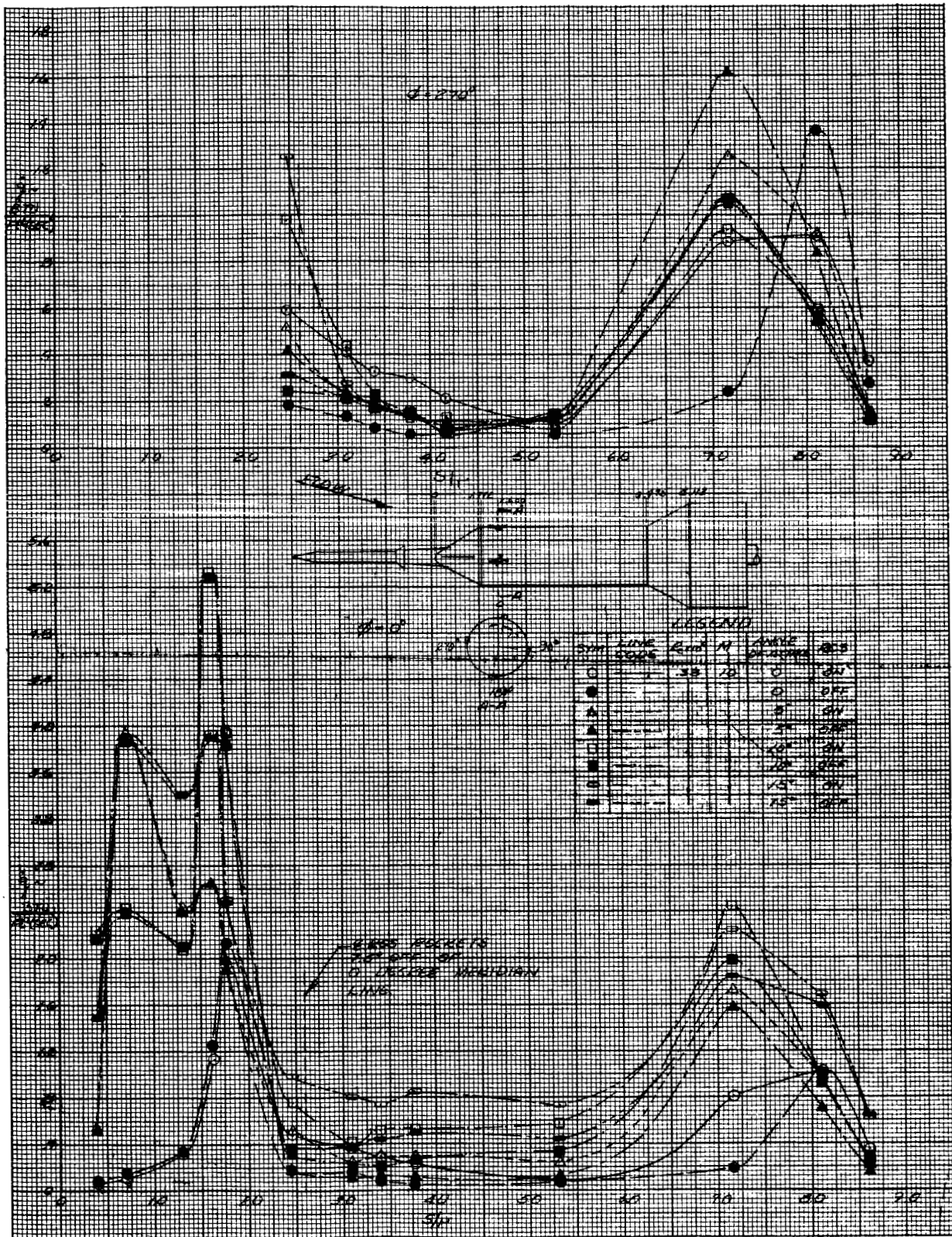


Figure 19. Effect of RCS Motors on Launch Configuration Heating Rates With Strakes (E₄₃T₂₇C₂L₂₈S₆R₅I₁B₈) (Re/in. = 27,000)

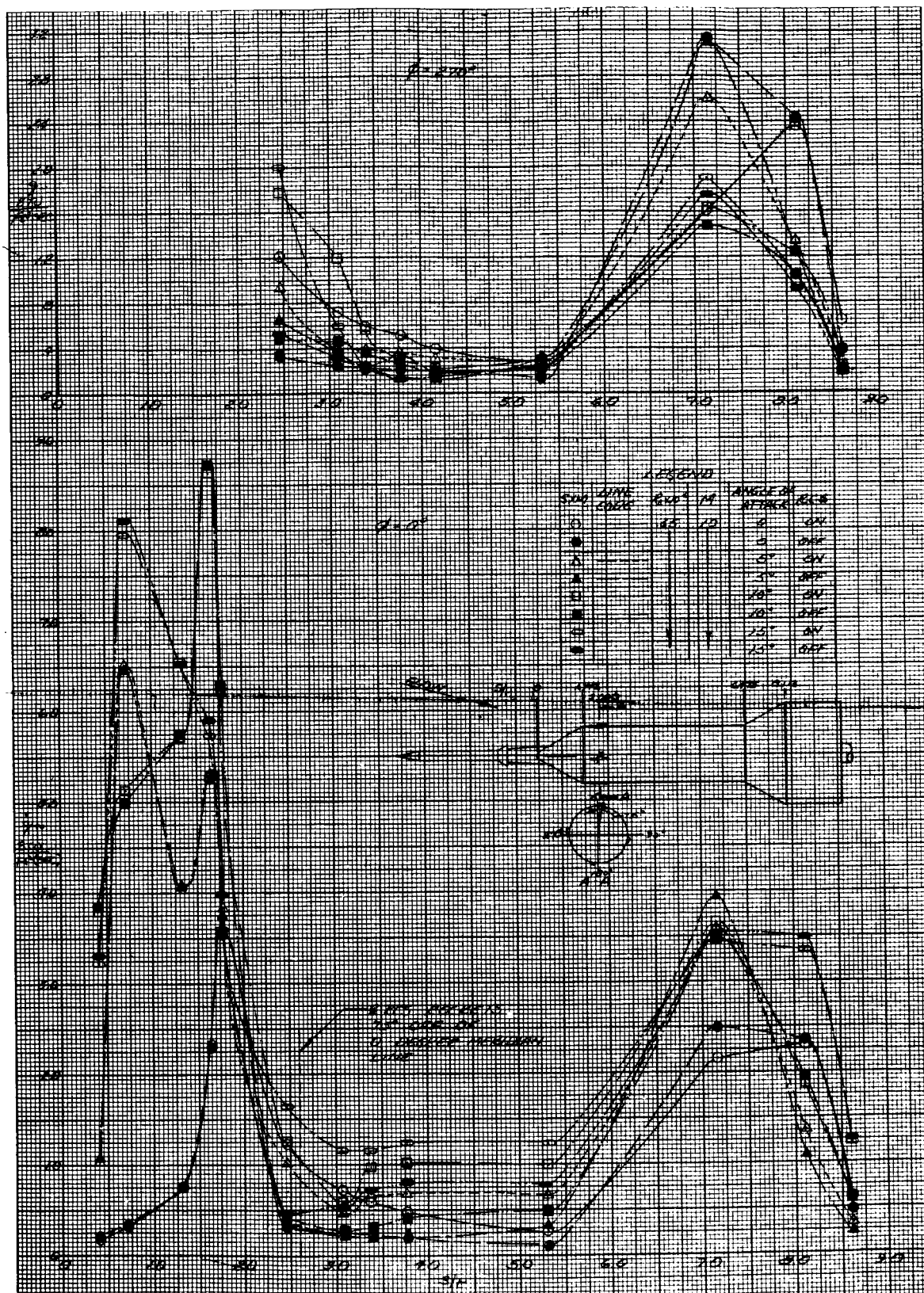
~~CONFIDENTIAL~~

Figure 20. Effect of RCS Motors on Launch Configuration Heating Rates With Strakes (E₄₃T₂₇C₂L₂₈S₆R₅I₁B₈)

~~CONFIDENTIAL~~

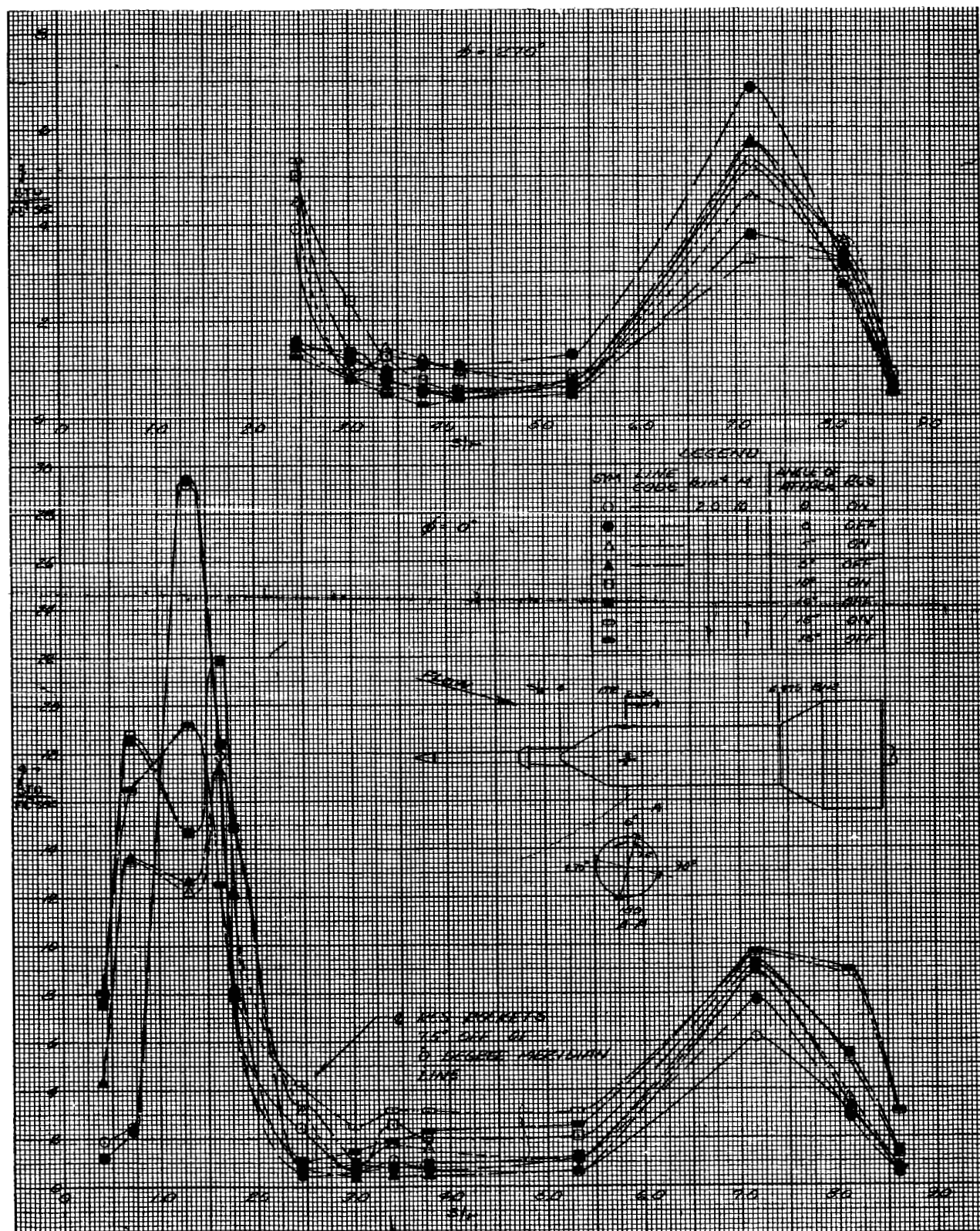
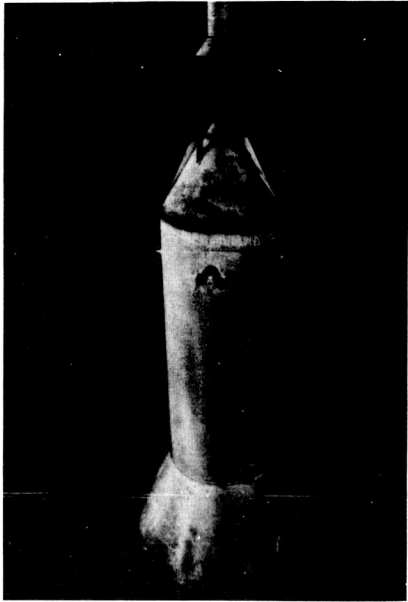
~~CONFIDENTIAL~~

Figure 21. Effect of RCS Motors on Launch Configuration Heating Rates With Strakes ($E_{43}T_{27}C_2L_{28}S_6R_5I_1B_8$) ($Re/in. = 166,000$)

~~CONFIDENTIAL~~

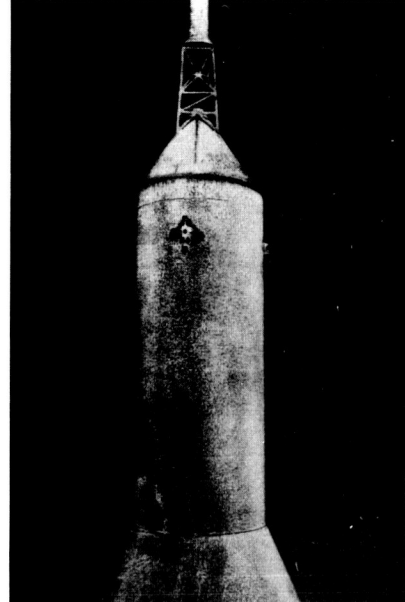
~~CONFIDENTIAL~~

AFTER FLOW PATTERN WAS ESTABLISHED
TIME ≈ 3.0 SEC.



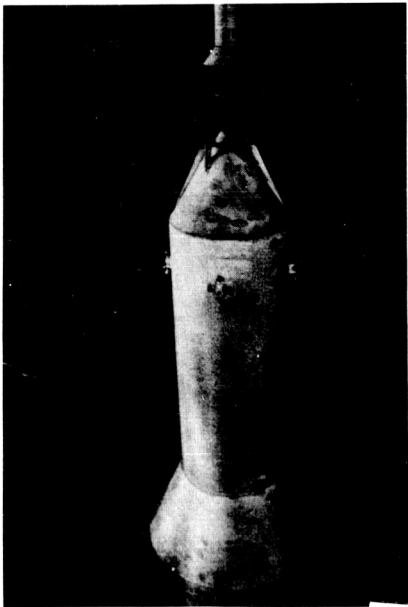
43 TOP VIEW

$\alpha = 0^\circ$
 $\phi = 0^\circ$
 $P_o = 215$ PSIA
 $T_o = 1670^\circ\text{R}$
 $M = 10.0$



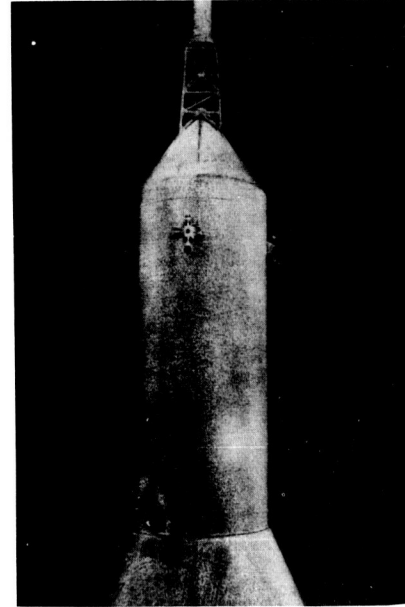
44 SIDE VIEW

INITIAL ENTRY INTO TUNNEL
TIME ≈ 0



41 TOP VIEW

$\alpha = 0^\circ$
 $\phi = 0^\circ$
 $P_o = 215$ PSIA
 $T_o = 1670^\circ\text{R}$
 $M = 10.0$



42 SIDE VIEW

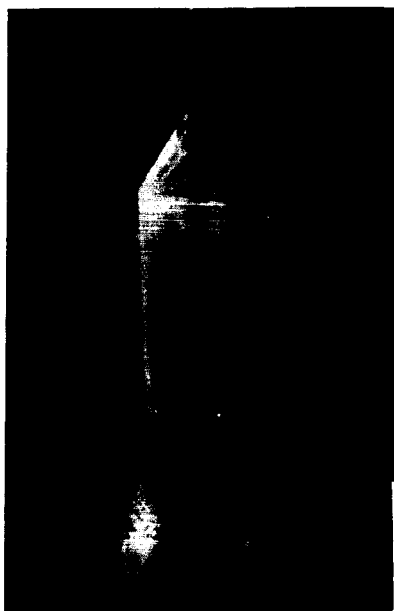
Figure 22. Photos of Oil Flow Photographs of Launch Configuration With Strakes and Service Module Reaction Control Motors at Zero-Degrees Angle of Attack ($Re/in. = 27,000$)

~~CONFIDENTIAL~~



CONFIDENTIAL

INITIAL ENTRY INTO TUNNEL
TIME ≈ 0



25 TOP VIEW

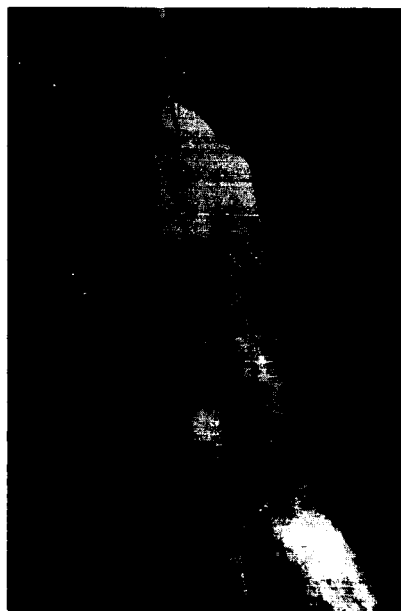
$\alpha = 10^\circ$
 $\phi = 0^\circ$
 $P_o = 215 \text{ PSIA}$ $M = 10.0$
 $T_o = 1670^\circ\text{R}$

AFTER FLOW PATTERN WAS ESTABLISHED
TIME $\approx 3.0 \text{ SEC.}$

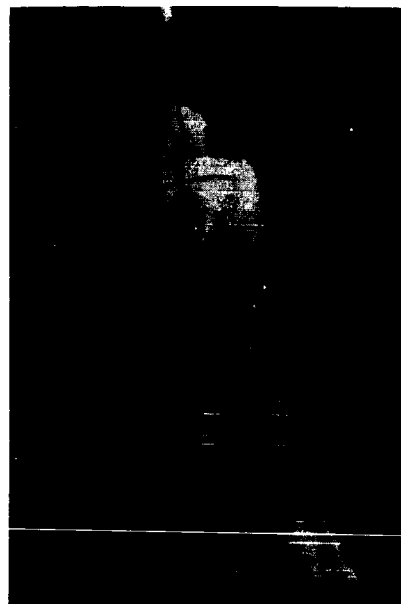


27 TOP VIEW

$\alpha = 10^\circ$
 $\phi = 0^\circ$
 $P_o = 215 \text{ PSIA}$ $M = 10.0$
 $T_o = 1670^\circ\text{R}$



26 SIDE VIEW



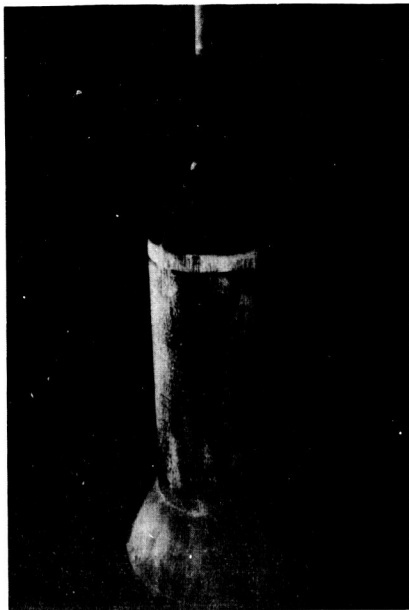
28 SIDE VIEW

Figure 23. Photos of Oil Flow Photographs of Launch Configuration With Strakes and Service Module Reaction Control Motors at 10 Degrees Angle of Attack ($Re/in. = 27,000$)

CONFIDENTIAL

~~CONFIDENTIAL~~

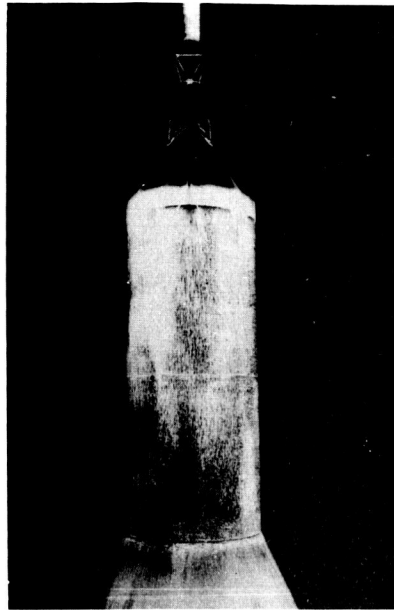
AFTER FLOW PATTERN WAS ESTABLISHED
TIME ≈ 1.5 SEC



TOP VIEW

$P_o = 215$ PSIA $M = 10.0$
 $T_o = 1670^\circ R$

$\alpha = 0^\circ$
 $\phi = 0^\circ$



SIDE VIEW

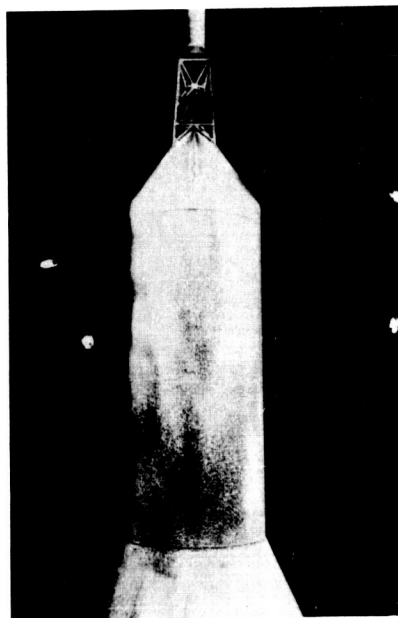
INITIAL ENTRY INTO TUNNEL
TIME ≈ 0



TOP VIEW

$P_o = 215$ PSIA $M = 10.0$
 $T_o = 1670^\circ R$

$\alpha = 0^\circ$
 $\phi = 0^\circ$



SIDE VIEW

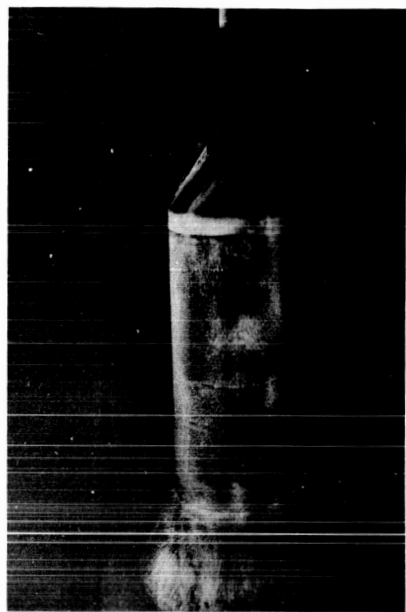
Figure 24. Photos of Oil Flow Photographs of Launch Configuration With Strakes at Zero-Degrees Angle of Attack ($Re/in. = 27,000$)

~~CONFIDENTIAL~~



~~CONFIDENTIAL~~

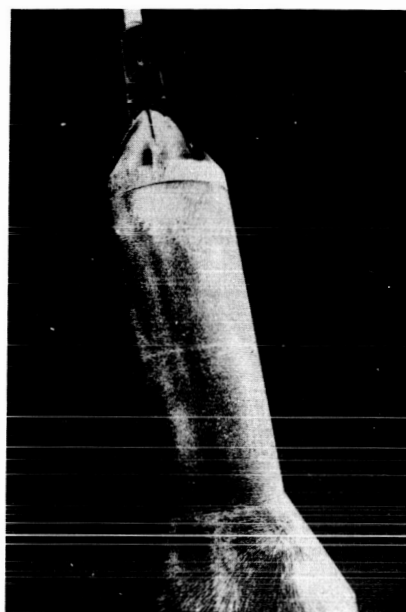
AFTER FLOW PATTERN WAS ESTABLISHED
TIME \approx 2.0 SEC



23 TOP VIEW

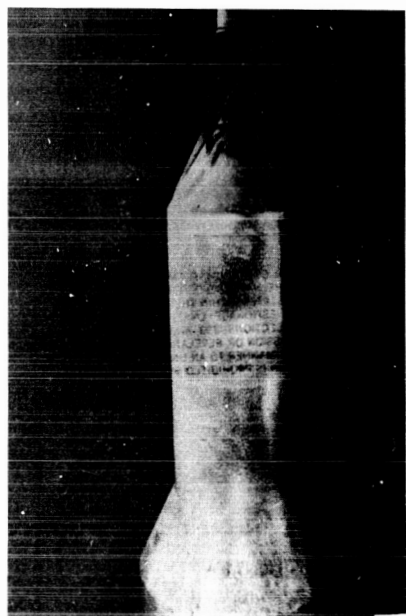
$P_o = 215$ PSIA $M = 10.0$
 $T_o = 1670^\circ R$

$\alpha = 10$
 $\phi = 0$



24 SIDE VIEW

INITIAL ENTRY INTO TUNNEL
TIME \approx 0



21 TOP VIEW

$P_o = 215$ PSIA $M = 10.0$
 $T_o = 1670^\circ R$

$\alpha = 10^\circ$
 $\phi = 0^\circ$



22 SIDE VIEW

Figure 25. Photos of Oil Flow Photographs of Launch Configuration With Strakes at 10 Degrees Angle of Attack ($Re/in. = 27,000$)

~~CONFIDENTIAL~~

~~CONFIDENTIAL~~

INITIAL ENTRY INTO TUNNEL
TIME ≈ 0



TOP VIEW

$\alpha = 0^\circ$
 $\phi = 0^\circ$

$P_o = 215 \text{ PSIA}$ $M = 10.0$
 $T_o = 1670^\circ\text{R}$

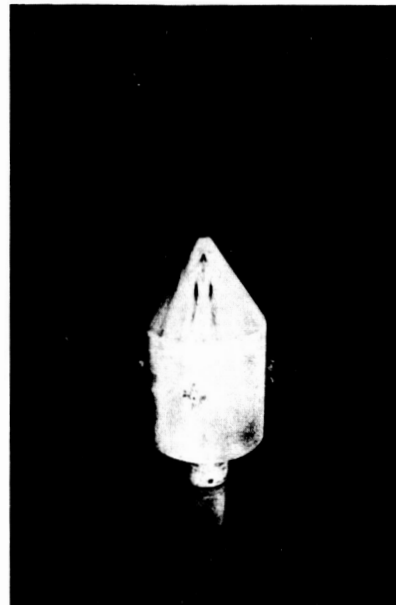
AFTER FLOW PATTERN WAS ESTABLISHED
TIME $\approx 3.0 \text{ SEC}$



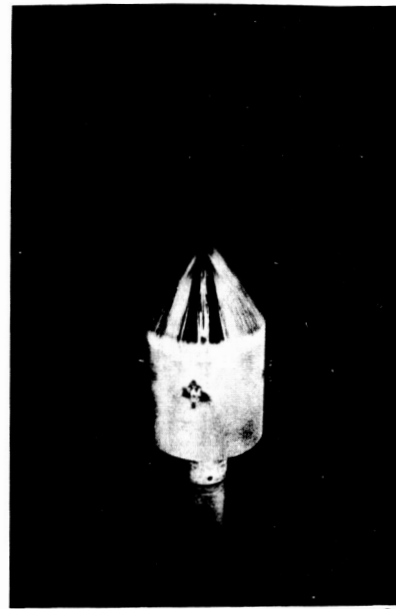
TOP VIEW

$\alpha = 0^\circ$
 $\phi = 0^\circ$

$P_o = 215 \text{ PSIA}$ $M = 10.0$
 $T_o = 1670^\circ\text{R}$



SIDE VIEW



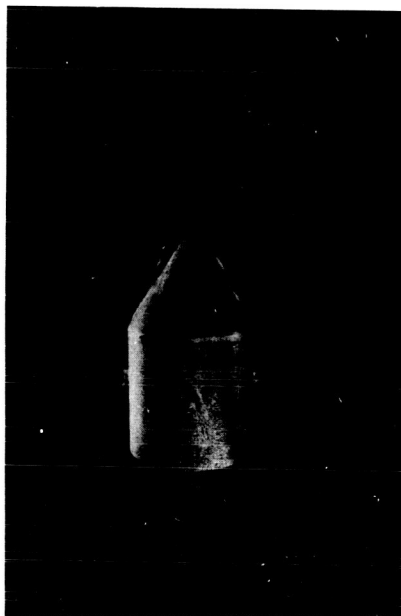
SIDE VIEW

Figure 26. Photos of Oil Flow Photographs of Command-Service Modules,
With Reaction Control Motors, at Zero Degrees
Angle of Attack ($Re/in. = 27,000$)

~~CONFIDENTIAL~~

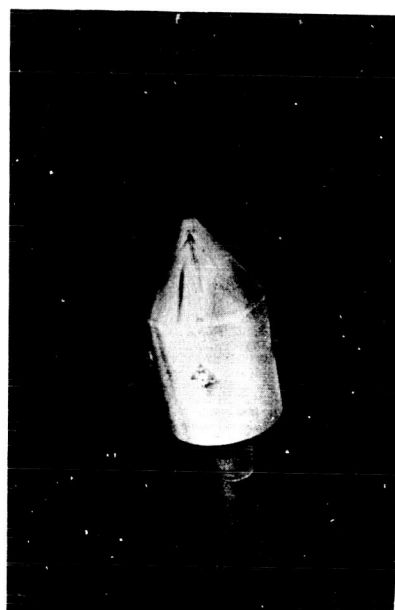
~~CONFIDENTIAL~~

INITIAL ENTRY INTO TUNNEL
TIME ≈ 0



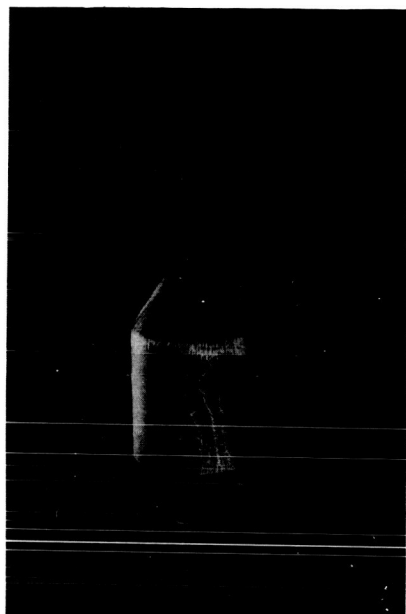
37 TOP VIEW

$\alpha = 10^\circ$
 $\phi = 0$
 $P_o = 215 \text{ PSIA}$ $M = 10.0$
 $T_o = 1670^\circ\text{R}$



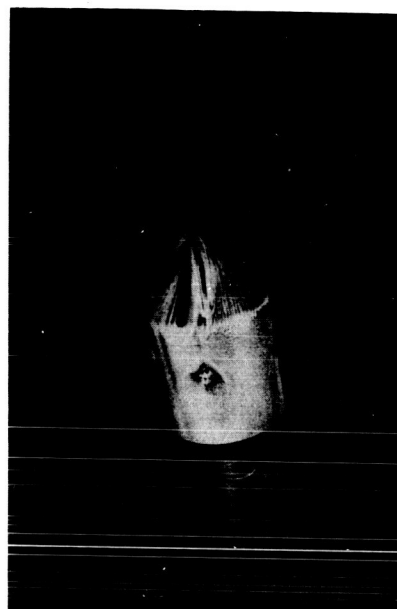
38 SIDE VIEW

AFTER FLOW PATTERN WAS ESTABLISHED
TIME $\approx 2.0 \text{ SEC}$



39 TOP VIEW

$\alpha = 10^\circ$
 $\phi = 0$
 $P_o = 215 \text{ PSIA}$ $M = 10.0$
 $T_o = 1670^\circ\text{R}$



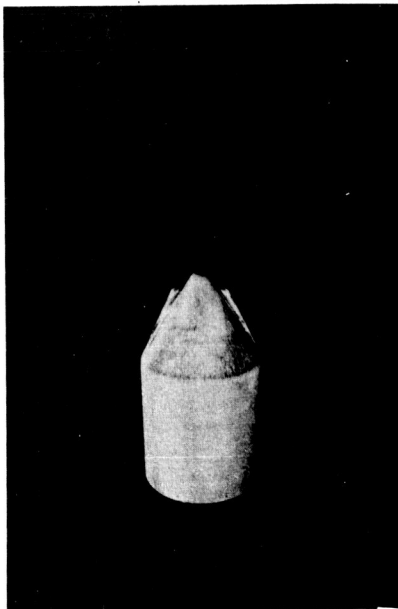
40 SIDE VIEW

Figure 27. Photos of Oil Flow Photographs of the Command-Service Module, With Strakes and Reaction Control Motors, at 10 Degrees Angle of Attack ($Re/in. = 27,000$)

~~CONFIDENTIAL~~

~~CONFIDENTIAL~~

INITIAL ENTRY INTO TUNNEL
TIME ≈ 0

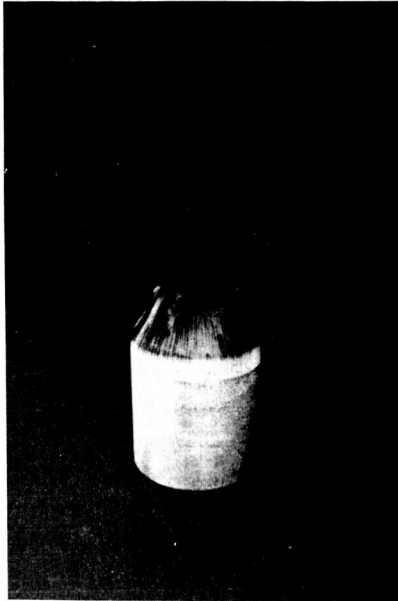


13

TOP VIEW

$\alpha = 0^\circ$
 $\phi = 0^\circ$
 $P_o = 215 \text{ PSIA}$ $M = 10.0$
 $T_o = 1670^\circ\text{R}$

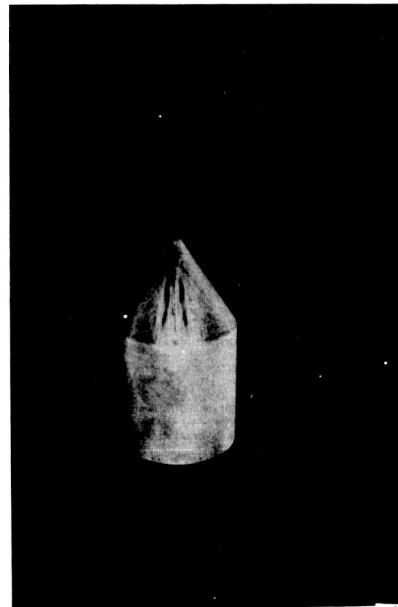
AFTER FLOW PATTERN WAS ESTABLISHED
TIME $\approx 3.0 \text{ SEC}$



15

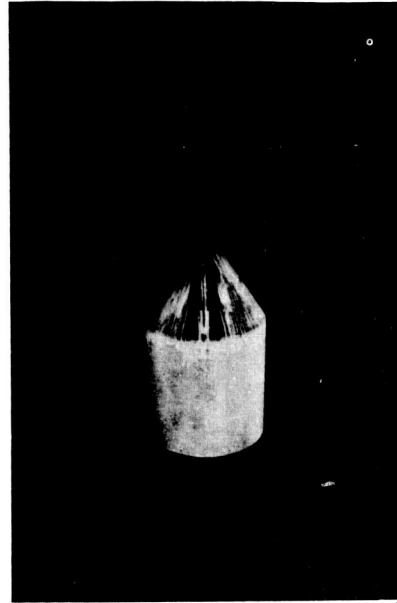
TOP VIEW

$\alpha = 0^\circ$
 $\phi = 0^\circ$
 $P_o = 215 \text{ PSIA}$ $M = 10.0$
 $T_o = 1670^\circ\text{R}$



14

SIDE VIEW



16

SIDE VIEW

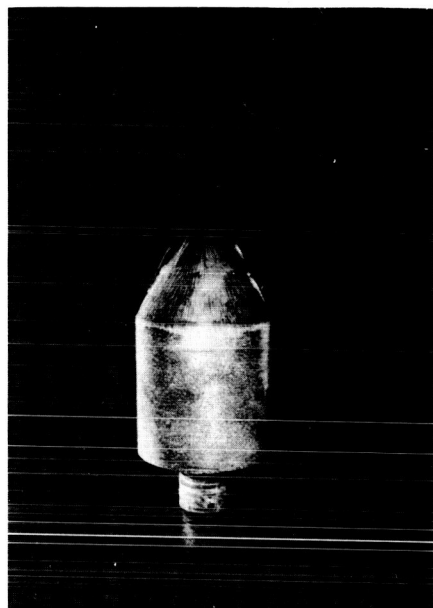
Figure 28. Photos of Oil Flow Photographs of Command-Service Module
With Strakes at Zero-Degrees Angle of Attack ($Re/in. = 27,000$)

~~CONFIDENTIAL~~



~~CONFIDENTIAL~~

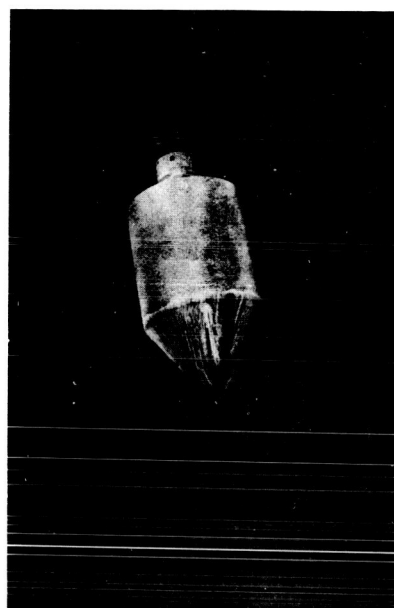
AFTER FLOW PATTERN WAS ESTABLISHED
TIME ≈ 1.5 SEC



35

TOP VIEW

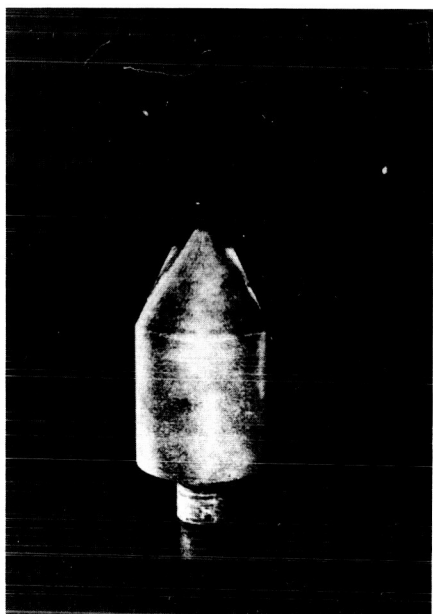
$\alpha = 10^\circ$
 $\phi = 0^\circ$
 $P_o = 215$ PSIA $M = 0$
 $T_o = 1670^\circ R$



36

SIDE VIEW

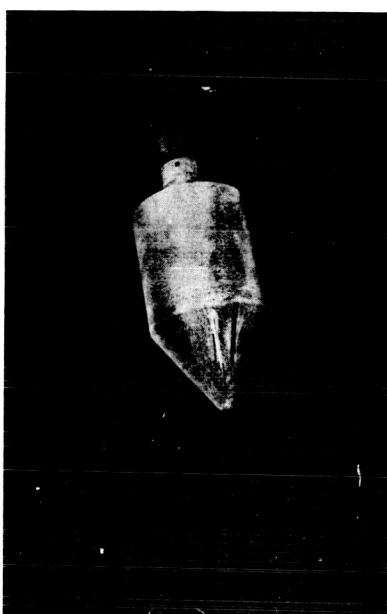
INITIAL ENTRY INTO TUNNEL
TIME ≈ 0



33

TOP VIEW

$\alpha = 10^\circ$
 $\phi = 0$
 $P_o = 215$ PSIA $M = 10.0$
 $T_o = 1670^\circ R$



34

SIDE VIEW

Figure 29. Photos of Oil Flow Photographs of Command-Service Module
With Strakes at 10-Degrees Angle of Attack ($Re/in. = 27,000$)

~~CONFIDENTIAL~~

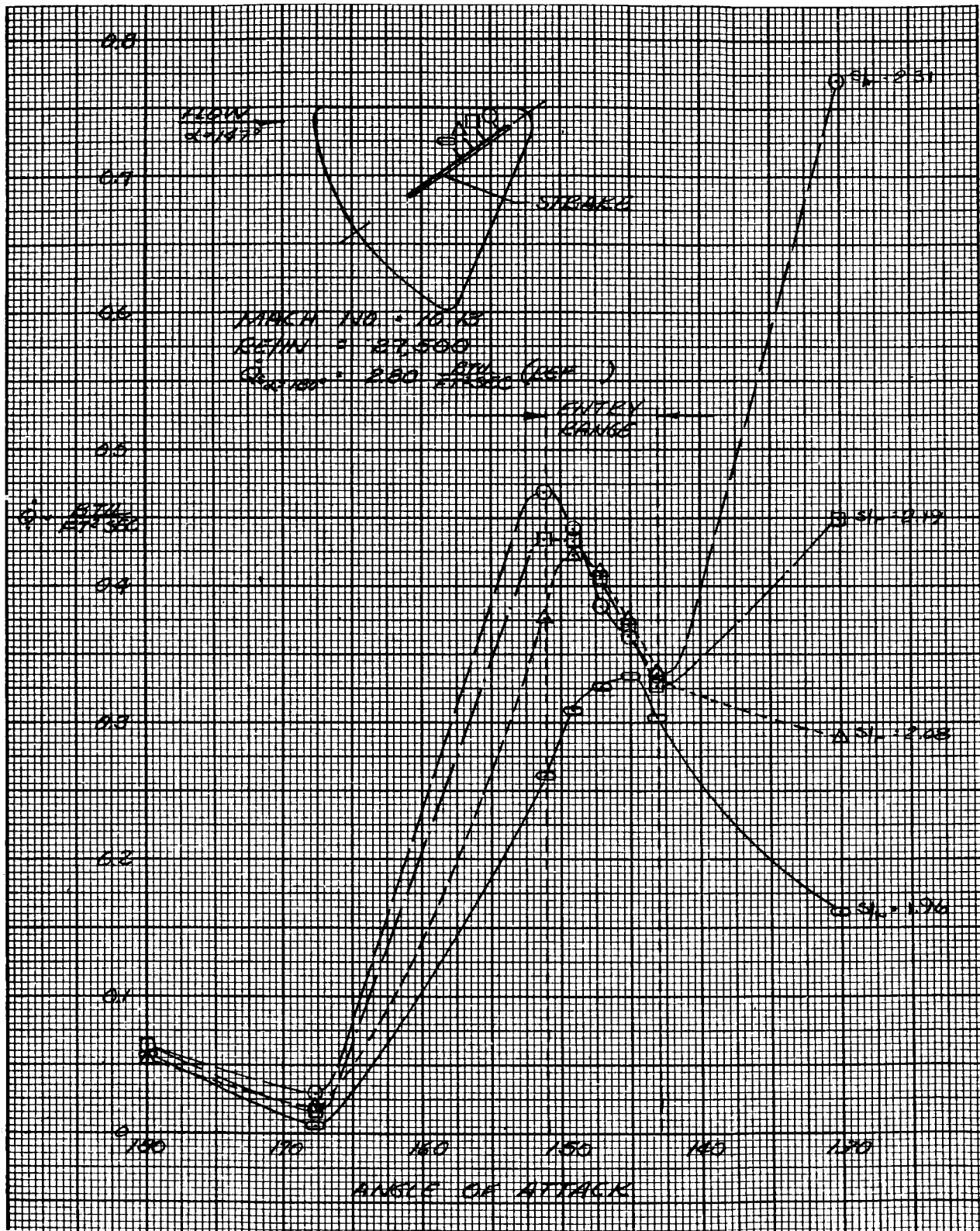


Figure 30. Heating Rates on Windward Side of Strake Versus Angle of Attack (C_2 Configuration) ($Re/in. = 27,000$)

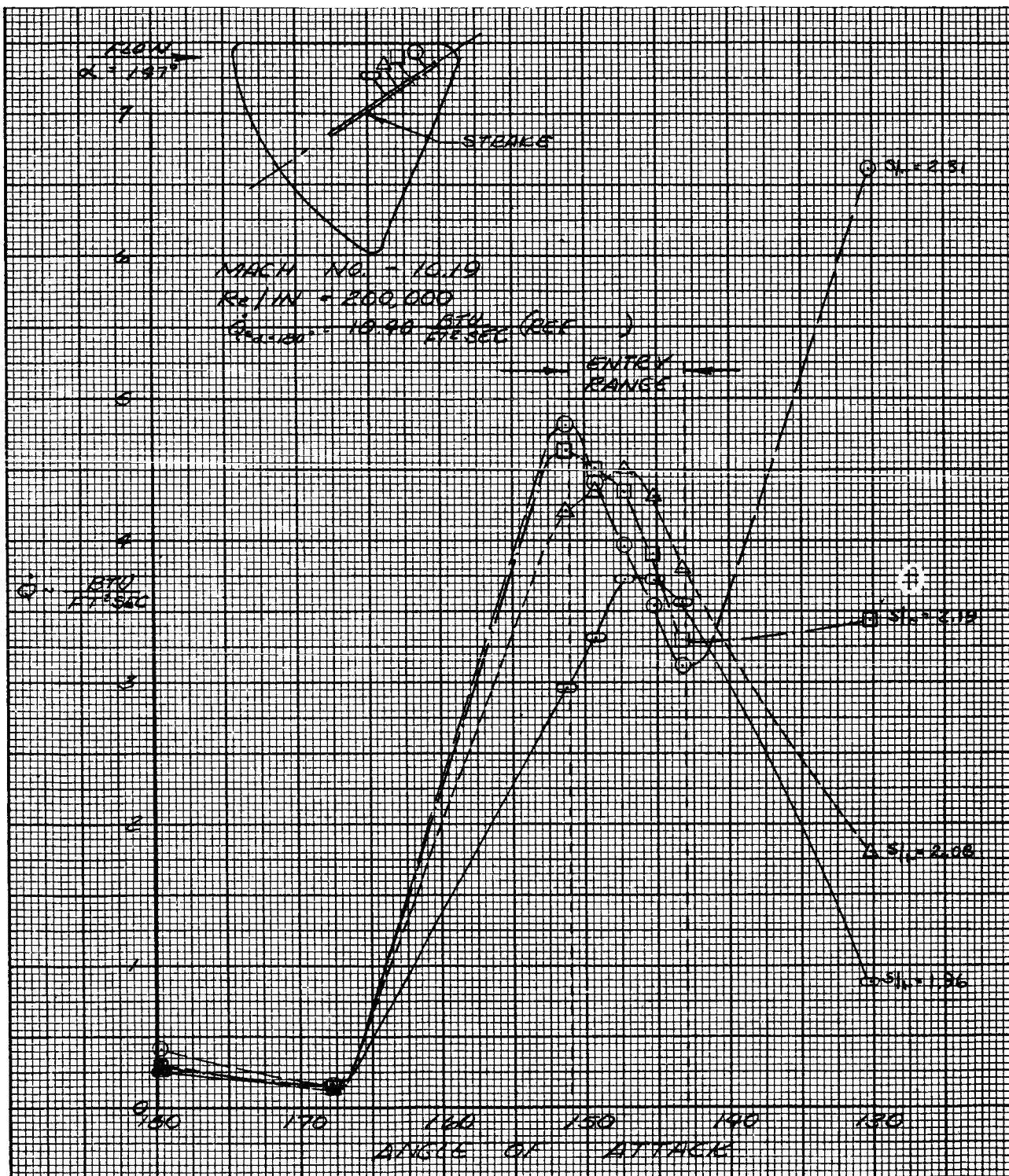
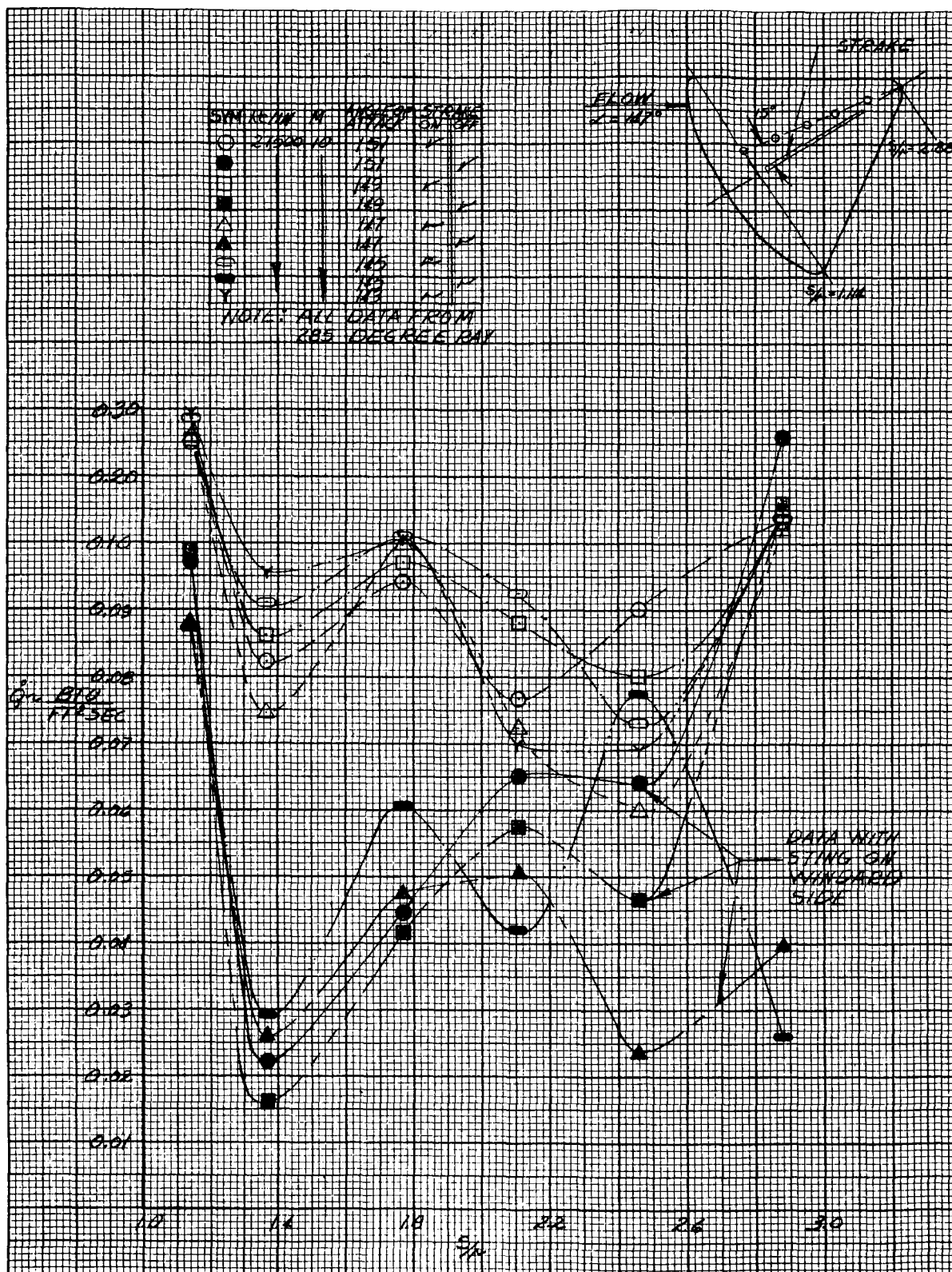
~~CONFIDENTIAL~~

Figure 31. Heating Rates on Windward Side of Strake Versus Angle of Attack (C_2 Configuration) ($Re/in. = 200,000$)

~~CONFIDENTIAL~~



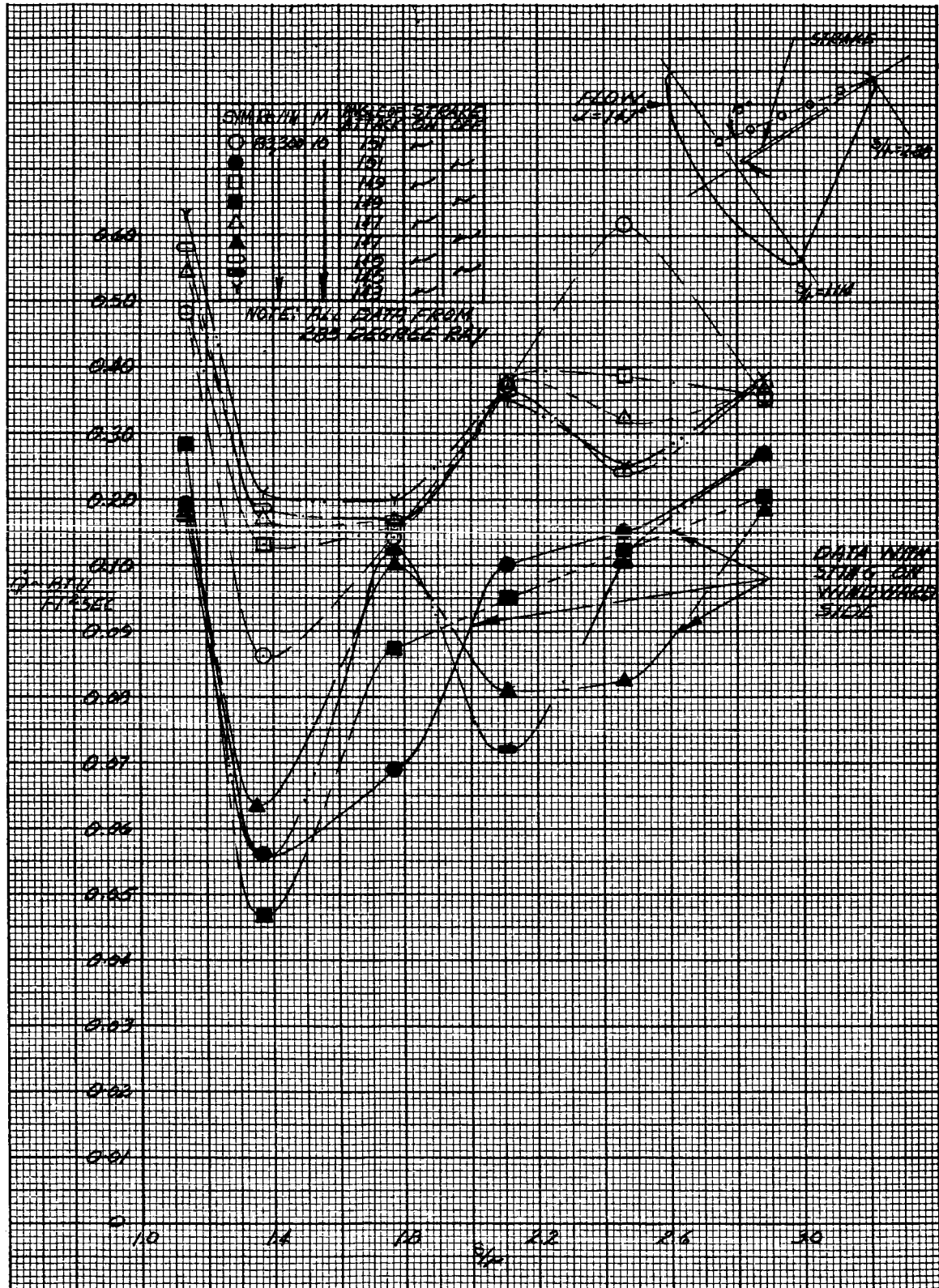
~~CONFIDENTIAL~~

Figure 33. Effect of Strakes on Windward Afterbody Heating Rate Near Entry Angle of Attack (C_2 configuration) ($Re/in. = 83,300$)

~~CONFIDENTIAL~~

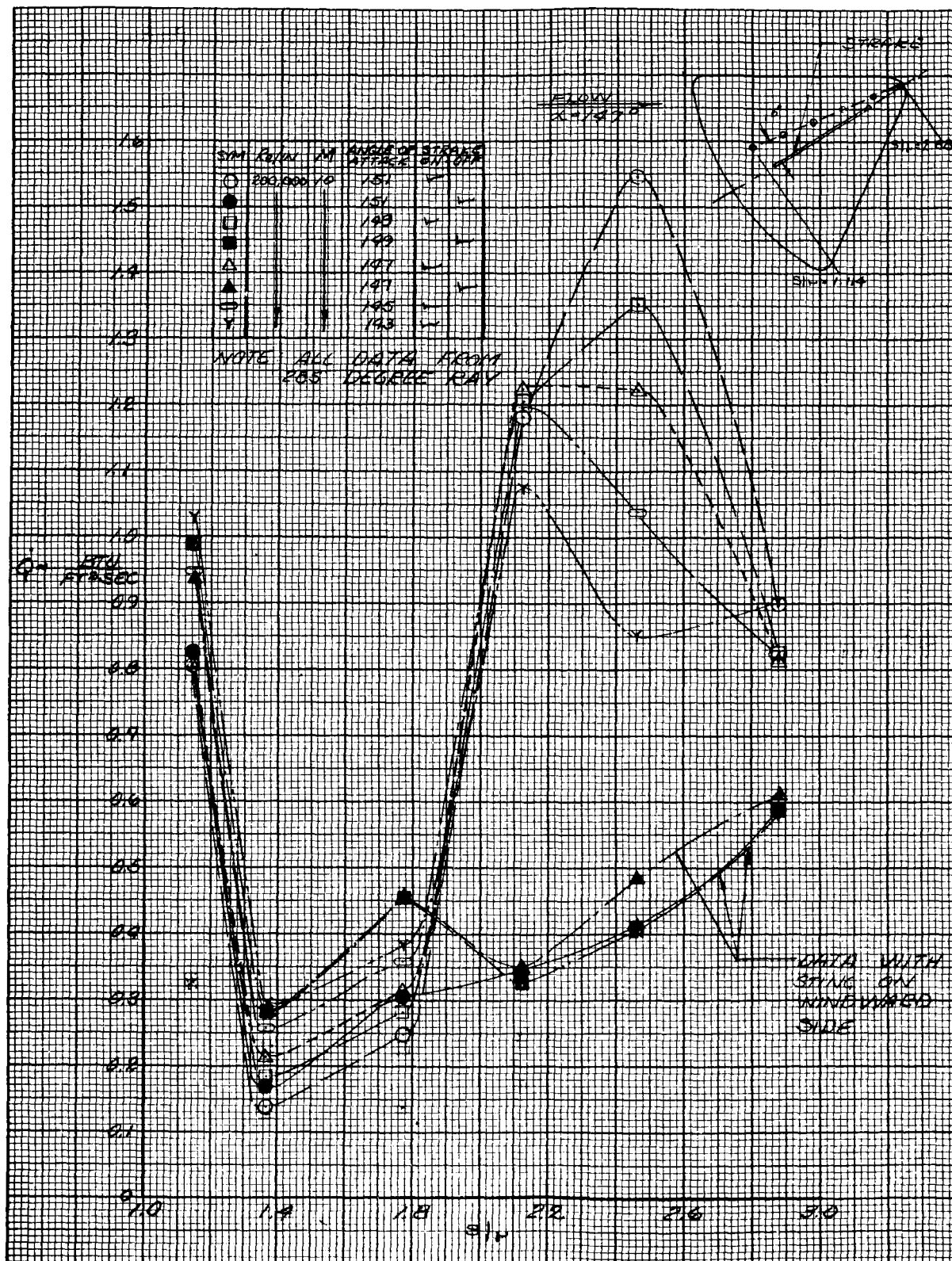
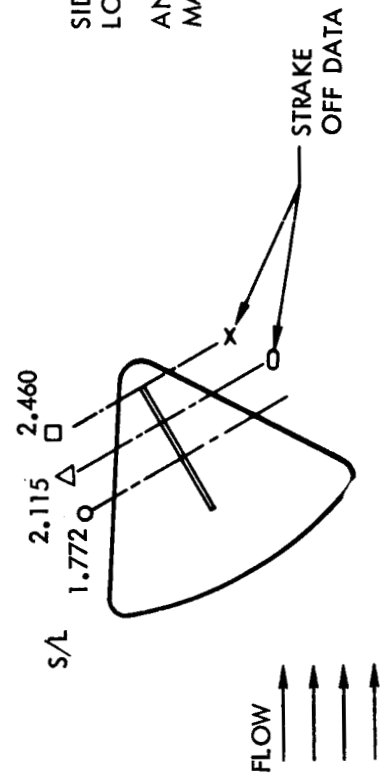
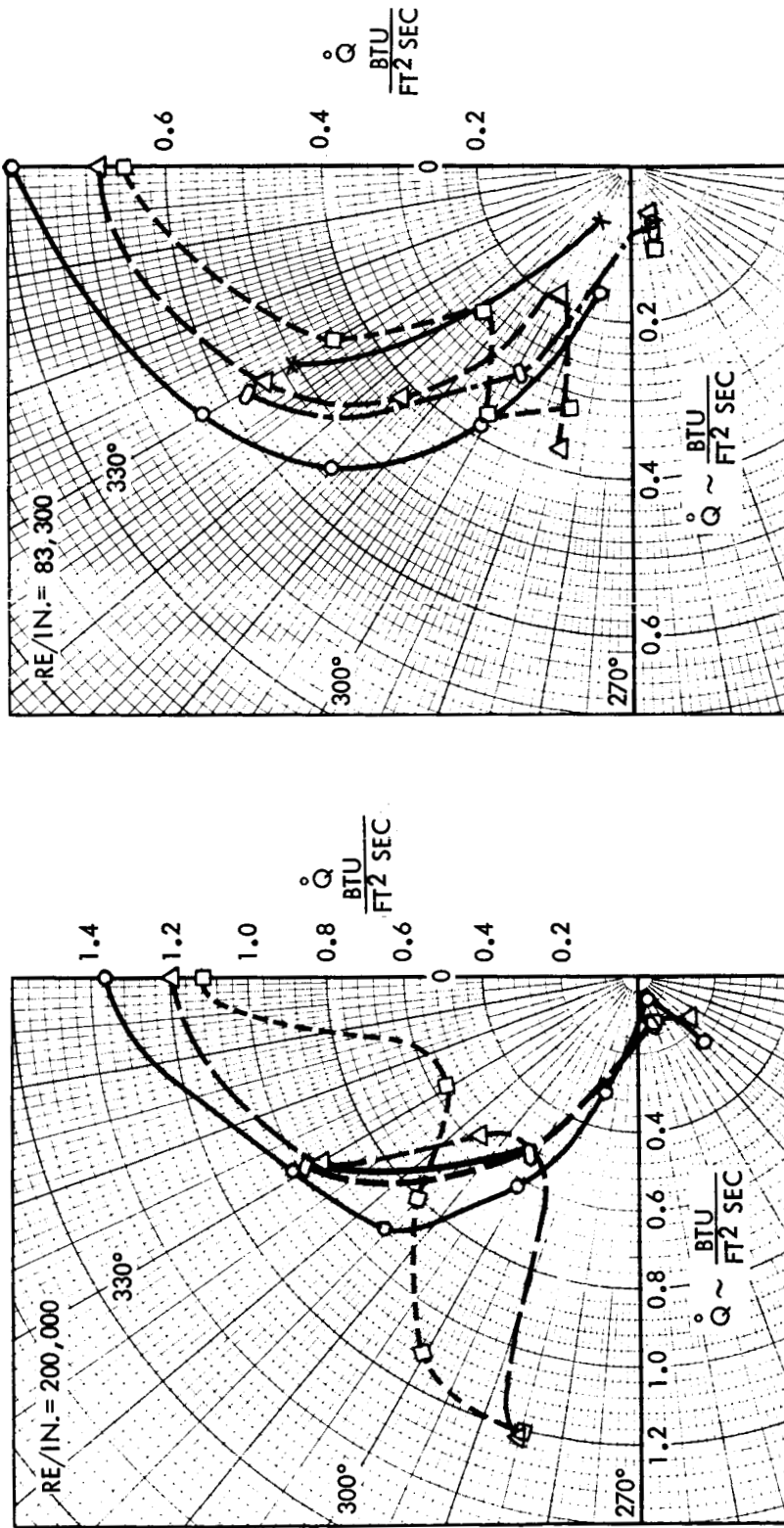
~~CONFIDENTIAL~~

Figure 34. Effect of Strakes on Windward Afterbody Heating Rates Near Entry Angle of Attack (C_2 configuration) ($Re/in. = 200,000$)

~~CONFIDENTIAL~~



~~CONFIDENTIAL~~



SIDE VIEW STRAKE
LOCATED ON 270° RAY
ANGLE OF ATTACK = 147°
MACH NO. = 10.0

Figure 35. The Effect of Strakes on Afterbody Heating at Two Reynolds Numbers ($Re/in. = 83,300$ and $200,000$) ($\alpha = 147^\circ$)

~~CONFIDENTIAL~~

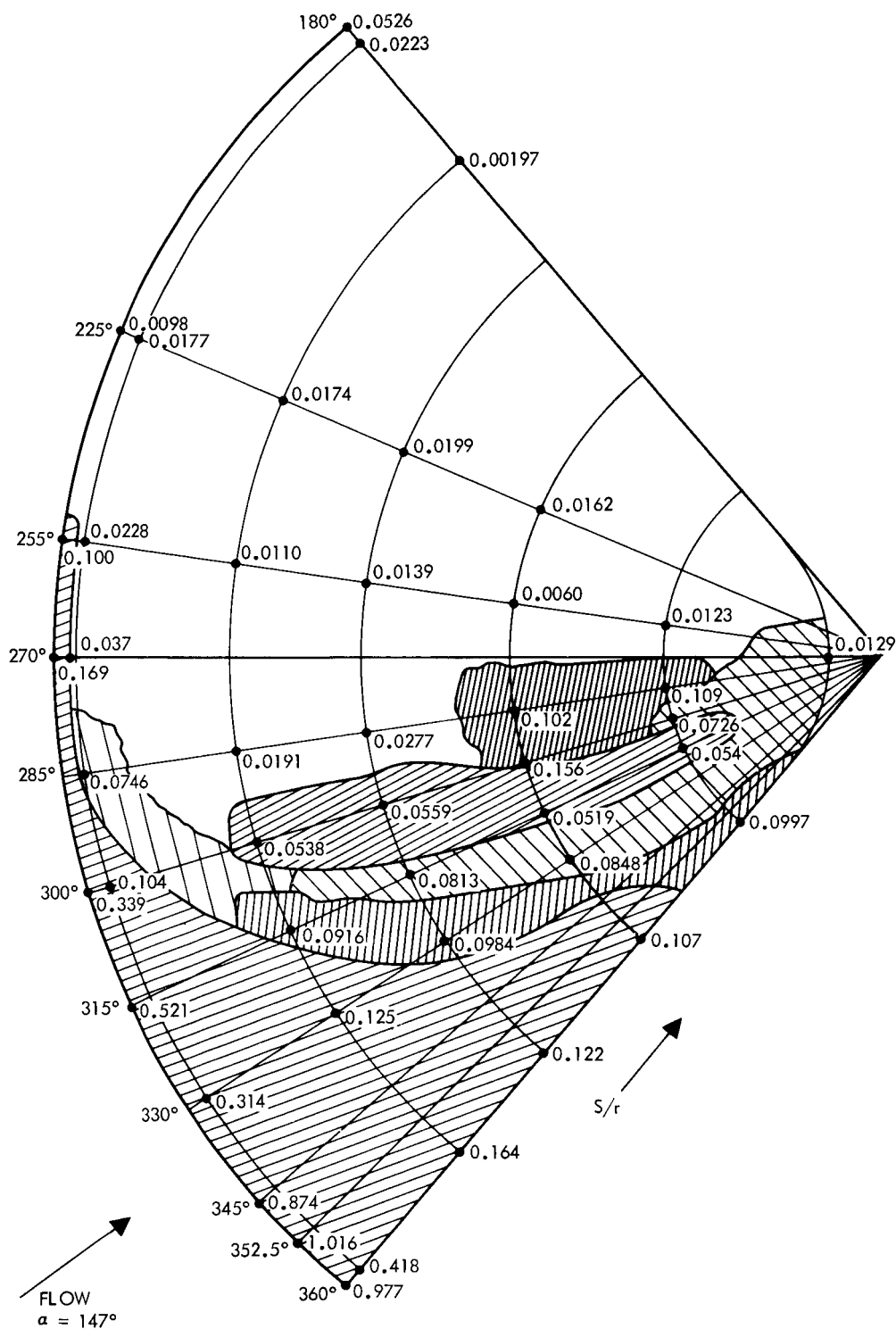
~~CONFIDENTIAL~~

Figure 36. Mapping of the Command Module Afterbody Heating Rate Ratio (H/H_0) ($Re/in. = 200,000$) ($\alpha = 147^\circ$)



~~CONFIDENTIAL~~

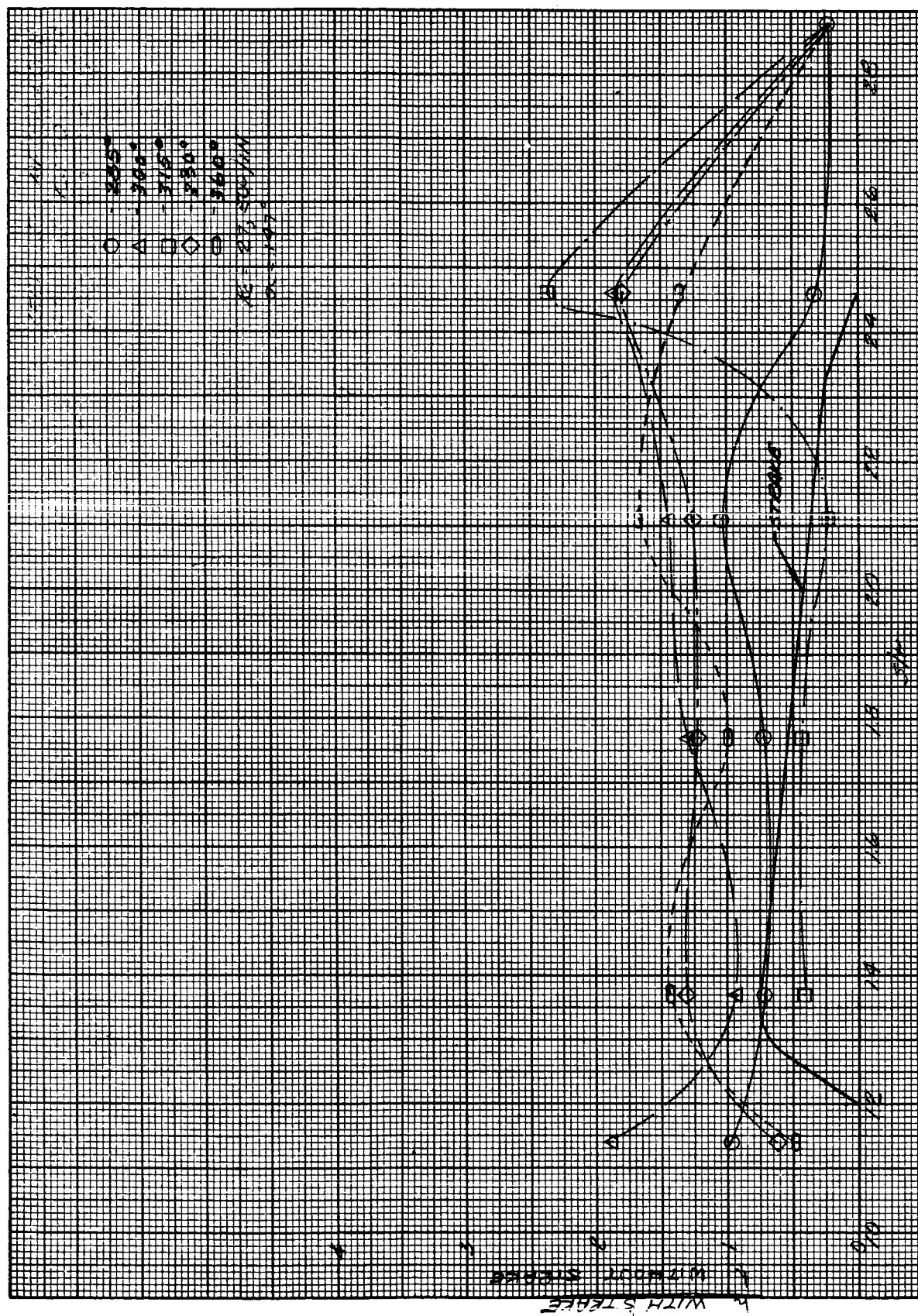


Figure 37. Leeward Afterbody Heating Ratio With and Without Strakes
($Re/in. = 27,500$) ($\alpha = 147^\circ$)

CONFIDENTIAL



~~CONFIDENTIAL~~

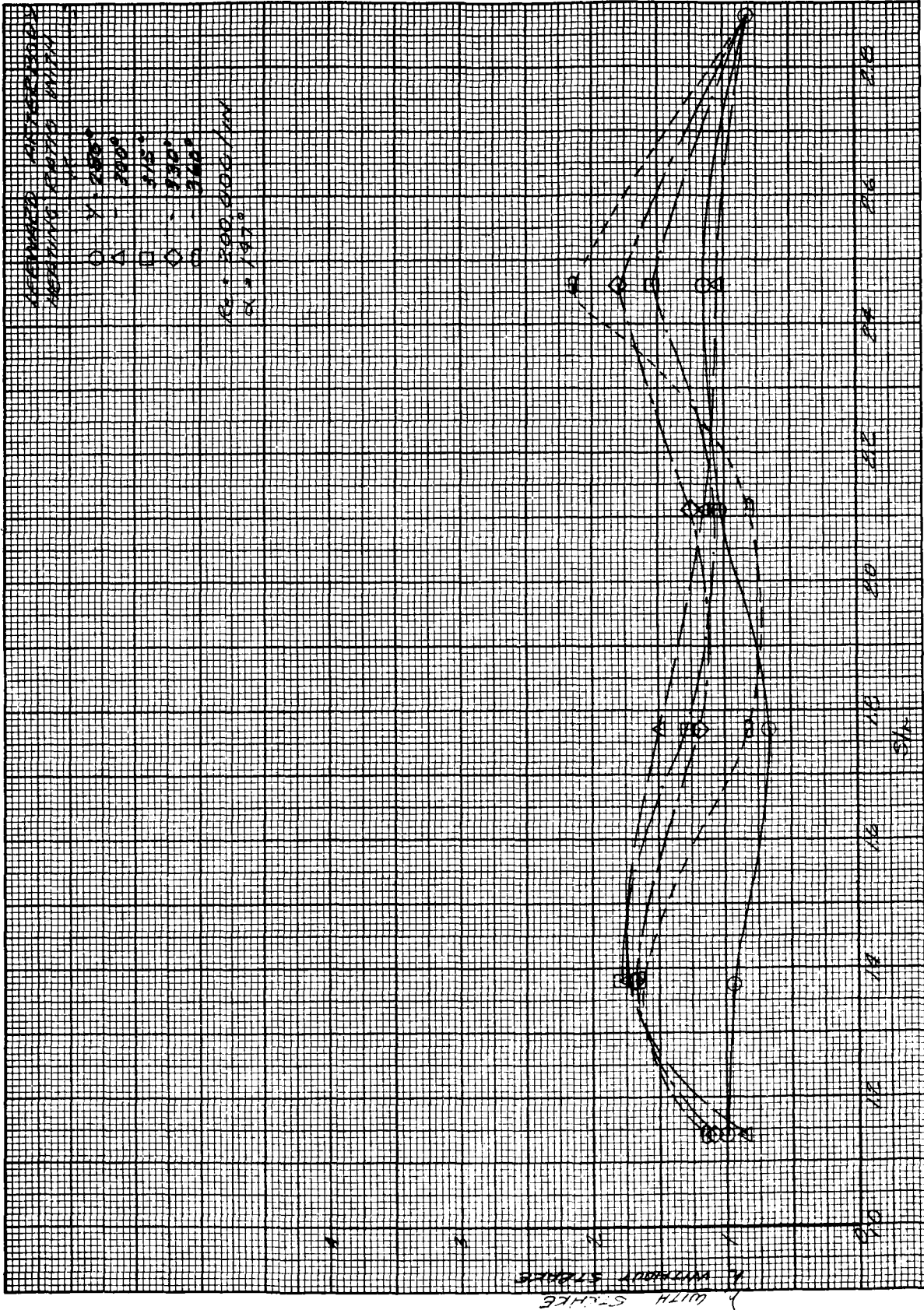
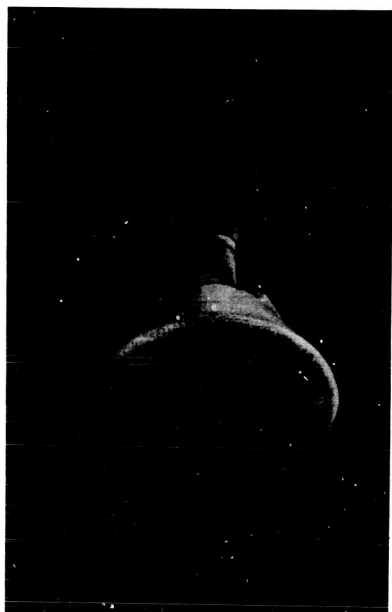


Figure 38. Leeward Afterbody Heating Ratio With and Without Strakes
 (Re/in. = 200,000) ($\alpha = 147^\circ$)

~~CONFIDENTIAL~~

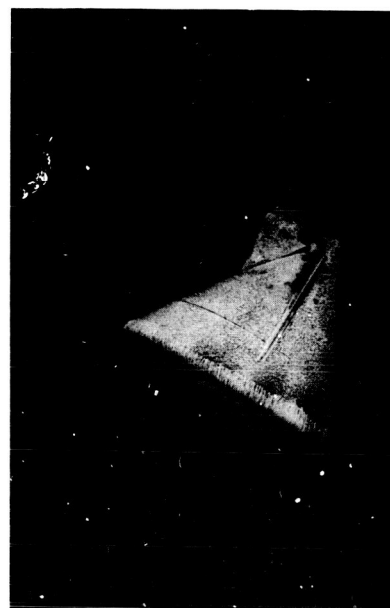
~~CONFIDENTIAL~~

INITIAL ENTRY INTO TUNNEL
TIME ≈ 0



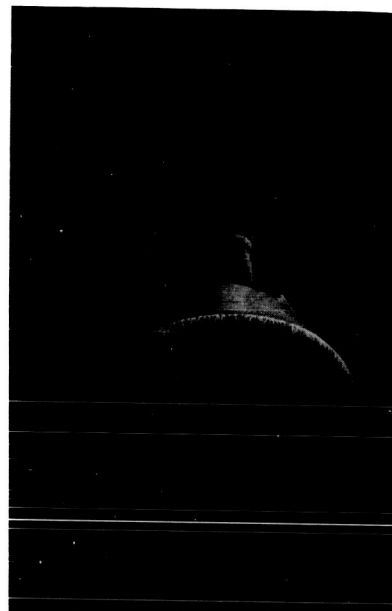
29 TOP VIEW

$\alpha = 147^\circ$
 $\phi = 0$
 $P_o = 215 \text{ PSIA}$ $M = 10.0$
 $T_o = 1670^\circ \text{R}$



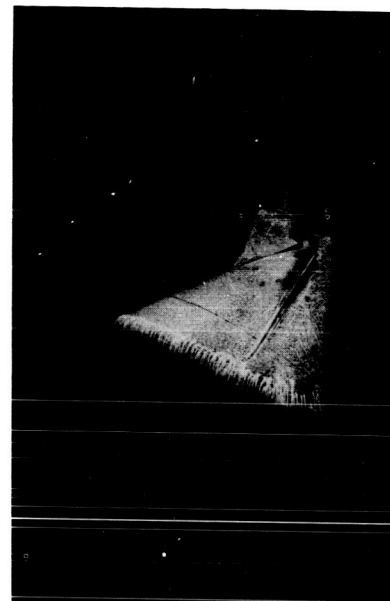
30 SIDE VIEW

AFTER FLOW PATTERN WAS ESTABLISHED
TIME $\approx 5.0 \text{ SEC}$



31 TOP VIEW

$\alpha = 147^\circ$
 $\phi = 0$
 $P_o = 215 \text{ PSIA}$ $M =$
 $T_o = 1670^\circ \text{R}$



32 SIDE VIEW

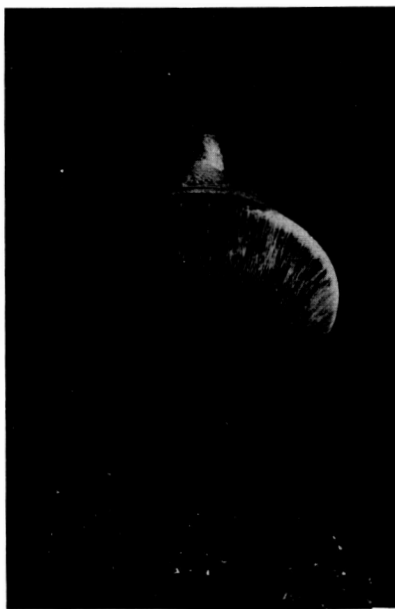
Figure 39. Photos of Oil Flow Photographs of Entry Configuration With Strakes at 147-Degrees Angle of Attack ($Re/in. = 27,500$)

~~CONFIDENTIAL~~



~~CONFIDENTIAL~~

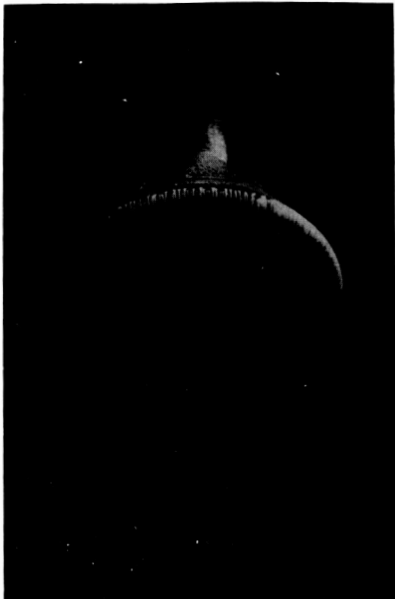
INITIAL ENTRY INTO TUNNEL
TIME ≈ 0



5 TOP VIEW

$\alpha = 147^\circ$
 $\phi = 180^\circ$
 $P_o = 215 \text{ PSIA}$ $M = 10.0$
 $T_o = 1670^\circ\text{R}$

AFTER FLOW PATTERN WAS ESTABLISHED
TIME $\approx 4.0 \text{ SEC}$

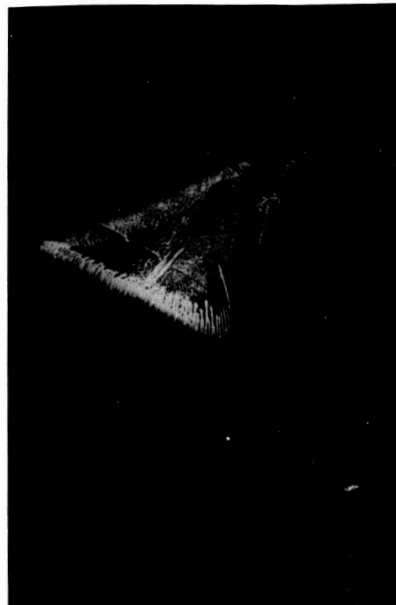


7 TOP VIEW

$\alpha = 147^\circ$
 $\phi = 180^\circ$
 $P_o = 215 \text{ PSIA}$ $M = 10.0$
 $T_o = 1670^\circ\text{R}$



6 SIDE VIEW



8 SIDE VIEW

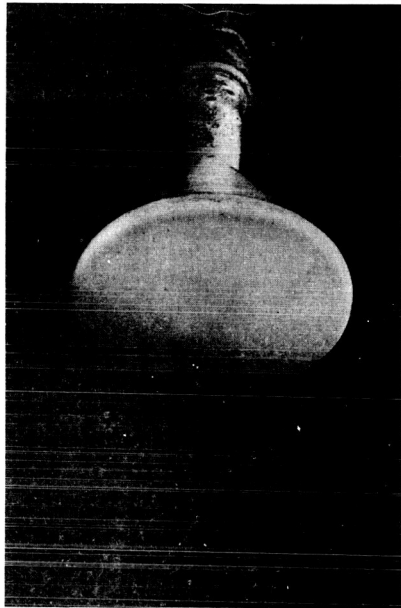
Figure 40. Photos of Oil Flow Photographs of Entry Configuration With Strakes at 147-Degrees Angle of Attack and Model Rolled 180 Degrees (Re/in. = 27,500)

~~CONFIDENTIAL~~



~~CONFIDENTIAL~~

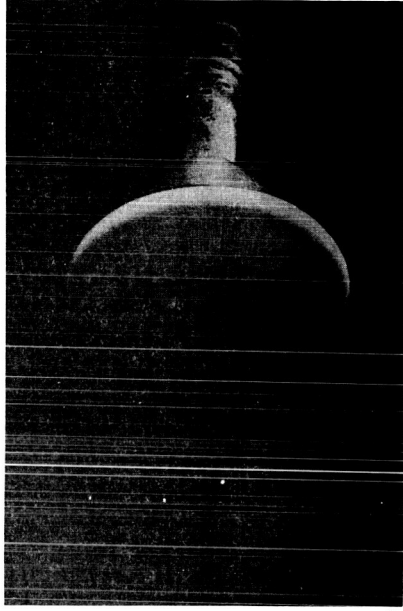
INITIAL ENTRY INTO TUNNEL
TIME 0



1 TOP VIEW

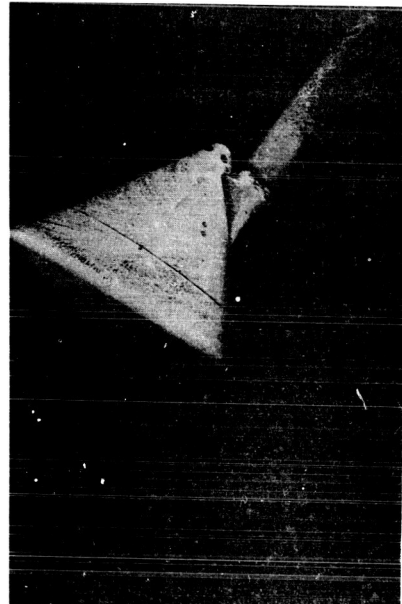
$\alpha = 147^\circ$ $P_o = 215 \text{ PSIA}$ $M = 10.0$
 $\phi = 180^\circ$ $T_o = 1670^\circ\text{R}$

AFTER FLOW PATTERN WAS ESTABLISHED
TIME 4.0 SEC

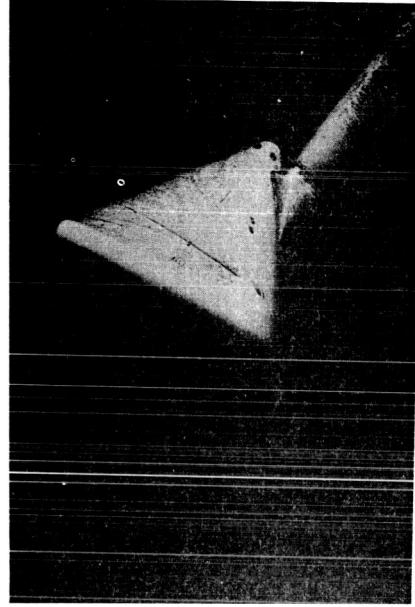


3 TOP VIEW

$\alpha = 147^\circ$ $P_o = 215 \text{ PSIA}$ $M = 10.0$
 $\phi = 180^\circ$ $T_o = 1670^\circ\text{R}$



2 SIDE VIEW



4 SIDE VIEW

Figure 41. Photos of Oil Flow Photographs of Entry Configuration Without Strakes at 147-Degrees Angle of Attack and Model Rolled 180 Degrees (Re/in. = 27,500)

~~CONFIDENTIAL~~

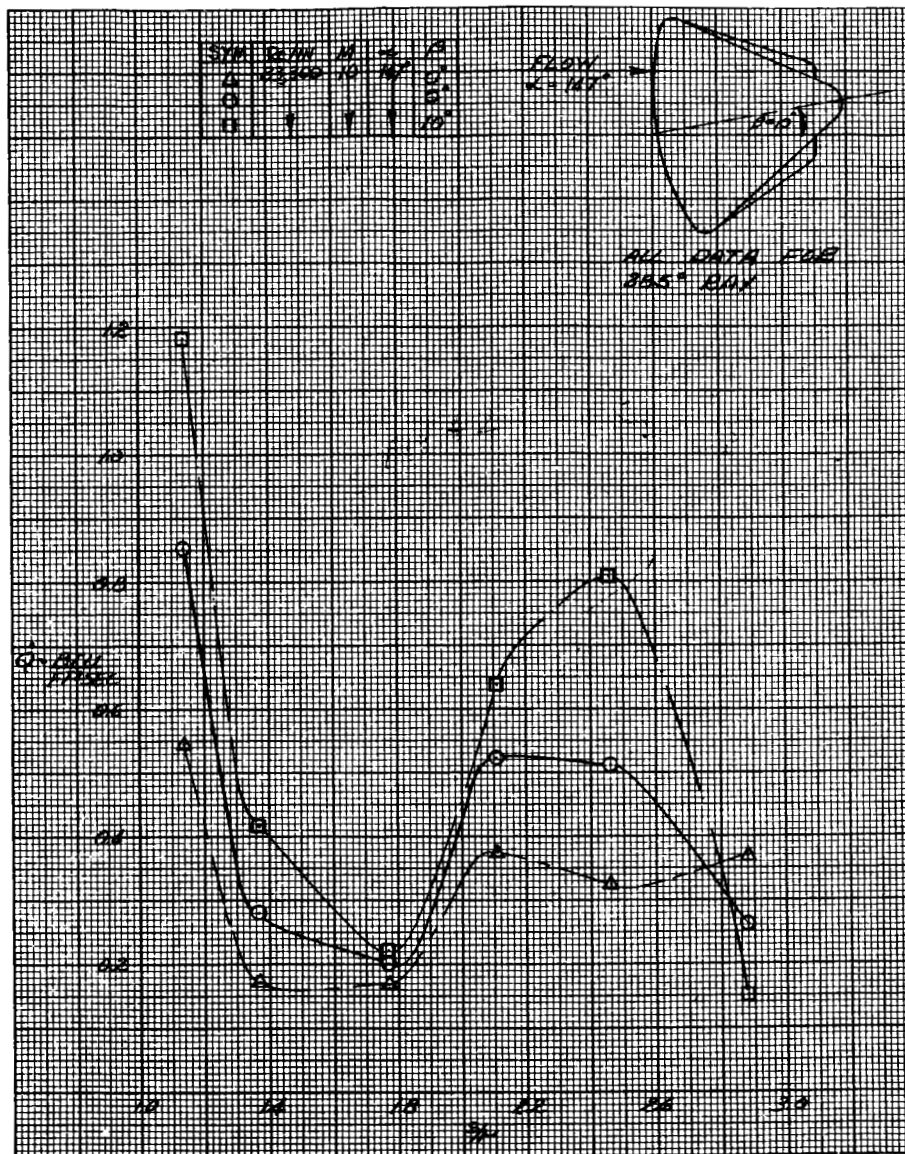
~~CONFIDENTIAL~~

Figure 42. Variation of Heat Transfer Rate on Afterbody of Command Module at 147-Degrees Angle of Attack at Various Yaw Angles
($Re/in. = 83,300$)

~~CONFIDENTIAL~~

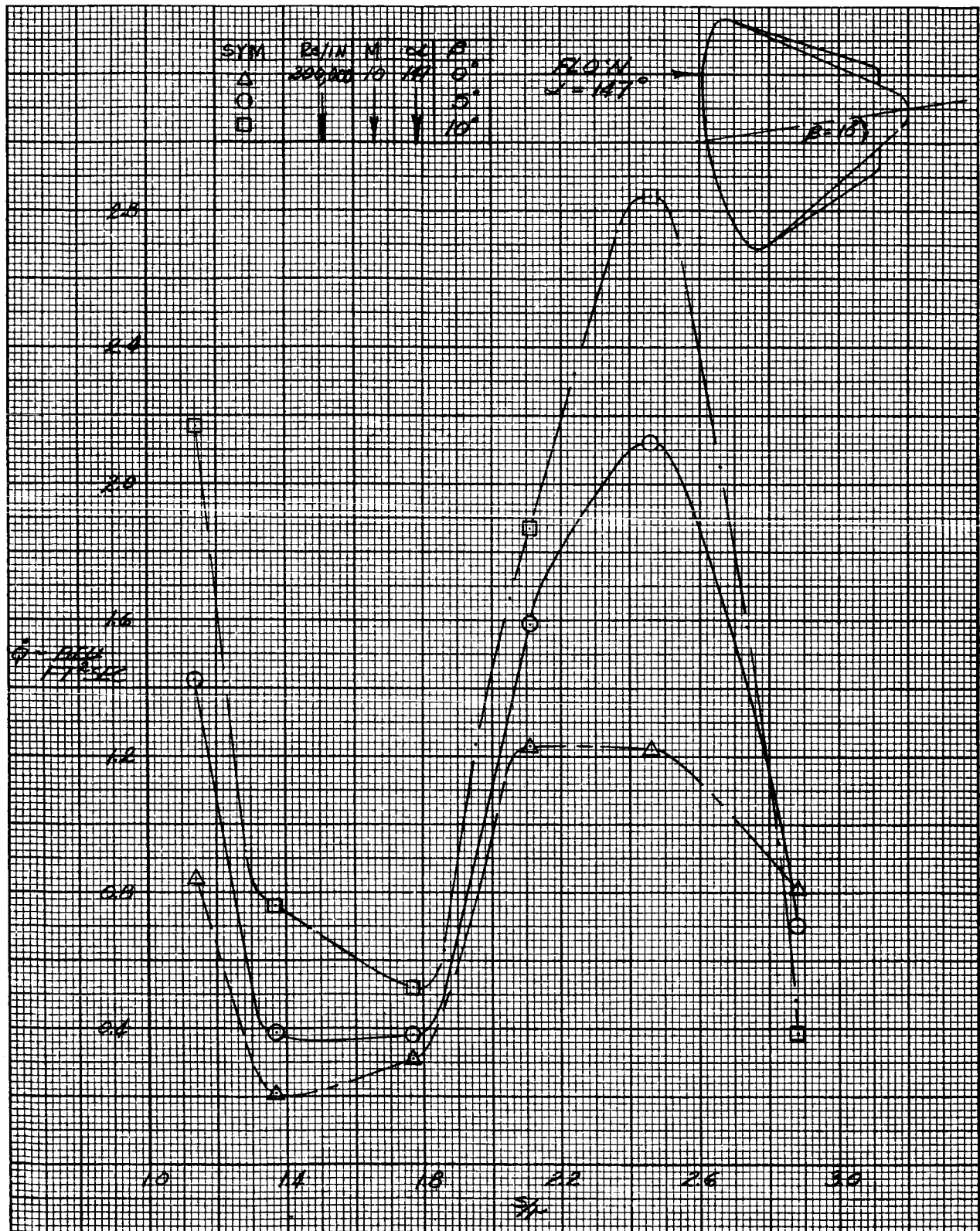
~~CONFIDENTIAL~~

Figure 43. Variation of Heat Transfer Rate on Afterbody of Command Module at 147-Degrees Angle of Attack at Various Yaw Angles
($Re/in. = 200,000$)

~~CONFIDENTIAL~~

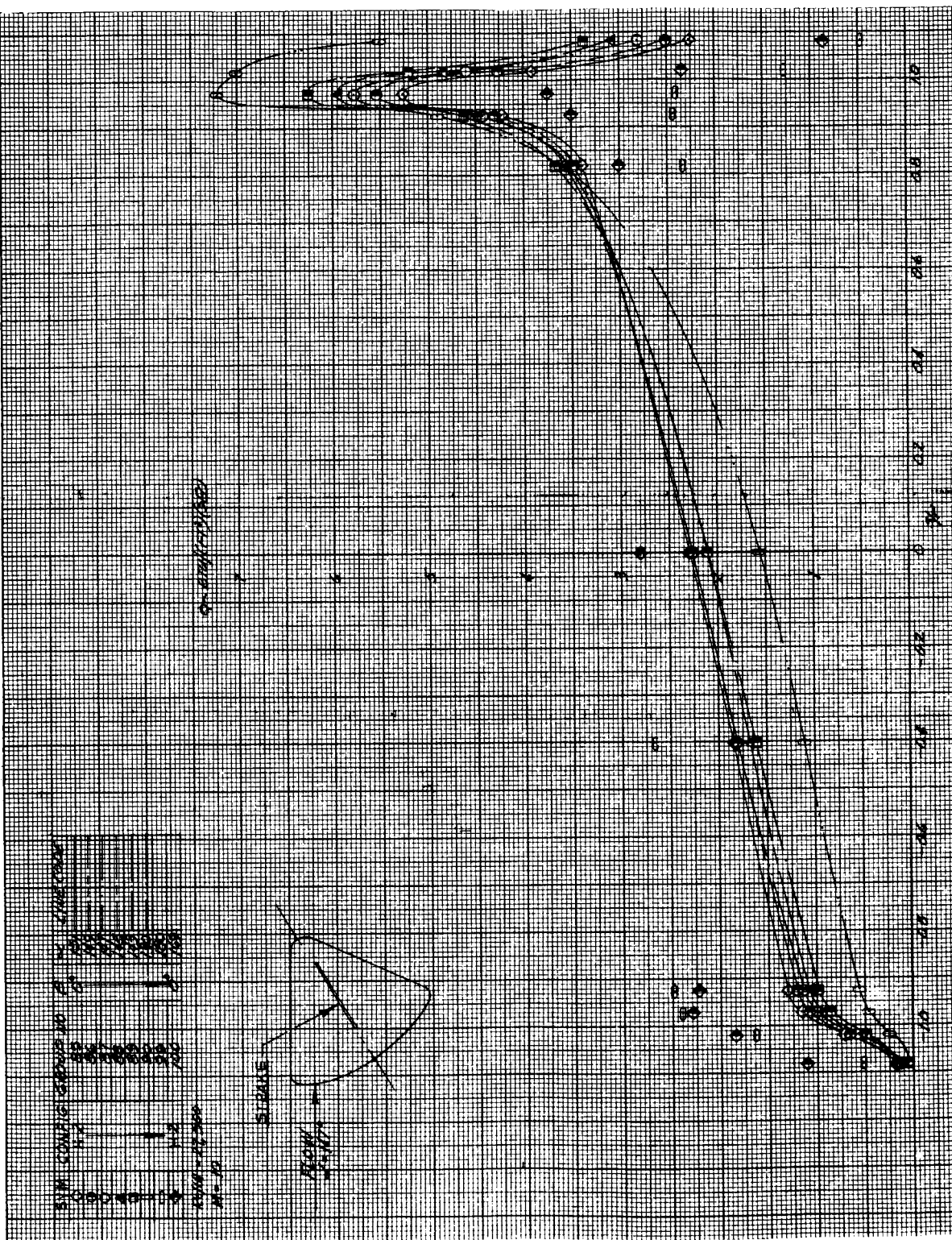


Figure 44. Variation of Heating Rates on the Command Module Entry Face at Various Angles of Attack ($Re/in. = 27,500$)

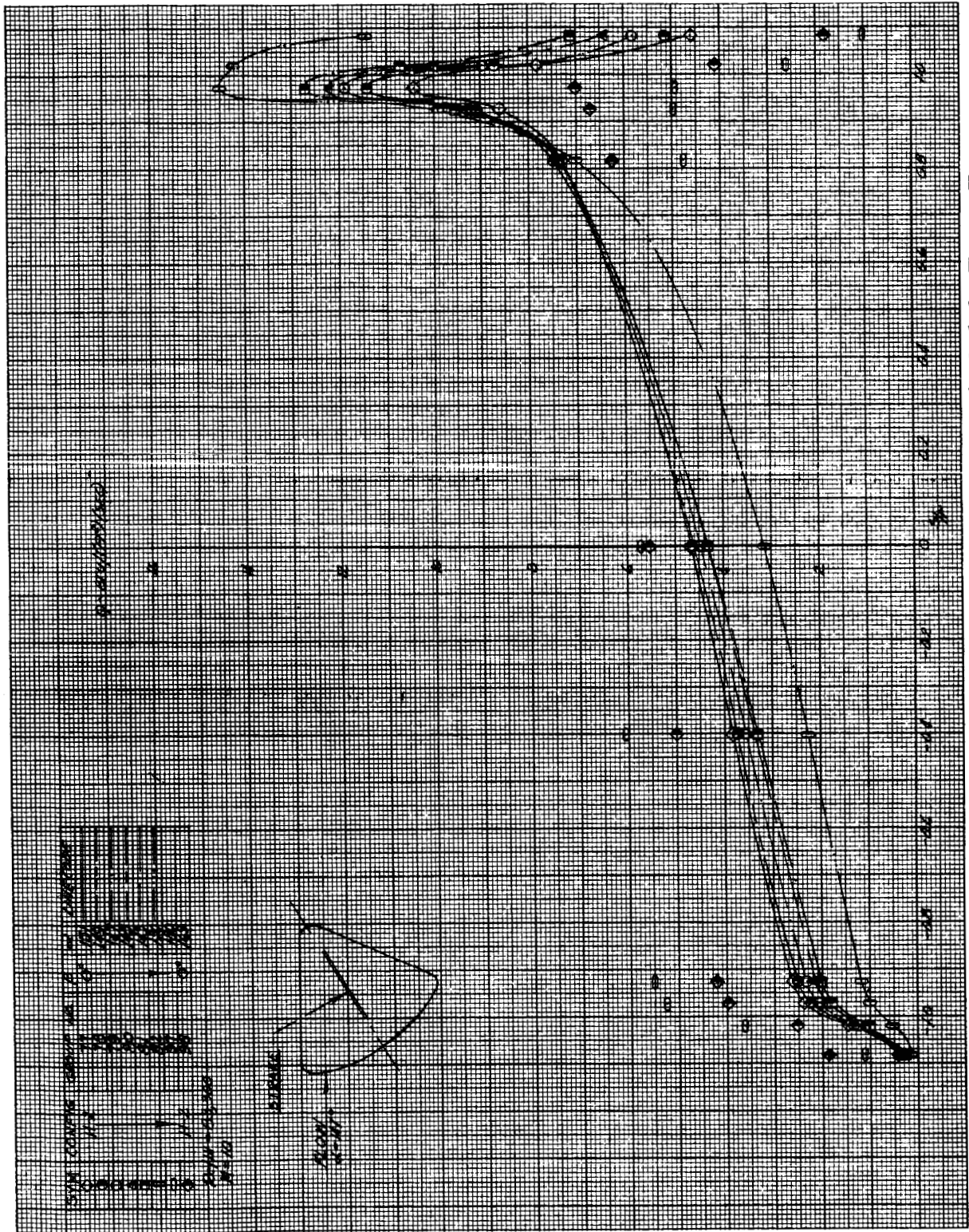
~~CONFIDENTIAL~~

Figure 45. Variation of Heating Rates on the Command Module Entry Face
at Various Angles of Attack ($Re/in. = 83,300$)

~~CONFIDENTIAL~~

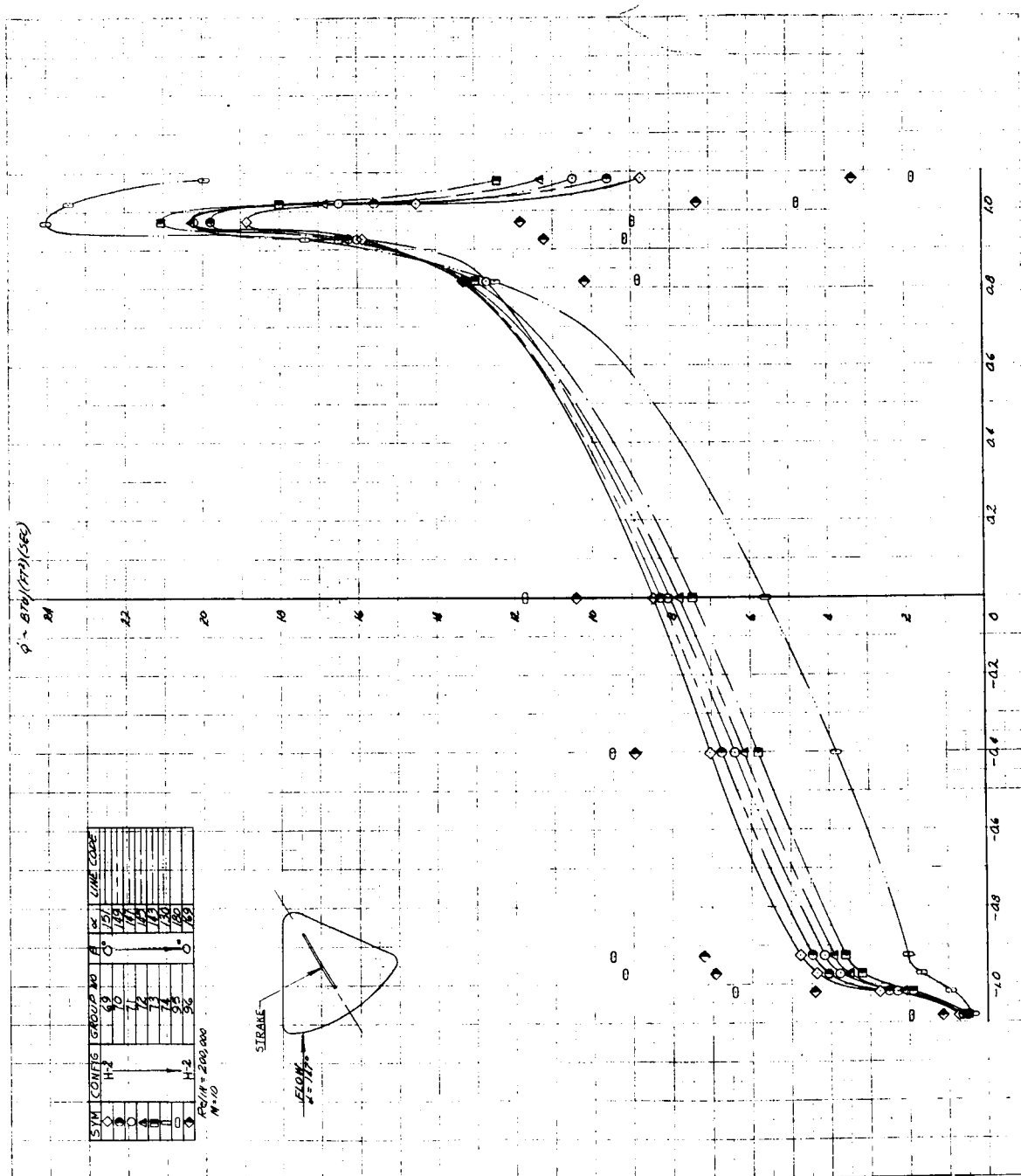
~~CONFIDENTIAL~~

Figure 46. Variation of Heating Rates on the Command Module Entry Face at Various Angles of Attack ($\text{Re}/\text{in.} = 200,000$)

~~CONFIDENTIAL~~